AD 740553

CALIBRATION OF C-131 and KC-135 AIRCRAFT AS HF TEST VEHICLES

Edward J. Christopher
Joseph L. Parry

Approved for Public Release.
Distribution Unlimited.

FOREWORD

Research described in this report was accomplished under Job Order No.: 441A0000.

The authors wish to acknowledge the technical guidance provided by Mr. Carmen Malagisi, Antenna Section (OCTA), in the preparation of this report and by Mr. C. Stincavage, Test Control Section (TSTC), for his valuable assistance in the reduction and preparation of the flight test pattern data.

This technical report was reviewed by the Office of Information (OI) and is releasable to the National Technical Information Service (NTIS).

This report has been reviewed and is approved.

Approved: ARTHUR J. FROHLICH
Chief, Techniques Branch
Surveillance & Control Division

GERALD D. CYGANOWSKI, Lt. Col., USAF
Chief, Test & Evaluation Branch
Technical Support Division

Approved: JAMES L. RYNNING
Colonel, USAF
Chief, Surveillance and
Control Division

QUENTIN J. PORTER
Chief, Technical Support Division

FOR THE COMMANDER:

FRED I. DIAMOND
Acting Chief, Plans Office

UNCLASSIFIED

Security Classification

DOCUMENT CONTROL DATA - R & D

(Security classification of title, body of abstract and indexing annotation must be entered when the overall report is classified)

1. ORIGINATING ACTIVITY *(Corporate author)* RADC (OCTA) Griffiss AFB NY 13440 RADC (TSTC) Griffiss AFB NY 13440	2a. REPORT SECURITY CLASSIFICATION UNCLASSIFIED 2b. GROUP N/A

3. REPORT TITLE

Calibration of C-131 and KC-135 Aircraft as HF Test Vehicles

4. DESCRIPTIVE NOTES *(Type of report and inclusive dates)*

Final Report - December 1970 to December 1971

5. AUTHOR(S) *(First name, middle initial, last name)*

Edward J. Christopher

Joseph L. Parry

6. REPORT DATE February 1972	7a. TOTAL NO OF PAGES 92	7b. NO OF REFS 9
8a. CONTRACT OR GRANT NO N/A b. PROJECT NO 441A0000 c. d.	9a. ORIGINATOR'S REPORT NUMBER(S) RADC-TR-72-14 9b. OTHER REPORT NO(S) *(Any other numbers that may be assigned this report)*	

10 DISTRIBUTION STATEMENT

Approved for Public Release. Distribution Unlimited.

11 SUPPLEMENTARY NOTES RADC PROJECT ENGRS: Edward J. Christopher OCTA/AC 315 330-2443 Joseph L. Parry TSTC/AC 315 330-2433	12 SPONSORING MILITARY ACTIVITY Rome Air Development Center Griffiss Air Force Base, NY 13440

13 ABSTRACT

A calibrated test vehicle provides a means by which absolute power gain measurements can be made on HF antennas without installing a ground reference antenna at each installation and making comparative measurements.

This report describes a method of accurately calibrating two aircraft test vehicles by using an HF standard gain ground reference antenna whose design includes ground conductivity parameters.

Analytical and experimental test programs were performed with a C-131 aircraft and its wing-tip mounted loop antenna and a KC-135 aircraft with its boom mounted loop antenna and fuselage mounted long wire antenna. Both type aircraft were calibrated as a complete receiving "unit", thereby taking into account variations in antenna pattern performance which result when the frequency of operation approaches the resonant frequency of the air frame.

After calibration at its home base these vehicles can embark on test missions to evaluate by means of radiation measurements the absolute power gain characteristics of HF antenna installation.

DD FORM 1 NOV 65 1473

UNCLASSIFIED

Security Classification

UNCLASSIFIED
Security Classification

14 KEY WORDS	LINK A ROLE	LINK A WT	LINK B ROLE	LINK B WT	LINK C ROLE	LINK C WT
Antennas						
HF Antennas						
Flight Testing						
Antenna Radiation Patterns						

UNCLASSIFIED
Security Classification

ABSTRACT

A calibrated test vehicle provides a means by which absolute power gain measurements can be made on HF antennas without installing a ground reference antenna at each installation and making comparative measurements.

This report describes a method of accurately calibrating two aircraft test vehicles by using an HF standard gain ground reference antenna whose design includes ground conductivity parameters.

Analytical and experimental test programs were performed with a C-131 aircraft and its wing-tip mounted loop antenna, and a KC-135 aircraft with its boom mounted loop antenna and fuselage mounted long wire antenna. Both type aircraft were calibrated as a complete receiving "unit", thereby taking into account variations in antenna pattern performance which result when the frequency of operation approaches the resonant frequency of the air frame.

After calibration at its home base, these vehicles can embark on test missions to evaluate by means of radiation pattern measurements the absolute power gain characteristics of HF antenna installations.

TABLE OF CONTENTS

Section		Page
I	Background	1
II	Analysis	3
III	Instrumentation	21
IV	Flight Test Plan	27
V	Data Analysis and Evaluation	31
VI	Gain Calculation	51
VII	Conclusions	81
Appendix A		83
References		85

LIST OF ILLUSTRATIONS

FIGURE		PAGE
1	Computed Elevation Pattern (15.9 MHz) Horizontal Polarization	7
2	Computed Elevation Pattern (17.9 MHz) Horizontal Polarization	7
3	Computed Elevation Pattern (27.9 MHz) Horizontal Polarization	8
4	Computed Elevation Pattern (27.9 MHz) Vertical Polarization	8
5	Computed Elevation Pattern (9.0 MHz) Horizontal Polarization	9
6	Computed Elevation Pattern (15.9 MHz) Horizontal Polarization	9
7	Computed Elevation Pattern (17.9 MHz) Horizontal Polarization	10
8	Computed Elevation Pattern (27.9 MHz) Horizontal Polarization	10
9	Computed Elevation Pattern (29.2 MHz) Horizontal Polarization	11
10	Computed Elevation Pattern (9.01 MHz) Vertical Polarization	11
11	Computed Elevation Pattern (15.9 MHz) Vertical Polarization	12
12	Computed Elevation Pattern (17.9 MHz) Vertical Polarization	12
13	Computed Elevation Pattern (27.9 MHz) Vertical Polarization	13
14	Computed Elevation Pattern (29.2 MHz) Vertical Polarization	13
15	Horizontally and Vertically Polarized Dipoles Over Ground	14
16	Horizontally Polarized Computed Elevation Pattern Over Sea Water	15
17	Horizontally Polarized Computed Elevation Pattern Over Rich Agricultural Land	17
18	Horizontally Polarized Computed Elevation Pattern Over Dry Sandy Soil	17
19	Vertically Polarized Computed Elevation Pattern Over Sea Water	18
20	Vertically Polarized Computed Elevation Pattern Over Rich Agricultural Land	18
21	Vertically Polarized Computed Elevation Pattern Over Dry Sandy Soil	19
22	Verona Dipole Configuration	21
23	C-131 Aircraft Instrumentation	22
24	KC-135 Aircraft Instrumentation	22

LIST OF ILLUSTRATIONS (CONTINUED)

FIGURE		PAGE
25	Flight Test Aircraft	23
26	Airborne Mounted Antenna	24
27	Verona Transmitting Ground Station	25
28	C-131 Orbital Flight Plan	28
29	Detailed Flight Plan Of C-131 Aircraft	28
30	KC-135 Radial Flight Plan	29
31	Detailed Flight Plan Of KC-135 Aircraft	29
32	Measured Elevation Pattern (15.9 MHz) Horizontal Polarization	32
33	Measured Elevation Pattern (17.9 MHz) Horizontal Polarization	32
34	Measured Elevation Pattern (27.9 MHz) Horizontal Polarization	33
35	Measured Elevation Pattern (27.9 MHz) Vertical Polarization	33
36	Measured Elevation Pattern (9.0 MHz) Horizontal Polarization	34
37	Measured Elevation Pattern (15.9 MHz) Horizontal Polarization	34
38	Measured Elevation Pattern (17.9 MHz) Horizontal Polarization	35
39	Measured Elevation Pattern (27.9 MHz) Horizontal Polarization	35
40	Measured Elevation Pattern (29.2 MHz) Horizontal Polarization	36
41	Measured Elevation Pattern (9.0 MHz) Vertical Polarization	36
42	Measured Elevation Pattern (15.9 MHz) Vertical Polarization	37
43	Measured Elevation Pattern (17.9 MHz) Vertical Polarization	37
44	Measured Elevation Pattern (27.9 MHz) Vertical Polarization	38
45	Measured Elevation Pattern (29.2 MHz) Vertical Polarization	38

LIST OF ILLUSTRATIONS (CONTINUED)

FIGURE		PAGE
46	Composite Elevation Profile (15.9 MHz) Horizontal Polarization	39
47	Composite Elevation Profile (17.9 MHz) Horizontal Polarization	39
48	Composite Elevation Profile (27.9 MHz) Horizontal Polarization	40
49	Composite Elevation Profile (27.9 MHz) Vertical Polarization	40
50	Composite Elevation Pattern (9.0 MHz) Horizontal Polarization	41
51	Composite Elevation Pattern (15.9 MHz) Horizontal Polarization	41
52	Composite Elevation Pattern (17.9 MHz) Horizontal Polarization	42
53	Composite Elevation Pattern (27.9 MHz) Horizontal Polarization	42
54	Composite Elevation Pattern (29.2 MHz) Horizontal Polarization	44
55	Composite Elevation Pattern (9.0 MHz) Vertical Polarization	44
56	Composite Elevation Pattern (15.9 MHz) Vertical Polarization	45
57	Composite Elevation Pattern (17.9 MHz) Vertical Polarization	45
58	Composite Elevation Pattern (27.9 MHz) Vertical Polarization	46
59	Composite Elevation Pattern (29.2 MHz) Vertical Polarization	46
60	Free Space Pattern of Loop Antenna	47
61	Model Measurement of Long Wire Antenna On Fuselage of KC-135 Aircraft	48
62	Field Set Up	51
63	Gain Contour (15.9 MHz) Horizontal Polarization	55
64	Gain Contour (17.9 MHz) Horizontal Polarization	56
65	Gain Contour (27.9 MHz) Horizontal Polarization	56
66	Gain Contour (27.9 MHz) Vertical Polarization	57
67	Gain Contour (9.0 MHz) Horizontal Polarization	57

LIST OF ILLUSTRATIONS (CONTINUED)

FIGURE		PAGE
68	Gain Contour (15.9 MHz) Horizontal Polarization	58
69	Gain Contour (17.9 MHz) Horizontal Polarization	58
70	Gain Contour (27.9 MHz) Horizontal Polarization	59
71	Gain Contour (29.2 MHz) Horizontal Polarization	59
72	Gain Contour (9.0 MHz) Vertical Polarization	60
73	Gain Contour (15.9 MHz) Vertical Polarization	60
74	Gain Contour (17.9 MHz) Vertical Polarization	61
75	Gain Contour (27.9 MHz) Vertical Polarization	61
76	Gain Contour (29.2 MHz) Vertical Polarization	62
77	High Frequency Antenna Installation	63
78	Effective Radiated Power and Field Strength Data (15.9 MHz)	64
79	Effective Radiated Power and Field Strength Data (17.9 MHz)	65
80	Effective Radiated Power and Field Strength Data (27.9 MHz)	66
81	Effective Radiated Power and Field Strength Data (27.9 MHz)	67
82	Effective Radiated Power and Field Strength Data (9.0 MHz)	68
83	Effective Radiated Power and Field Strength Data (15.9 MHz)	69
84	Effective Radiated Power and Field Strength Data (17.9 MHz)	70
85	Effective Radiated Power and Field Strength Data (27.9 MHz)	71
86	Effective Radiated Power and Field Strength Data (29.2 MHz)	72
87	Effective Radiated Power and Field Strength Data (9.0 MHz)	73
88	Effective Radiated Power and Field Strength Data (15.9 MHz)	74
89	Effective Radiated Power and Field Strength Data (17.9 MHz)	75
90	Effective Radiated Power and Field Strength Data (27.9 MHz)	76
91	Effective Radiated Power and Field Strength Data (29.2 MHz)	77

LIST OF TABLES

TABLE		PAGE
I-A	Verona Dipole (C-131 Aircraft)	5
I-B	Verona Dipole (KC-135 Aircraft)	6
II-A	Dipole Gain For C-131 Aircraft Measurements	20
II-B	Dipole Gain For KC-135 Aircraft Measurements	20
III	Dipole Design Frequencies	21
IV-A	Dipole Gain For C-131 Aircraft Measurements	49
IV-B	Dipole Gain For KC-135 Aircraft Measurements	49
V	Airborne Receiving System Losses	50
VI	Ground Transmitter System Losses	50
VII-A	"Unit Gain" Calculation (C-131)	54
VII-B	"Unit Gain" Calculation (KC-135)	54

SECTION I

BACKGROUND

Airborne techniques to measure absolute power gain of high frequency antennas (3 - 30 MHz) are limited by the inability to estimate the gain of airborne antennas used in making radiation pattern measurements in this frequency range. The limiting factor is the difficulty in isolating the airborne antenna from the aircraft upon which it is mounted. This report describes an effort to more precisely estimate the gain of such airborne antennas. The gain obtained can be used to determine the absolute power gain of several existing HF receiving and transmitting antenna installations.

Ground-based horizontal and vertical transmitting dipoles, designed to operate at discrete frequencies within the HF spectrum, were fabricated and installed at RADC's Verona Test Annex. Elevation pattern profiles were computed at different frequencies and for various dipole heights above ground, taking into account the effects on pattern performance which result from locating the antenna over a real ground environment, that is, one in which the ground is not considered a perfectly reflecting plane, as is usually assumed. The elevation profiles computed for this report correlated well with those results reported by other authors.* The computer programs used in these computations were used previously in other antenna pattern analyses supported by field measurements. A high degree of confidence in the use of these programs resulted. Direct use was made of the computed pattern-gain characteristics of the dipole in determining, as a function of the receiving aircraft's slant range and angular position, relative to the dipole, the absolute gain of the aircraft and its antennas as a single calibrated unit.

*Refer to references listed in Bibliography

SECTION II

ANALYSIS

To compute the elevation pattern-gain characteristics of the dipole and to incorporate into the computations the effects of a real ground environment on pattern performance, combined reflection coefficient and height factor analyses were performed. A brief description follows of these programs and the manner in which they were employed.

When a plane wave strikes a surface of infinite conductivity at an oblique angle, the reflected wave has the same amplitude as the incident (direct) wave and the same phase, or exactly the opposite phase, as the incident wave, depending upon the sense of polarization. However, in a more realistic situation, the incident wave strikes a surface of finite conductivity, resulting in a decrease in the amplitude of the reflected wave versus that of the incident wave. The phase relations are also modified.

The vector ratio of the reflected to incident wave is termed the reflection coefficient and is defined as

$$R \angle \rho$$

where

R = ratio of the magnitude of the reflected to incident wave

ρ = phase difference of reflected to incident wave

The exact value of the reflection coefficient is dependent upon the dielectric constant and conductivity of the earth, the angle of incidence with which the wave strikes the earth and the frequency of operation. It may be expressed as follows:

$$R_V = \text{Vertical Polarization} = \frac{\text{Reflected Wave}}{\text{Incident Wave}} = \frac{\varepsilon^1 \sin \psi_2 - \sqrt{\varepsilon^1 - \cos^2 \psi_2}}{\varepsilon^1 \sin \psi_2 - \sqrt{\varepsilon - \cos^2 \psi_2}} \quad (1)$$

$$R_H = \text{Horizontal Polarization} = \frac{\text{Reflected Wave}}{\text{Incident Wave}} = \frac{\sqrt{\varepsilon^1 - \cos^2 \psi_2} - \sin \psi_2}{\sqrt{\varepsilon^1 - \cos^2 \psi_2} + \sin \psi_2} \quad (2)$$

PRECEDING PAGE BLANK

where

ψ_2 = angle of incidence

$\varepsilon^1 = \varepsilon - j\, 6\, \sigma\, \lambda\, X\, 0^{12}$

ε = assumed dielectric constant of the earth environment

σ = earth conductivity (EMU)

λ = wavelength of operating frequency

$j = \sqrt{-1}$

Results of the reflection coefficient analysis for horizontal and vertical polarization were substituted into the following "resultant field equation" to take into account variations in pattern shape due to adjustments in antenna height.

$$E = I_1 \sin(\beta H \sin \psi_2) + I_1 \cos(\beta H \sin \psi_2) + I_2 \sin[-\beta H (\sin \psi_2) + \beta_2] + I_2 \cos[\beta - \beta H (\sin \psi_2) + \beta_2] \quad (3)$$

where

E = Electric Field

I_1 = 1

I_2 = Current in antenna N (obtained from reflection coefficient analysis)

β = $2\pi/\lambda$

β_2 = Relative phase of antenna current (obtained from reflection coefficient analysis)

ψ_2 = Angle of elevation

H = Antenna electrical height in wavelengths

The reflection coefficient analysis was programmed for the Honeywell 635/645 Computer. It was performed at the frequencies for which the ground-based dipole was specifically designed, namely 9.01 MHz, 15.92 MHz, 17.99 MHz, 27.92 MHz and 29.20 MHz. "Rich agricultural land and low hills" best describes the ground conditions at the Verona Test Site. These ground conditions were represented in the computer program by a conductivity (σ) of 1 X 10^{-13} EMU and a dielectric constant (ε) of 15 ESU. In an attempt to further support the reasonableness of the ground conditions assumed at the Verona Test Site, the reflection coefficient analysis was performed using Verona ground constants which were measured in support of an earlier project.[9] The comparative data correlated within 1 dB over 5° to 45° in elevation.

Results of the reflection coefficient analysis were then employed in the resultant field equation which was also programmed for the Honeywell 635/645 Computer. This extension to the reflection coefficient analysis will be referred to as the height factor analysis.

Tables 1A and 1B list the basic parameters included in the combined reflection coefficient and height factor analyses. The extremely flat terrain at the Verona Test Site resulted in the assumption that the physical and electrical dipole heights were at the same level. Overall results of the analysis for Table 1A are shown in Figures 1 through 3, for Horizontal Polarization and Figure 4 for Vertical Polarization. Correspondingly, results of the analysis for Table 1B are shown in Figures 5 through 9 for horizontal polarization and Figures 10 through 14 for vertical polarization. The vertical profile pattern data consists of a plot of relative signal level as a function of elevation angle, where the relative signal level has been normalized to that obtained when operating over an infinitely conducting ground. Cross referencing this data with height factor analysis performed in References (1), (2), (3), and (6) provided excellent correlation in terms of overall pattern shape, particularly with regard to the angular positions of the various peaks and nulls for the antenna electrical heights assumed.

Table 1A

VERONA [illegible]

[illegible] 131 [illegible] AFF [illegible]

GROUND CONDITIONS

Rich Agricultural Land and Low Hills

Conductivity = 1 x 10^{-13} [illegible]

Dielectric Constant = 15 (ESU)

Aircraft	Antenna	Polarization	Freq (MHz)	[illegible]	Physical Dipole Height (ft)	Electrical Dipole Height
[illegible]	Wing [illegible] Loop	[illegible]	[illegible]	[illegible]	[illegible]	[illegible]
[illegible]	Wing [illegible] Loop	[illegible]	[illegible]	[illegible]	[illegible]	[illegible]
[illegible]	[illegible]	[illegible]		[illegible]	[illegible]	[illegible]
[illegible]	[illegible]	[illegible]	[illegible]			[illegible]

TABLE 1B

VERONA DIPOLE

(KC-135 #125 Aircraft)

GROUND CONDITIONS:

Rich Agricultural Land and Low Hills

Conductivity $\sigma = 1 \times 10^{-13}$ (EMU)

Dielectric Constant $\epsilon = 15$ (ESU)

Antenna	Polarization	Freq (MHz)	λ(Ft)	Physical Dipole Height (Ft)	Electrical Dipole Height
Boom/Mtd Loop	HOR	9.01	109.1	29.5	.27 λ
Boom/Mtd Loop	HOR	15.92	61.8	17.3	.28 λ
Boom/Mtd Loop	HOR	17.99	54.6	13.8	.25 λ
Boom/Mtd Loop	HOR	27.92	35.2	9.9	.28 λ
Long Wire	HOR	29.20	33.7	33.7	.75 λ
Boom/Mtd Loop	VER	9.01	109.1	25.5	.27 λ
Boom/Mtd Loop	VER	15.92	61.8	17.3	.28 λ
Boom/Mtd Loop	VER	17.99	54.6	13.8	.25 λ
Boom/Mtd Loop	VER	27.92	35.2	9.9	.28 λ
Long Wire	VER	29.20	33.7	33.7	1 λ

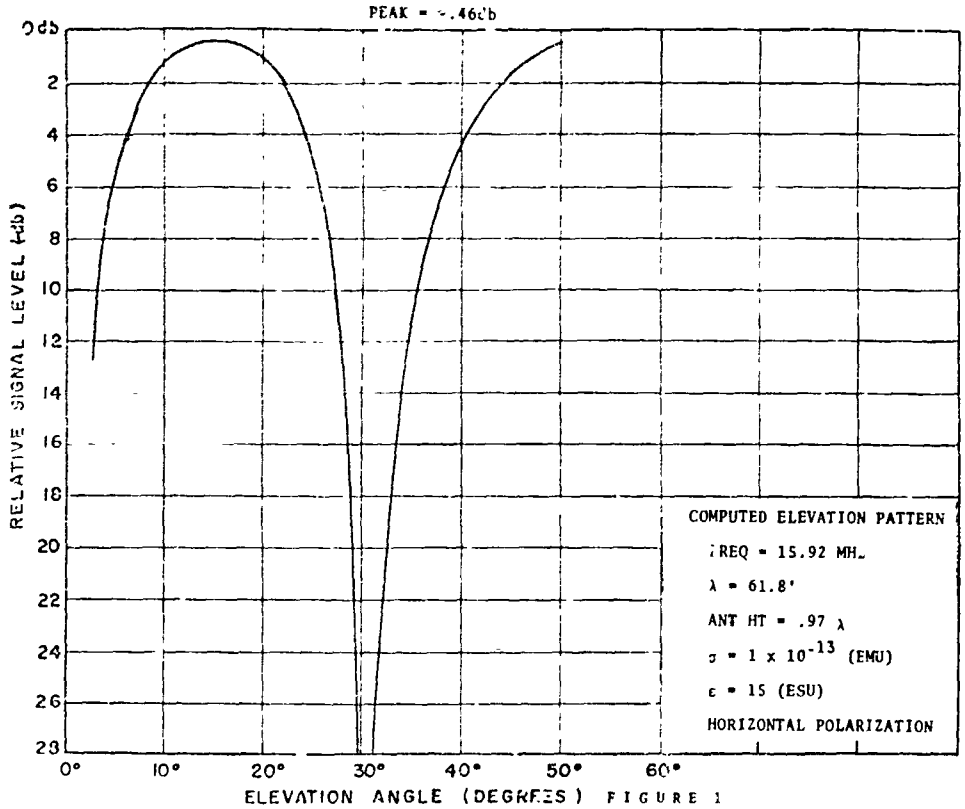

FIGURE 1

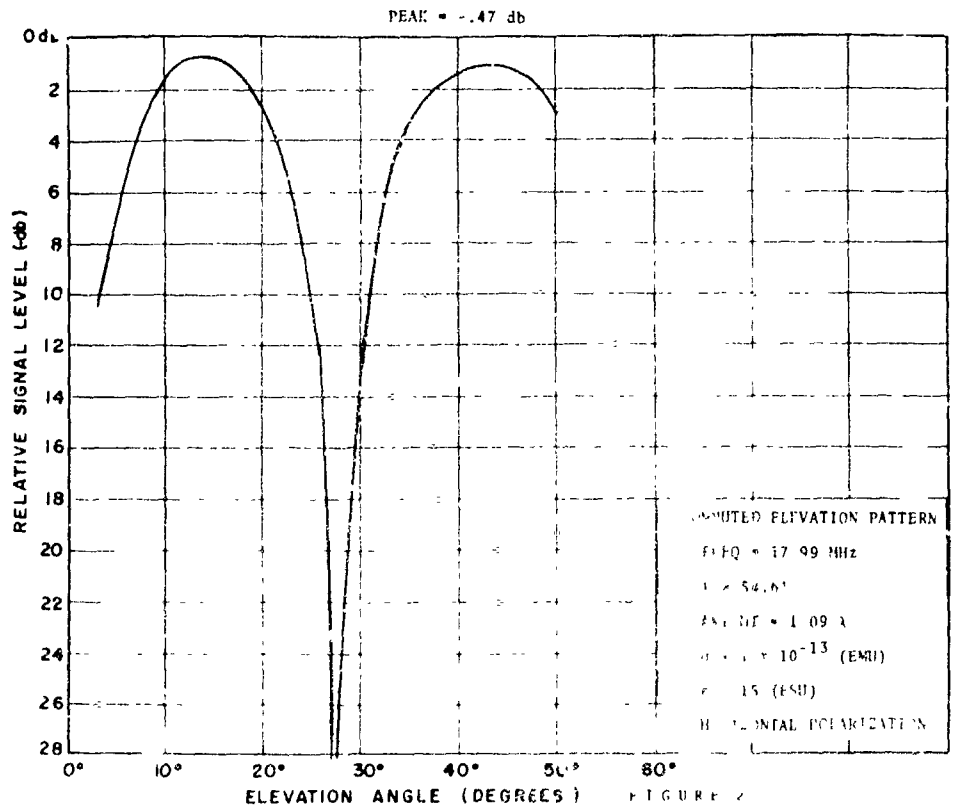

FIGURE 2

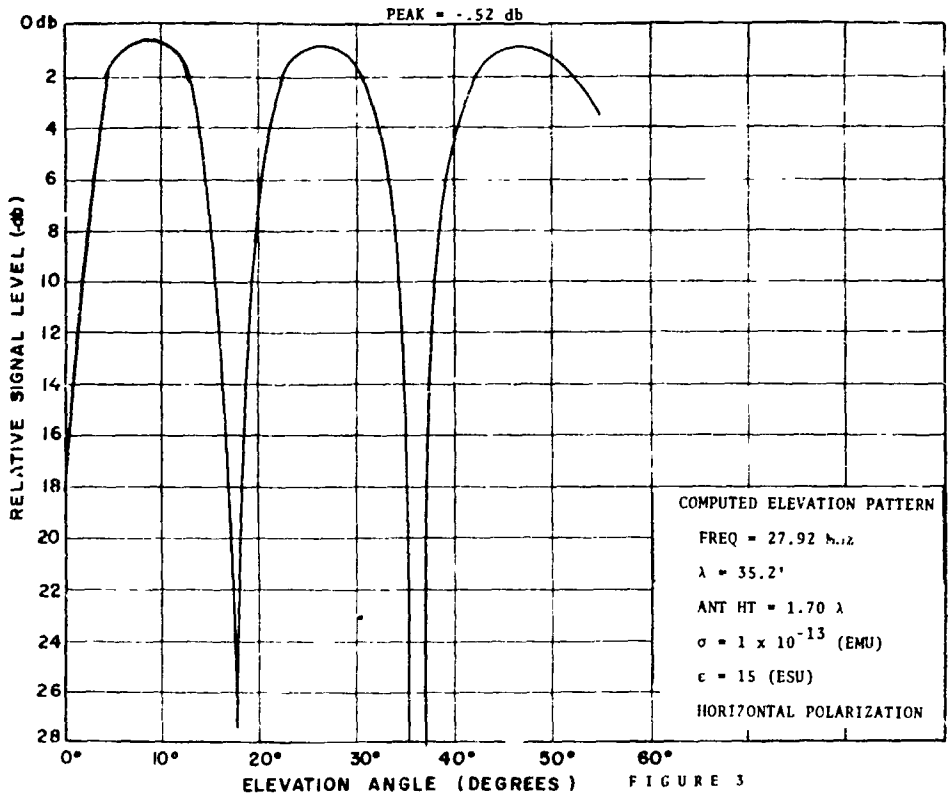

FIGURE 3

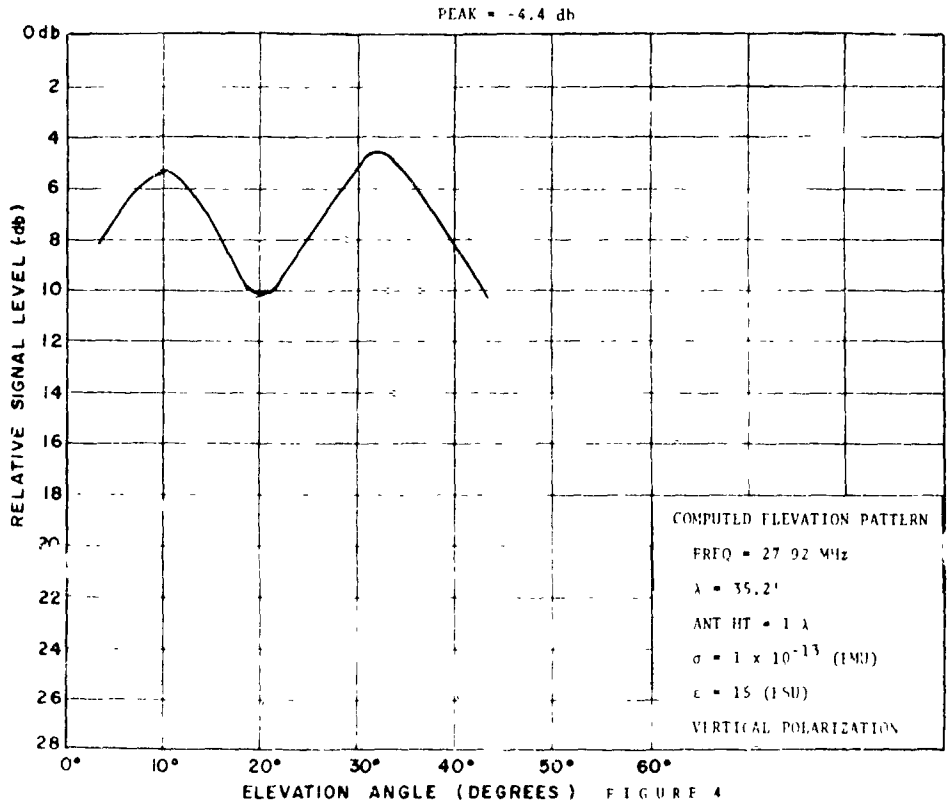

FIGURE 4

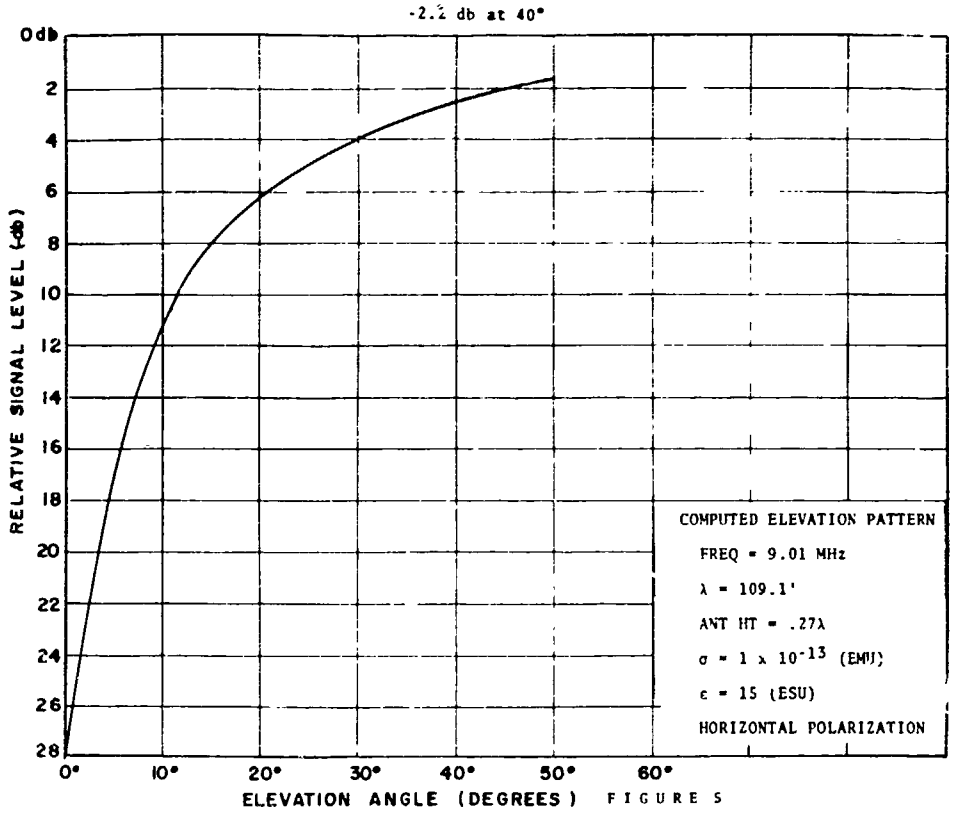

FIGURE 5

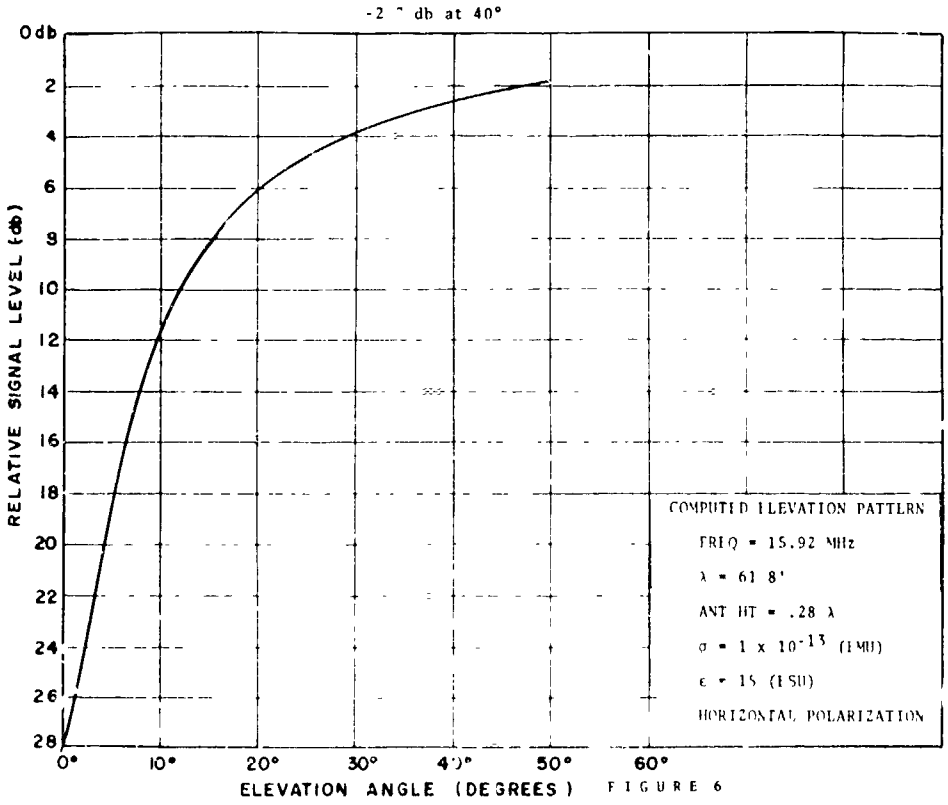

FIGURE 6

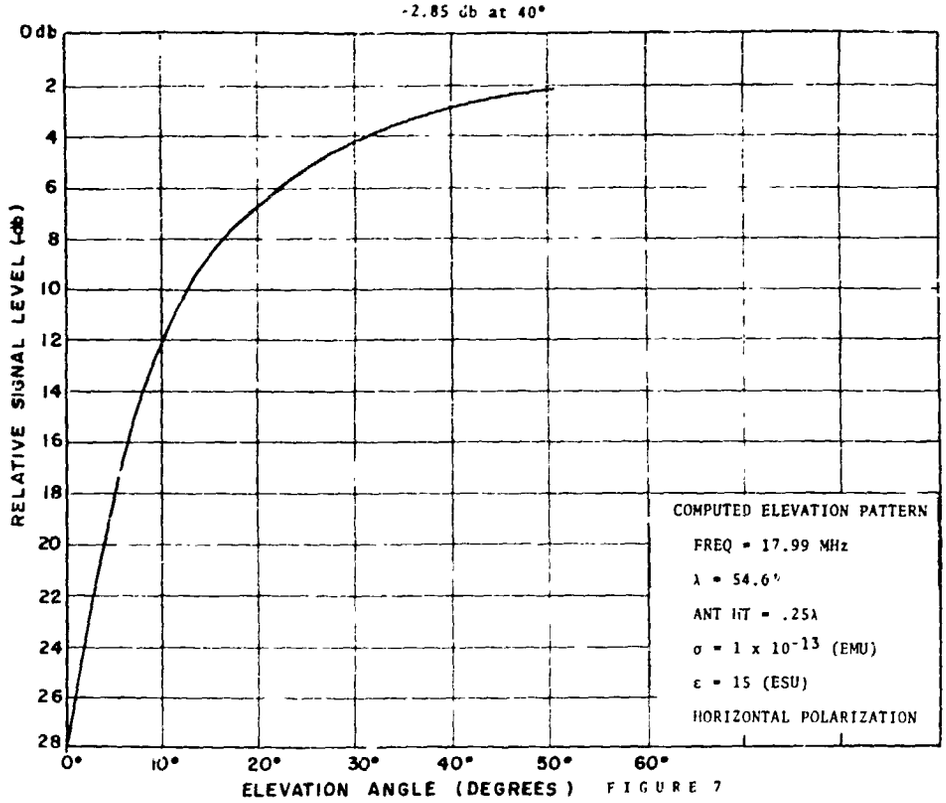

FIGURE 7

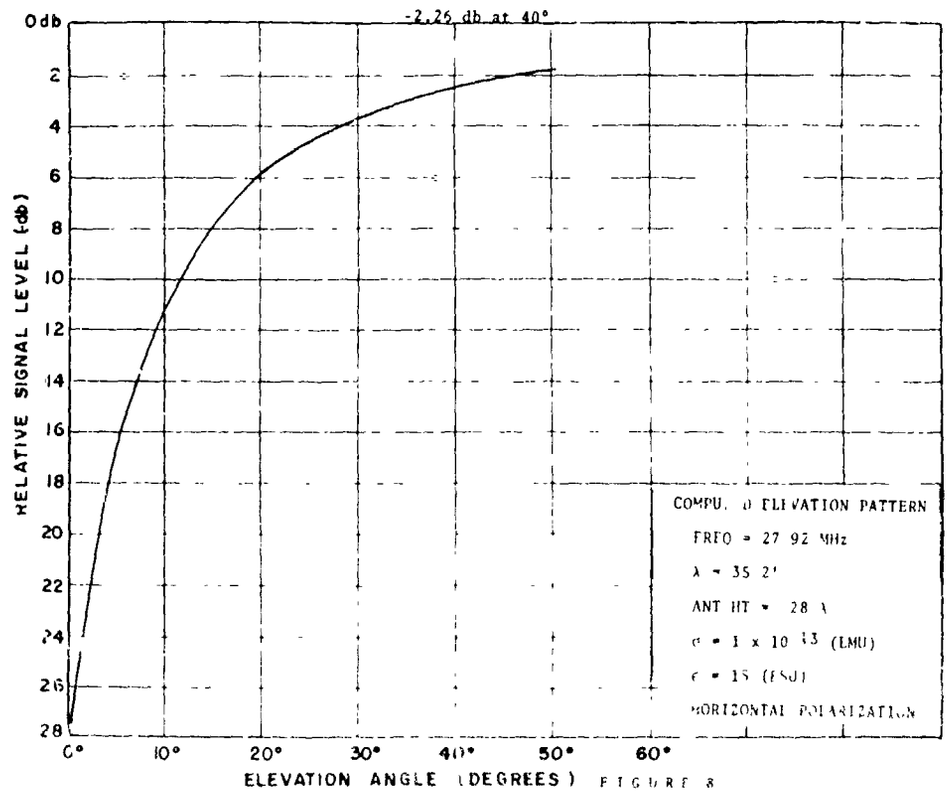

FIGURE 8

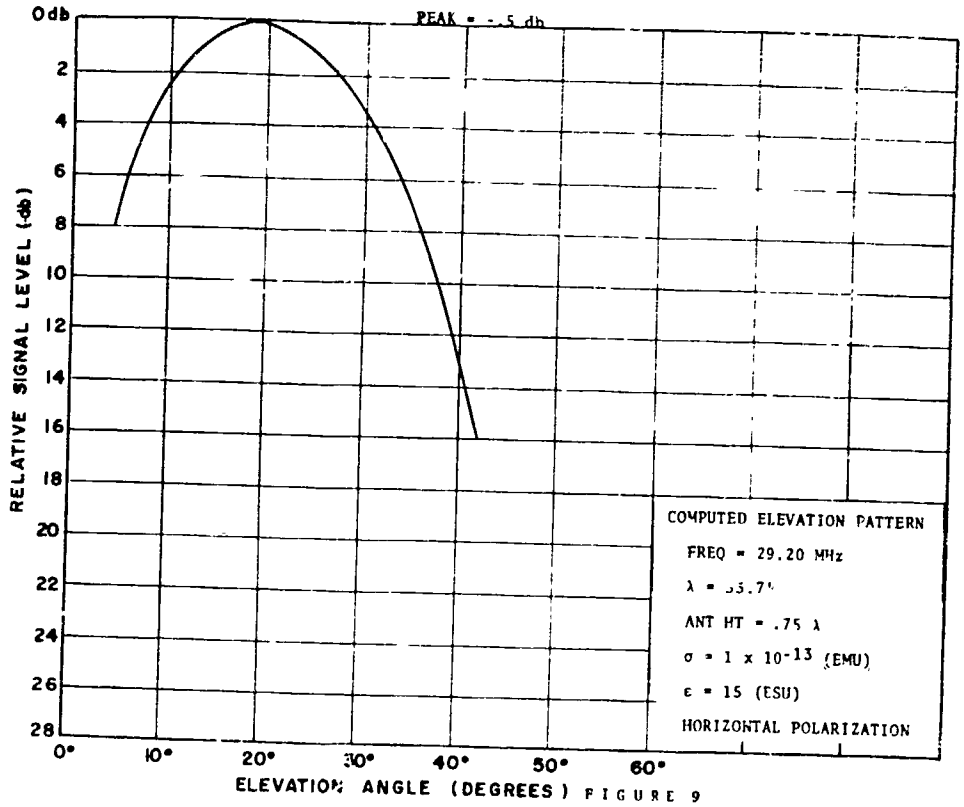

FIGURE 9

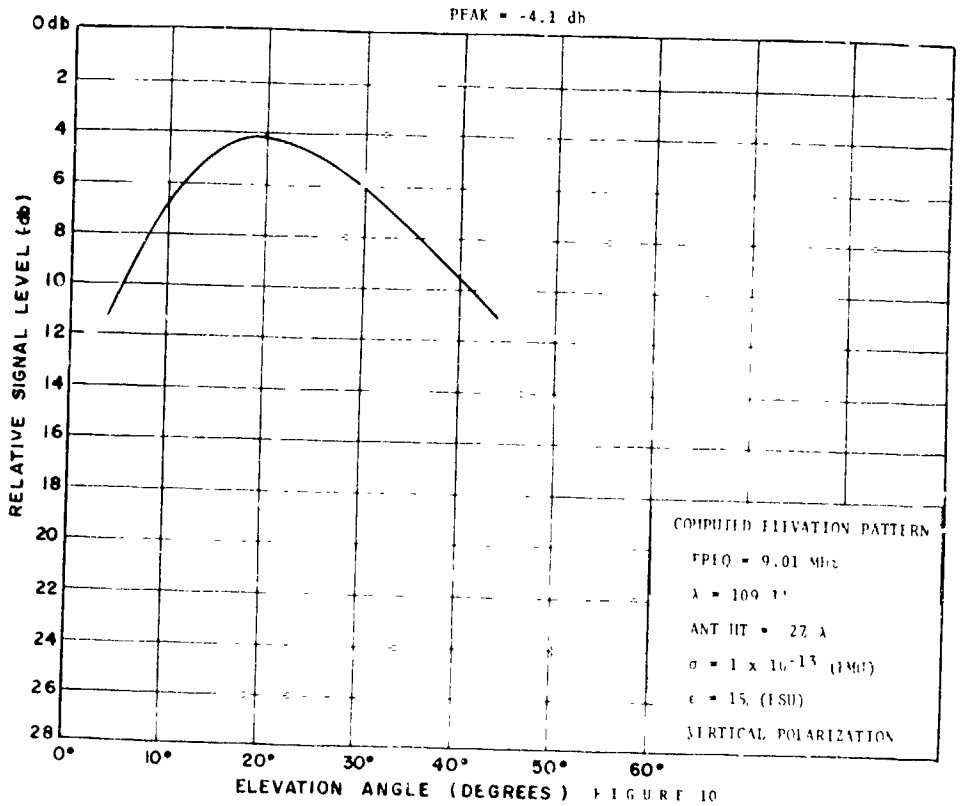

FIGURE 10

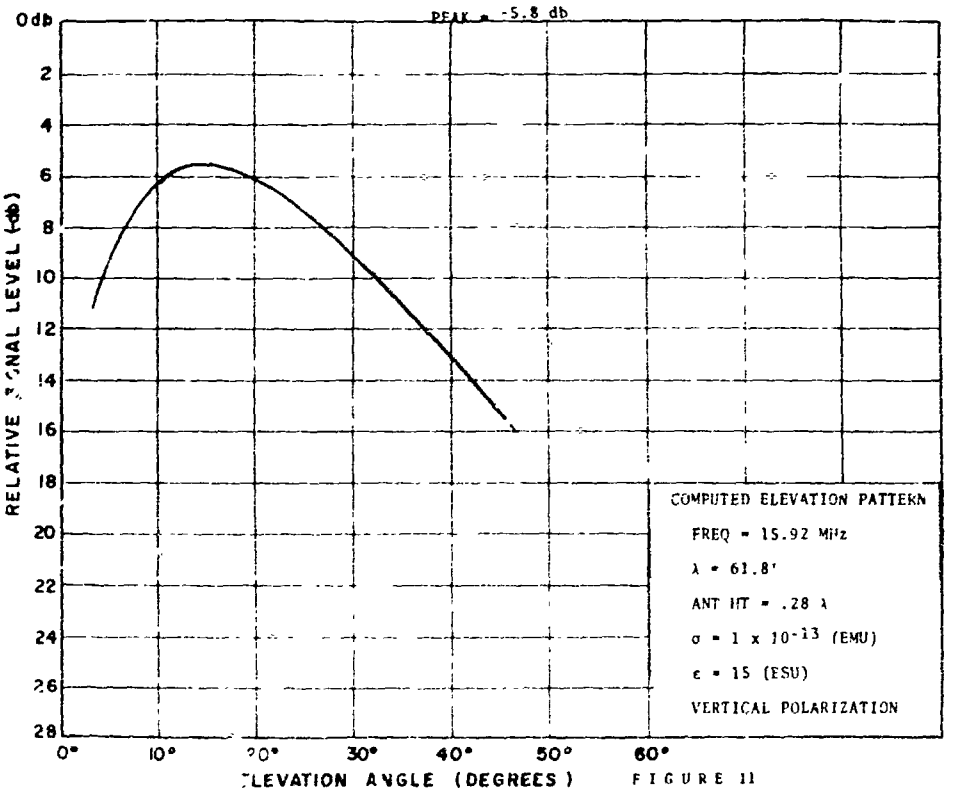

FIGURE 11

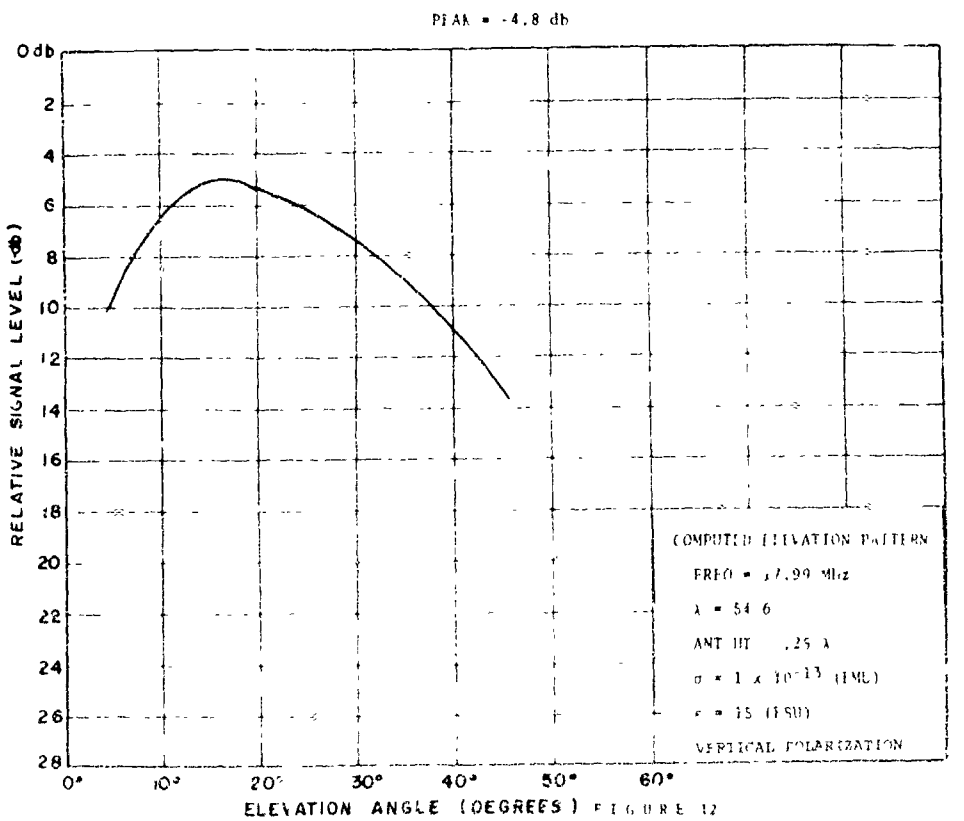

FIGURE 12

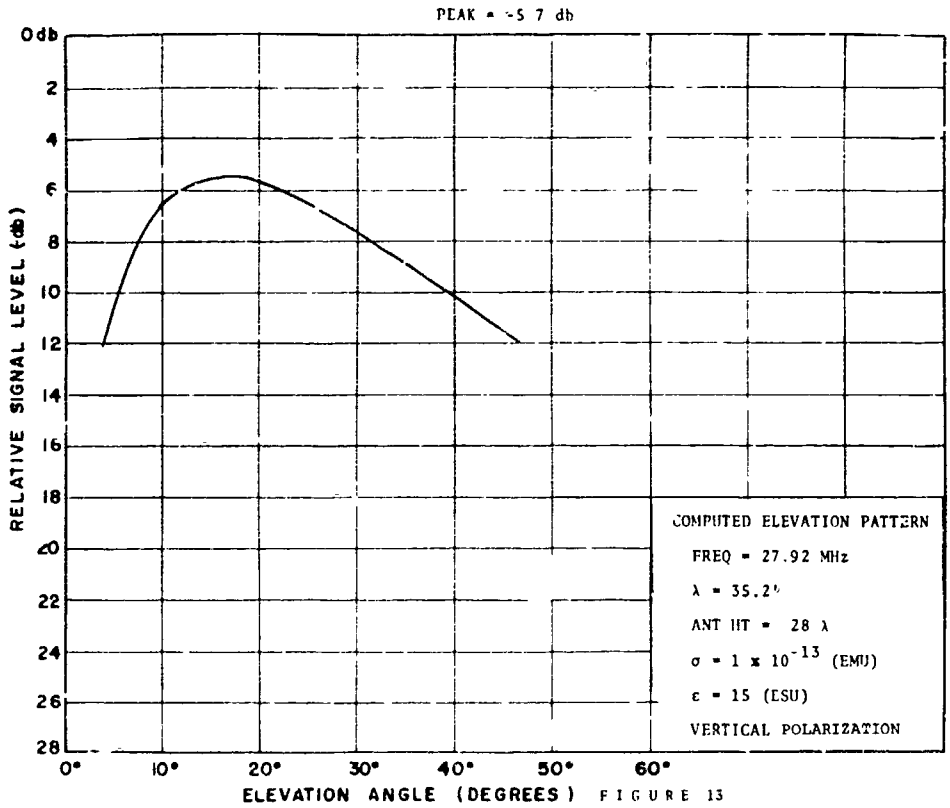

FIGURE 13

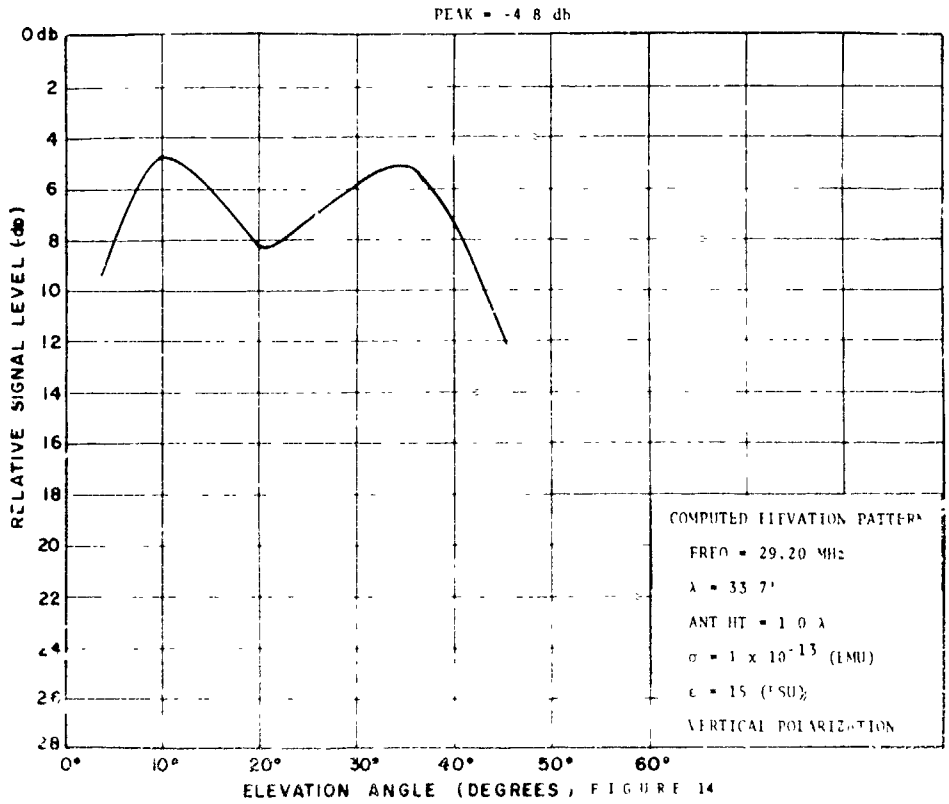

FIGURE 14

The following background information will facilitate interpretation of the data of Figures 1 through 14. As an antenna is brought from a free space environment to that of a ground environment, its pattern alters due to the proximity of ground. Over infinitely conducting ground a six-db improvement in antenna gain relative to that of free space conditions ideally should be realized. This gain improvement is accounted for in Figure 15. As shown in Figure 15A, B, antenna radiation in free space consists only of direct waves. However, in the presence of ground, the resultant field is obtained or described by the interference, either constructively or destructively, between the direct and ground-reflected rays, as shown in Figure 15.

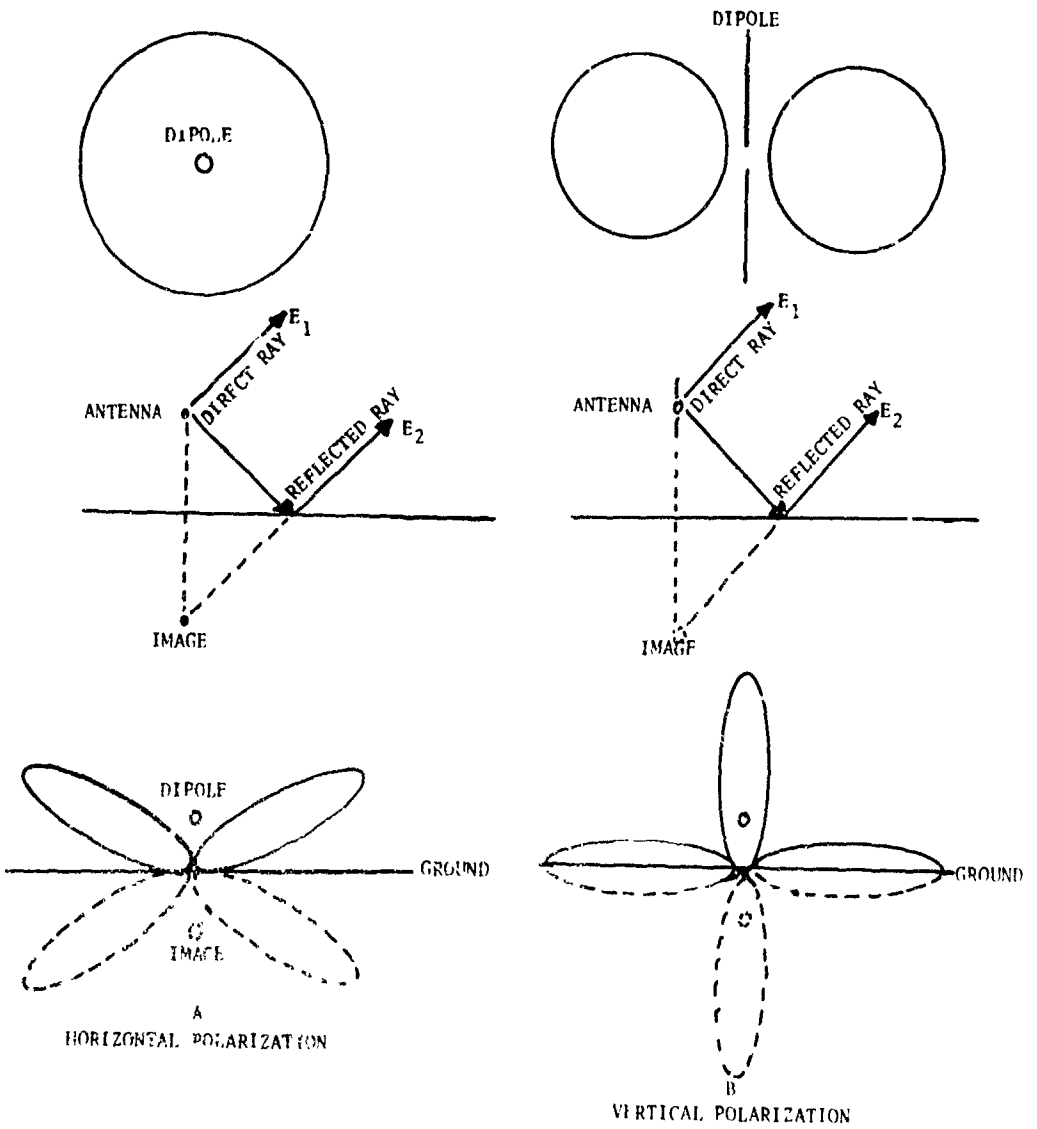

Dipole Antenna Positioned $\frac{\lambda}{2}$ Above Ground

Figure 15

With ground:

$E_1 + E_2 = 2E$, where $2E$ is the magnitude in the far field, when E_1 and E_2 add in phase.

With no ground (i.e., free space):

$E_1 = E$, where E is the magnitude in the far field. Gain improvement in the presence of ground is given, therefore, by the ratio of the squares of the field:

$$\frac{(2E)^2}{E^2} = \frac{4E^2}{E^2} = 4, \text{ corresponding to 6 db.}$$

At a perfectly conducting ground plane, the reflected wave amplitude equals that of the incident wave and the reflected wave phase is either exactly that of the incident wave, as in the case of vertical polarization, or exactly the opposite, as in the case of horizontal polarization. The effect is shown in the computed patterns of Figure 16 where the nearly perfect ground environment

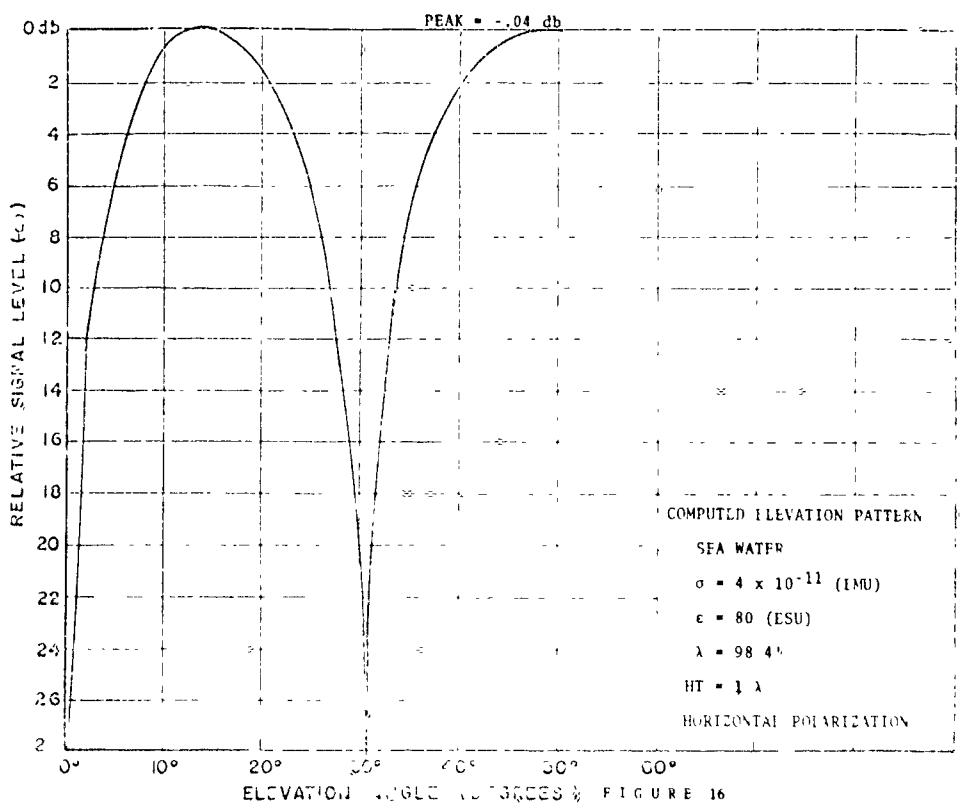

Figure 16

is represented by seawater, which most closely simulates an infinitely conducting reflecting surface. This figure shows a minimum reduction in signal level of .04 db at the peak of the vertical pattern profile, due to the less than perfect conductivity of the seawater environment assumed. As mentioned, in the presence of infinitely conducting ground, an antenna gain improvement of 6 db over that obtained in free space would be realized. However, over ground of finite conductivity, there is a decrease in the amplitude of the reflected versus direct wave and the phase relations between the direct and reflected waves are modified. Therefore, when operating over a ground of finite conductivity, the resultant field amplitude at a point in space varies as a function of the finite conductivity of the existent ground environment. As a consequence of this variation in amplitude, less than the maximum 6 db gain improvement realized over perfect ground is obtained. This effect is shown in the computed patterns of Figures 17 and 18 which are plots for the same antenna electrical heights, polarization, and operating frequency as that of Figure 16. Only the ground environment was varied. Examination of Figures 17 and 18 indicate that as the ground becomes progressively less conductive, the signal attenuation at the peak of the vertical pattern profile increases.

Similarly, Figures 19, 20, and 21 are computed patterns for a vertically polarized half-wave dipole located over the same extreme ground environments used in Figures 16 through 18. It is particularly interesting to note how slight the difference in single attenuation is at the peak of the vertical pattern profiles shown in Figures 16 through 18, for the extreme ground environment considered. Ground attenuation varies only between .04 dB for seawater to .63 dB for a dry sandy environment. However, the greater sensitivity of vertical polarization to ground conductivity is demonstrated in Figures 19 through 21. Here, the ground attenuation varies from a minimum of 1.2 dB for a seawater environment to a maximum of 4.7 dB for a dry sandy soil environment. Allowing for this attenuation factor, the maximum 6 dB gain improvement expected, due to proximity of an antenna over perfectly conducting ground, has to be modified accordingly. Tables IIA and IIB were prepared to relate this behavior for all frequencies and polarizations for which flight test measurements were made. The angles after the entries in the "Ground attenuation" column of Tables IIA and IIB are those angles at which the listed attenuation values were taken off the computed patterns of Figures 1 through 14. The significance of these selected angles will become more apparent in the "Data Analysis" section of this report. In Figures 1 through 14 and 16 through 21, the maximum realizable gain has been normalized to 0 dB. This normalization factor will be used on all vertical pattern profile data to be presented throughout this report.

The pattern data of Figures 1 through 14 is representative of the ground conditions at the Verona Test Site where the flight

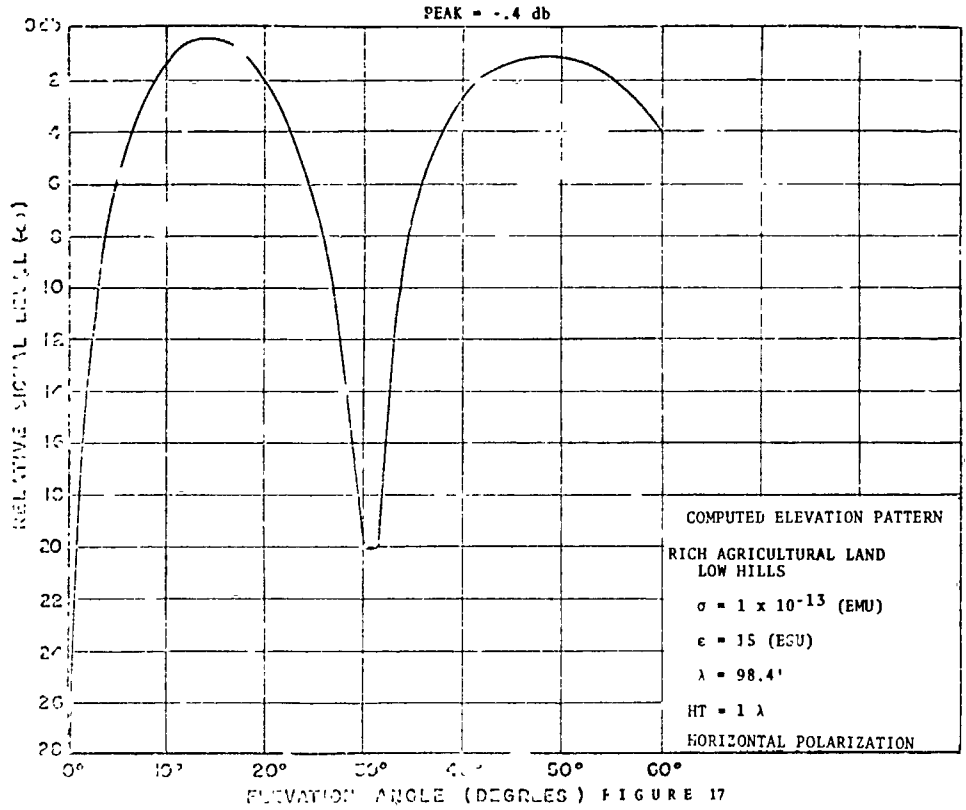

ELEVATION ANGLE (DEGREES) FIGURE 17

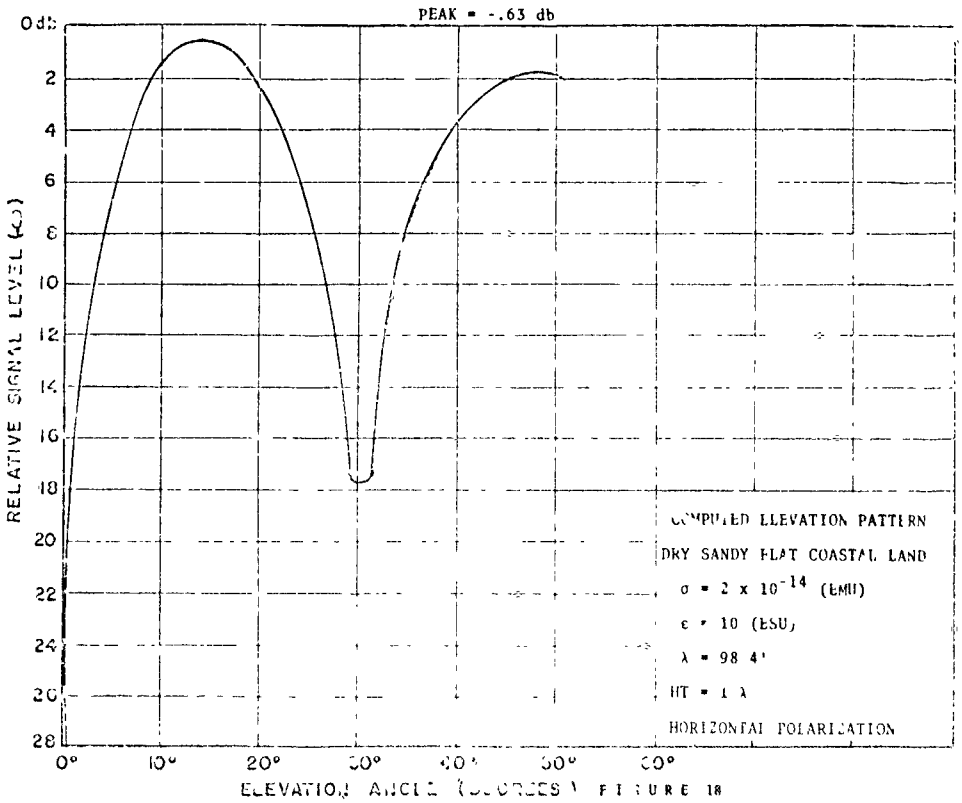

ELEVATION ANGLE (DEGREES) FIGURE 18

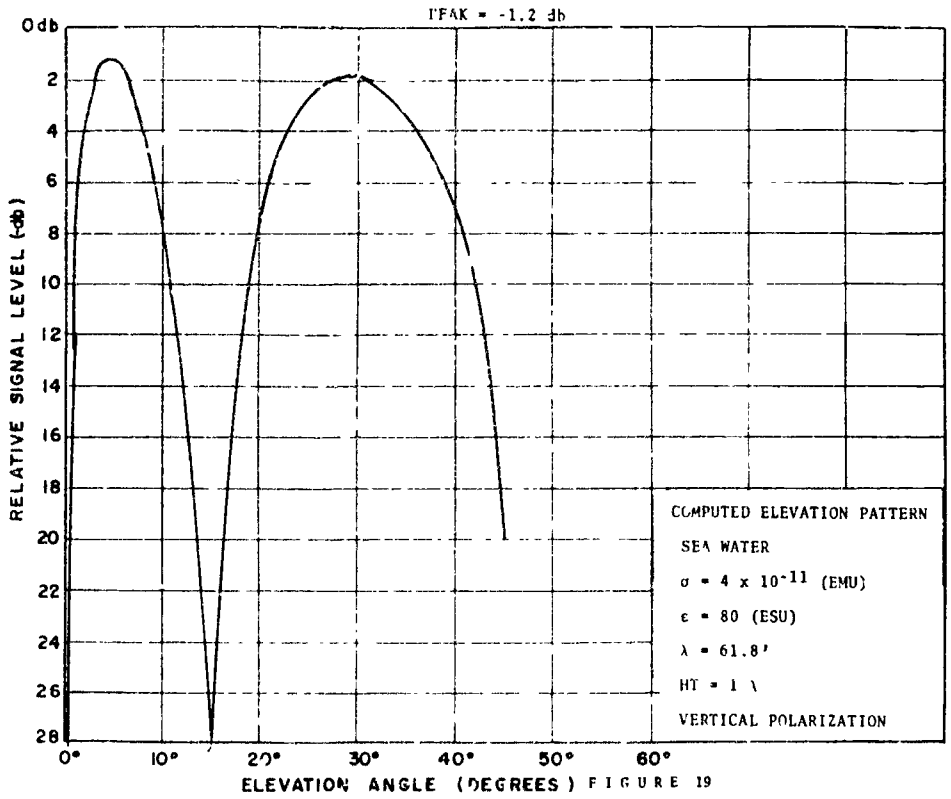

FIGURE 19

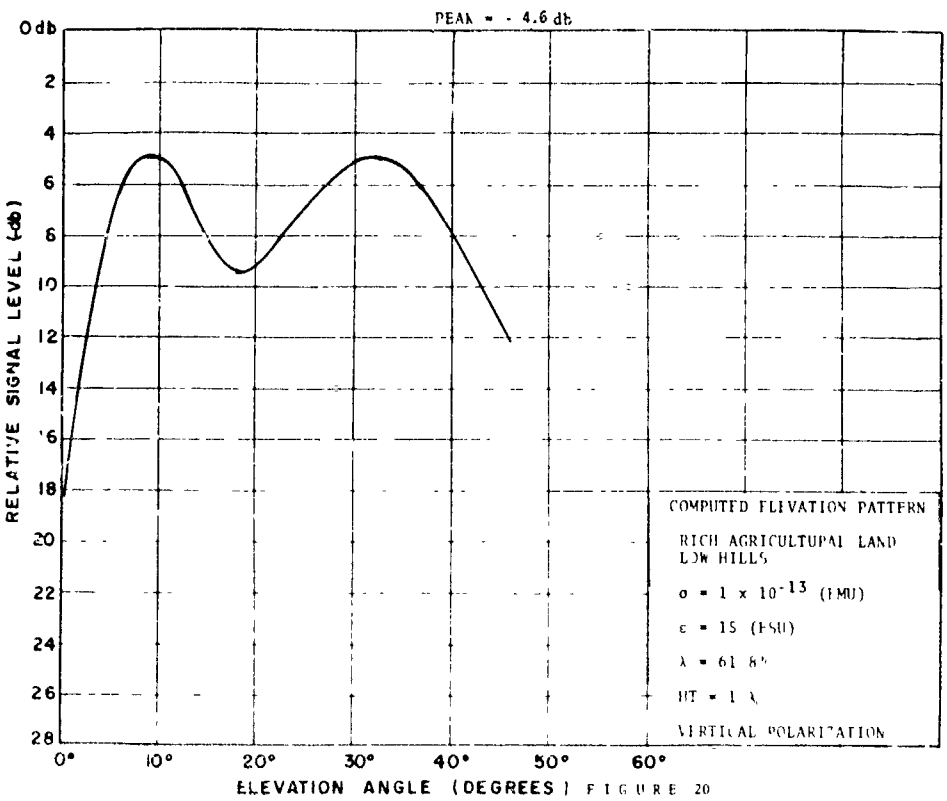

FIGURE 20

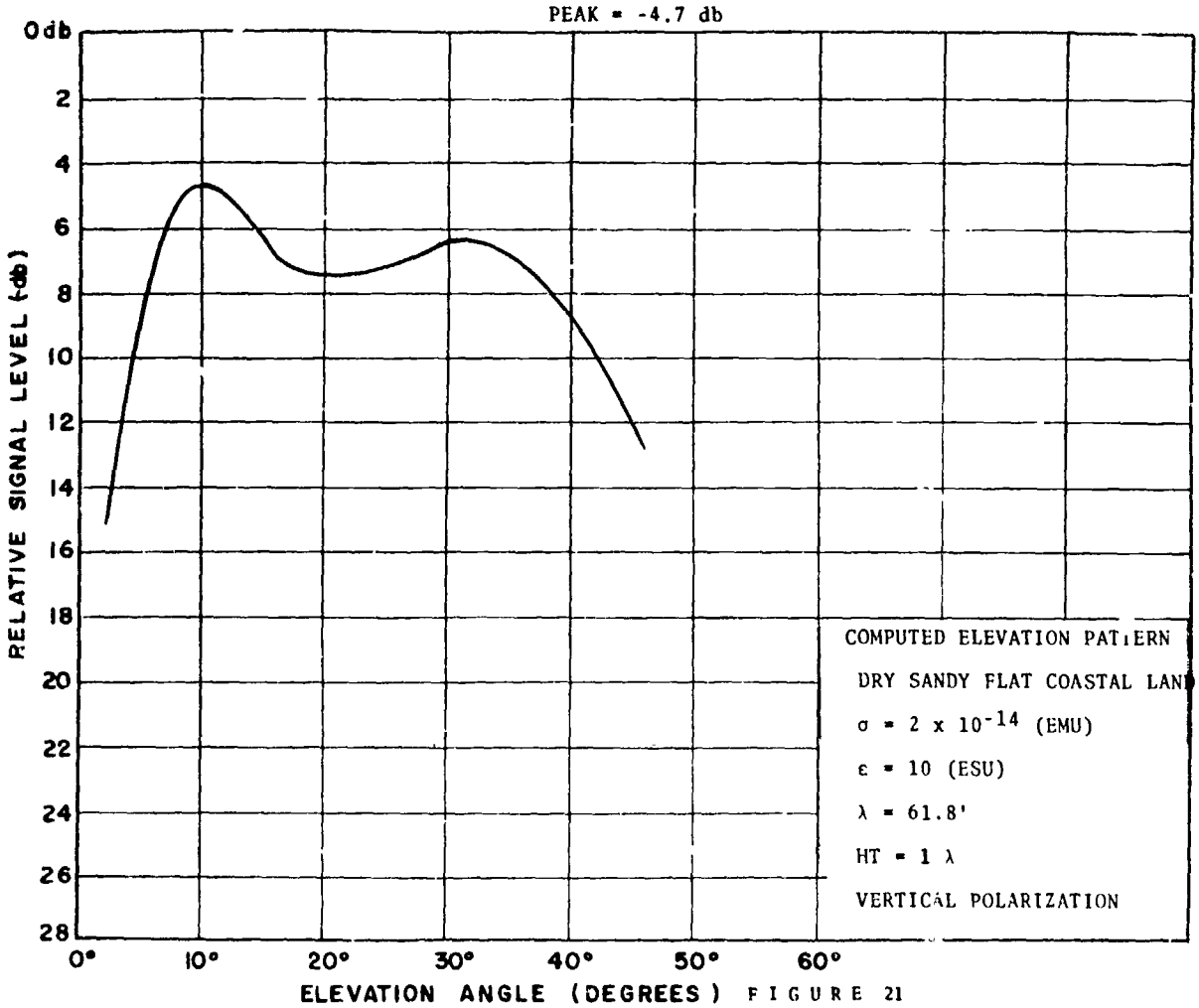

Figure 21

test measurements were made. It will be used, therefore, in direct support of the report objective.

Having analytically established the radiation field of a ground dipole of controlled geometry, which was installed in a site where terrain and ground conductivity were known, the measured energy distribution at the airborne probe was determined by flight tests. The dipole installation, site instrumentation, flight test plan, and overall field measurements are discussed in the following sections.

TABLE II a

Aircraft	Polarization	Frequency	Dipole Free Space (db/iso)	Gain Over Ground (db)	Maximum Combined Gain (db)	Ground Attenuation (db)	Absolute Dipole Gain G_2
C-131#799	Horizontal	15.92	2.15	6.0	8.15	-.5 @ 15°	7.6 dbi
C-131#799	Horizontal	17.99	2.15	6.0	8.15	-.5 @ 14°	7.6 dbi
C-131#799	Horizontal	27.92	2.15	6.0	8.15	-.5 @ 9°	7.6 dbi
C-131#799	Vertical	27.92	2.15	6.0	8.15	-4.4 @ 32°	3.8 dbi

TABLE II b

Aircraft	Polarization	Frequency	Dipole Free Space (db/iso)	Gain Over Ground (db)	Maximum Combined Gain (db)	Ground Attenuation (db)	Absolute Dipole Gain G_2
KC135#125	Horizontal	9.01	2.15	6.0	8.15	-2.2 @ 40°	6.0 dbi
KC135#125	Horizontal	15.92	2.15	6.0	8.15	-2.2 @ 40°	6.0 dbi
KC135#125	Horizontal	17.99	2.15	6.0	8.15	-2.85 @ 40°	5.3 dbi
KC135#125	Horizontal	27.92	2.15	6.0	8.15	-2.26 @ 40°	5.9 dbi
KC135#125	Horizontal	29.2	2.15	6.0	8.15	-.5 @ 15°	7.6 dbi
KC135#125	Vertical	9.01	2.15	6.0	8.15	-4.1 @ 21°	4.0 dbi
KC135#125	Vertical	15.92	2.15	6.0	8.15	-5.8 @ 15°	2.4 dbi
KC135#125	Vertical	17.99	2.15	6.0	8.15	-4.8 @ 16°	3.4 dbi
KC135#125	Vertical	27.92	2.15	6.0	8.15	-5.7 @ 18°	2.5 dbi
KC135#125	Vertical	29.2	2.15	6.0	8.15	-4.8 @ 10°	3.4 dbi

SECTION III

INSTRUMENTATION

Horizontal and Vertically Polarized half-wave dipoles were fabricated and installed at RADC's Verona Test Annex. Table III lists those specific frequencies and corresponding element half-wave lengths for which the dipoles were fabricated.

Table III

FREQUENCY (MHz)	HALF-WAVE LENGTH (Feet)
9.0	54.5
15.9	30.9
18.0	27.3
27.9	17.6
29.2	16 8

As shown in Figure 22A, the horizontal dipole was supported on two 60-foot wooden poles. A simple pulley arrangement permitted the dipole height to be altered as desired. Similarly, the vertical dipole, as shown in Figure 22B, was supported on two 60-foot wooden poles and used the same pulley arrangement for antenna height adjustment.

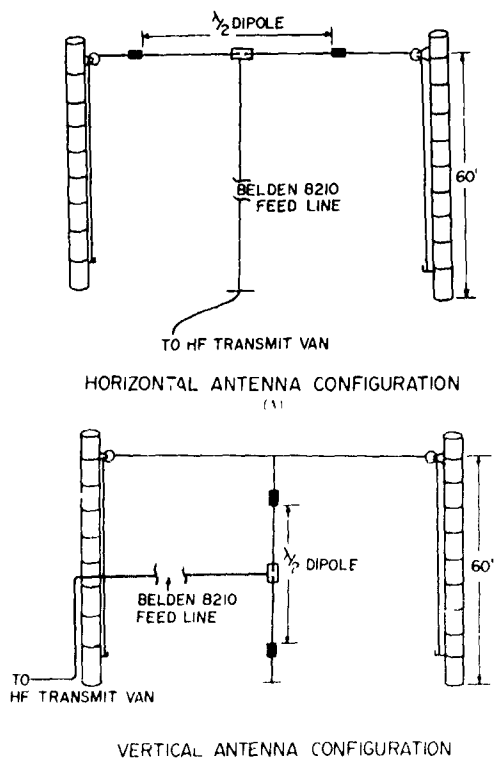

Figure 22

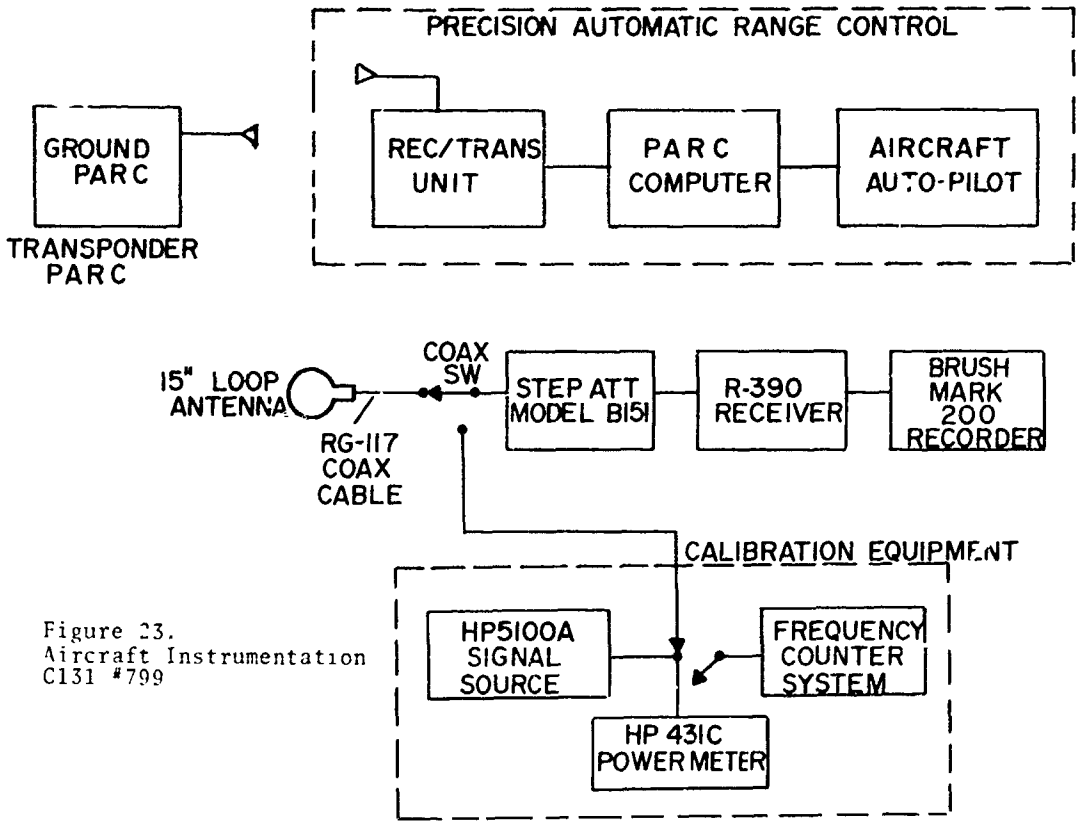

Figure 23.
Aircraft Instrumentation
C131 #799

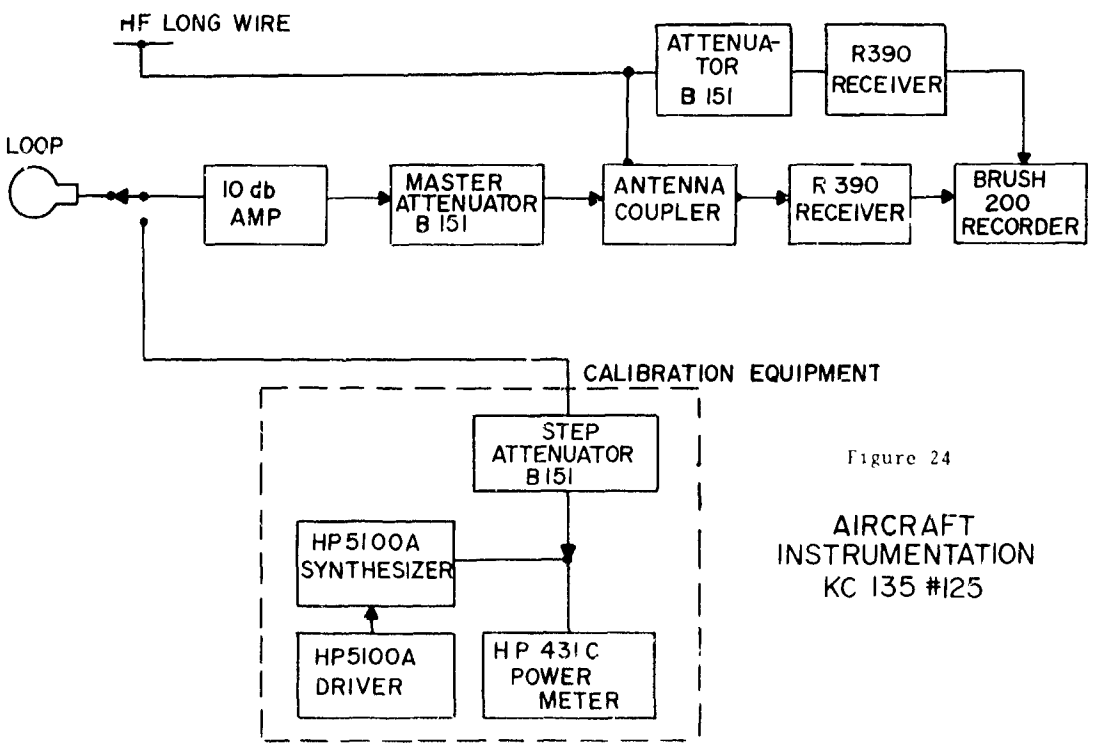

Figure 24

AIRCRAFT INSTRUMENTATION KC 135 #125

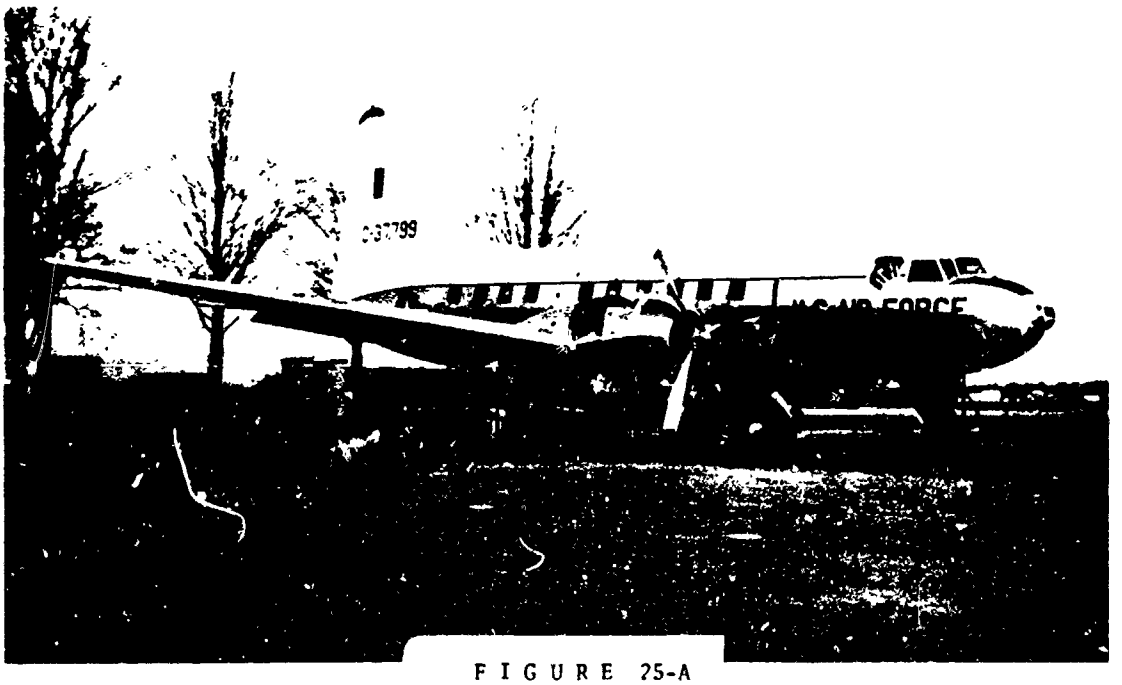

FIGURE 25-A

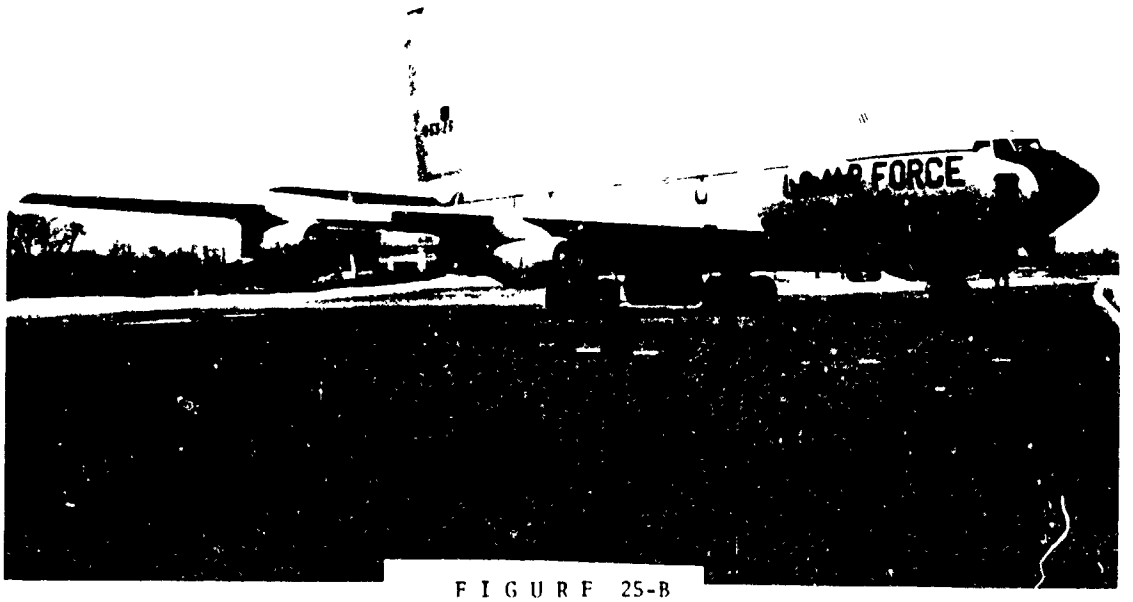

FIGURE 25-B

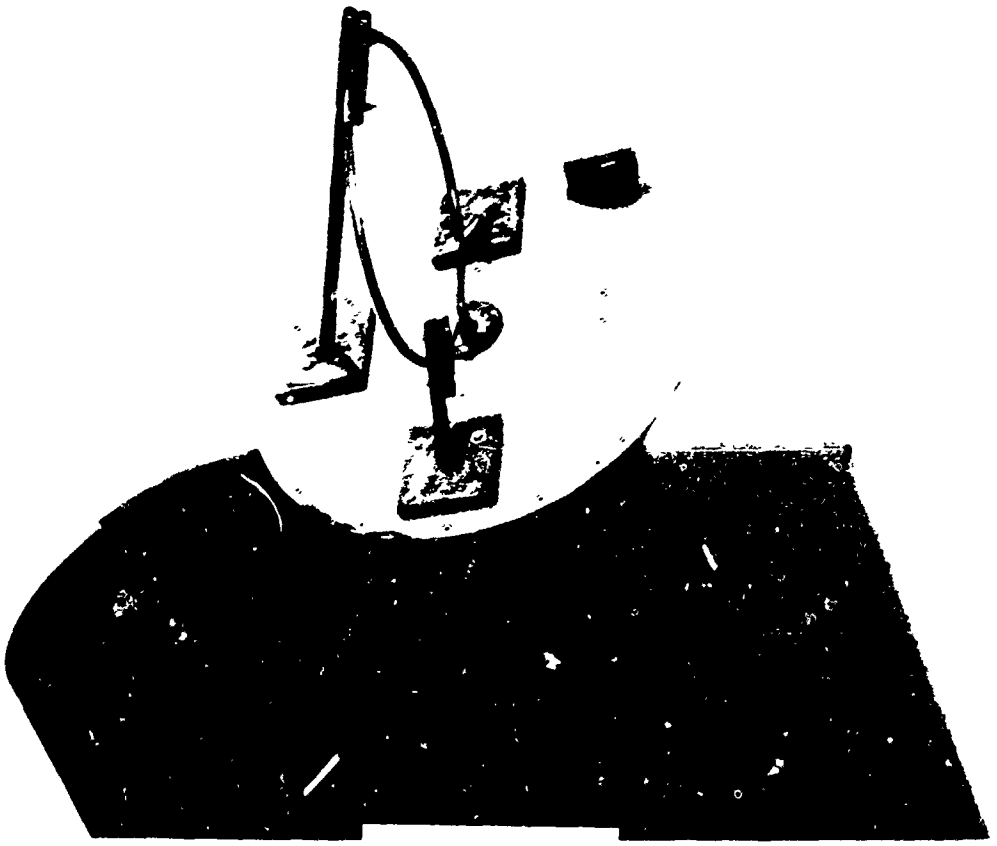

FIGURE 26-A

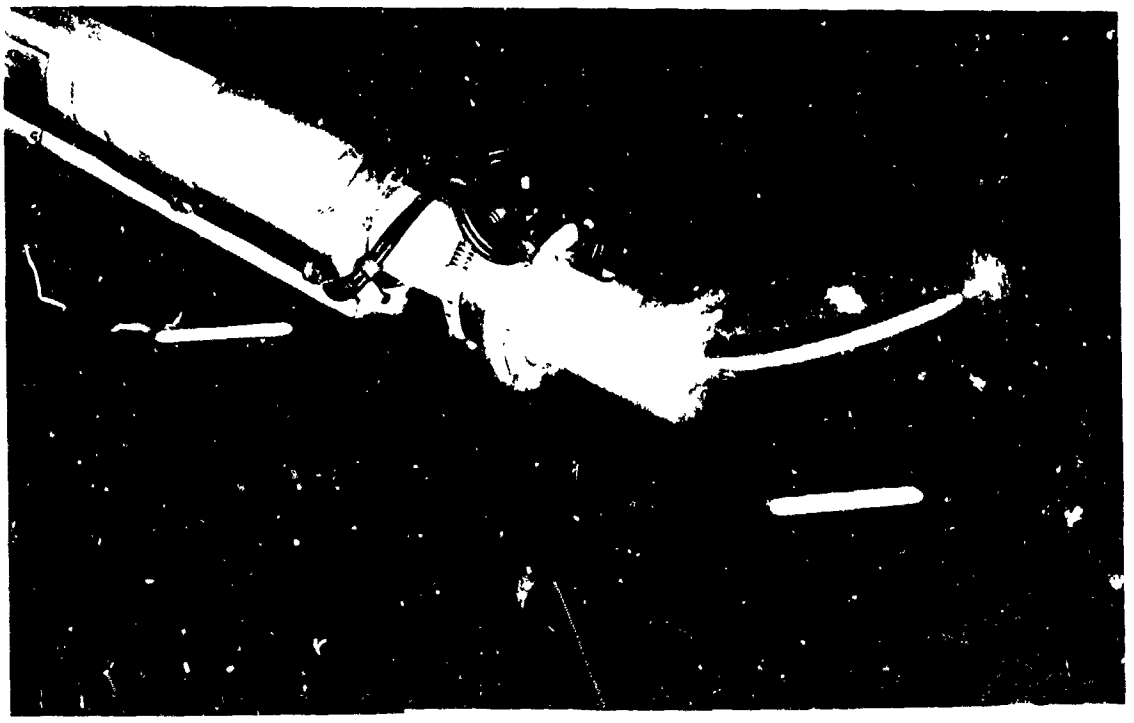

FIGURE 26-B

Figures 23 and 24 are block diagrams of the aircraft instrumentation for the C-131 and KC-135 aircraft, respectively. Stepped calibration curves were made before and after each set of vertical coverage pattern data at each of the operating frequencies. These comparative curves did not vary more than 0.5 dB throughout the tests. As a transmitting source, the signal generator was set on frequency and the receiver was tuned for maximum recorder deflection. A reference was then set using the built-in attenuator of the signal generator. External attenuation was inserted using the variable step attenuators to select the dynamic range of the recording chart. The receiver and recorder combination was thus calibrated. In the reduction of all data, use was made of the calibration charts, since linearity was not assumed to exist throughout the dynamic range of the receiving equipment.

Figures 25-A and 25-B are photographs of the C-131 and KC-135 aircraft used throughout the flight test measurements. Figures 26-A and 26-B are closeups of the two receiving loop antennas used on the C-131 and KC-135 aircraft, respectively. Figure 27 is a diagram of the ground transmitting equipment configuration. A Collins KWT 6/5 transceiver was used as the HF transmitting signal source. Throughout the flight tests, a ground log was maintained of the forward and reflected signal levels of the transmitter output. The output of the KWT 6/5 was fed to a Coupler Monitor CU-737/URC. This coupler arrangement allowed the reflected power to be maintained at less than four percent across the entire operating band, which corresponds to a reduction in transmitted signal level of approximately .3 dB. The radiated power was monitored during the flight tests and any change in power level was noted. The radiated power was maintained within ± .3 dB across the operating band.

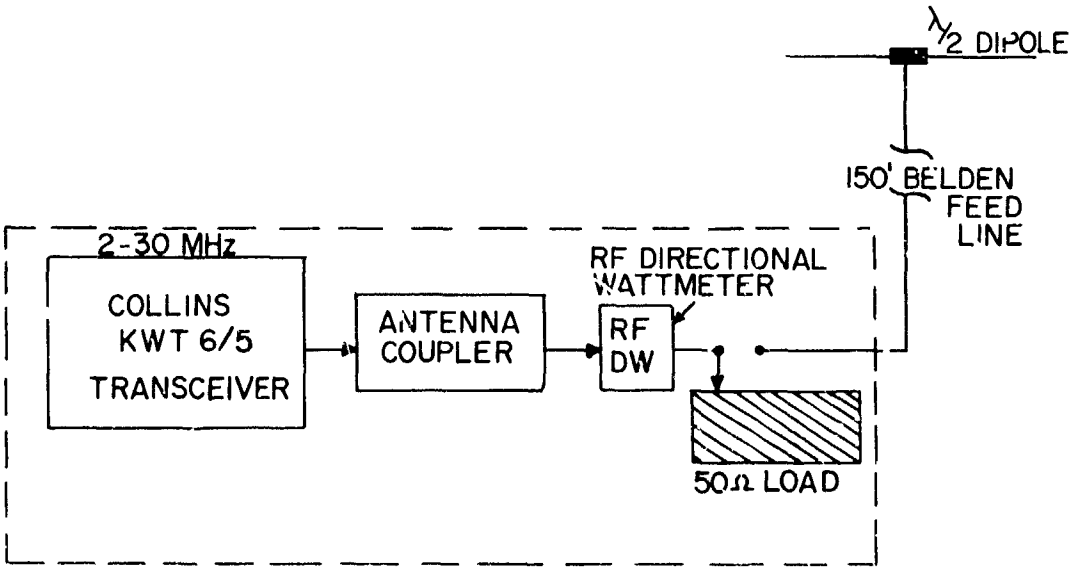

Figure 27. Verona Transmitting Ground Station

SECTION IV

FLIGHT TEST PLAN

A. Orbital Flights with C-131 Aircraft

Figure 28 shows the field setup at the Verona Test Site. Along a flight path parallel to the dipole axis and at a slant range of five nautical miles, the absolute signal levels at several elevation angles boresight to the dipole were measured. To generate the vertical profile of the unit, i.e., the aircraft with its antennas, it was essential that the attitude of the aircraft remain level at all elevation angles of interest. Throughout the flight tests attitude instruments were periodically monitored by the pilot to assure that a level attitude was maintained. In the absence of severe variations in the received signal level and the periodic monitoring of pertinent attitude instruments, the aircraft stability was maintained within $\pm 2^{\circ}$. It was estimated that a roll of this magnitude would vary the received signal level by approximately .2 dB. To insure that a flight path parallel to the dipole axis was maintained, an S-band tracking radar, Close Support Control Set AN/MSQ-1A, was employed. Prior to each day's measurements, the scheduled flight paths for successive elevation angles were preplotted by the AN/MSQ-1A operator for a coverage sector of $\pm 30^{\circ}$ either side of boresight, as shown in Figure 28. The plots were then used as a reference guide by the AN/MSQ-1A operator to control and maintain the aircraft's flight along those paths. Reruns were made of all flights in which the pilot experienced any effects such as turbulence and/or gusting which might have altered the aircraft's heading and/or attitude. After each pass, the AN/MSQ-1A plots were examined to assure that deviations from the desired flight path were no greater than $\pm 2^{\circ}$ in elevation angle.

The AN/MSQ-1A van and the HF van communicated by wire to relay aircraft range and heading information to the pattern recorder operator. A triggering device incorporated into the recorder permitted the aircraft's aximuthal heading relative to the dipole boresight to be incrementally strobed onto the recorded pattern. The Precision Automatic Range Control System (PARC) was used to keep the aircraft in a constant orbit. Combined use of the AN/MSQ-1A and the PARC system provided an excellent cross check on the aircraft's exact range. This range information was appropriately recorded on each of the measured patterns. In the reduction of all pattern data appropriate compensation was made for departure of the aircraft from the desired five nautical mile slant range off boresight.

Figure 29 is a detailed diagram of the orbital flight plan.

PRECEDING PAGE BLANK

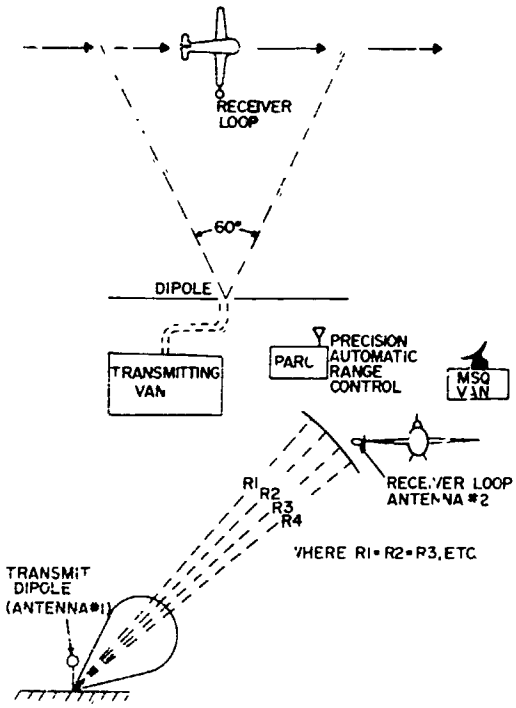

ORBITAL FLIGHT PLAN C131 #799

Figure 28. Orbital Flight Plan C131 #799

Detailed Flight for C 131 Aircraft

A Spiraling C-K Orbits. Data taken between 210° and 270°. Remainder of orbit used to change altitude

B Elevation Angles overage [illegible]

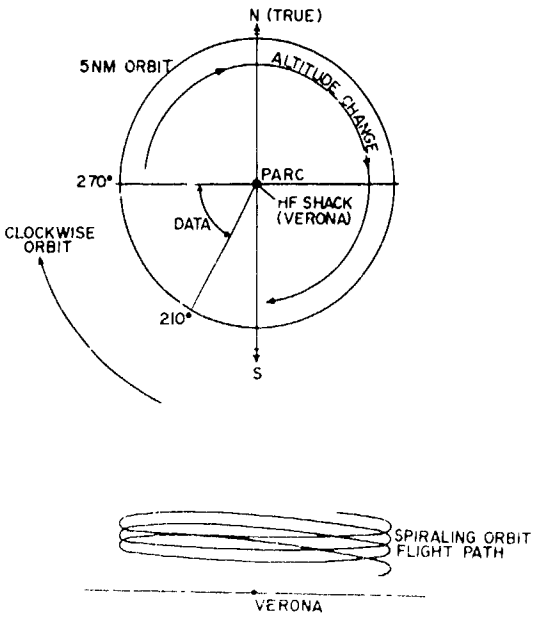

Figure 29

B. Radial Flights with KC-135 aircraft

Figure 30 shows the field setup used at the Verona Test Site to perform the radial flight test measurements required in the calibration of the KC-135 aircraft and its associated loop antenna as a single calibrated unit. Sixty nautical mile radials, originating at Verona, were flown along an outbound heading of 240° (true) at an altitude of 29,000 feet, MSL. Initial bearing was established by the Verona TACAN. To ensure that this bearing was maintained, an S-band tracking radar, the AN/MSQ-1A was employed. Prior to each day's measurements, the scheduled flight path, as shown in Figure 30, was preplotted and used as a reference guide by the AN/MSQ-1A operator to control and maintain the aircraft's flight along those paths. After each radial, the AN/MSQ-1A plots were examined to assure that deviations from the desired flight path were no greater than ± 1° in azimuth.

The AN/MSQ-1A van and the HF van communicated by wire to relay aircraft range and heading information to the pattern recorder operator A triggering device incorporated into the recorder permitted the aircraft's range relative to the dipole to be incrementally strobed onto the recorder pattern. Range data was recorded in five NM increments on each of the measured patterns. In the reduction of all radial measurements, the test data was normalized to 5.0 NM slant range.

Figure 31 is a detailed diagram of the radial flight plan.

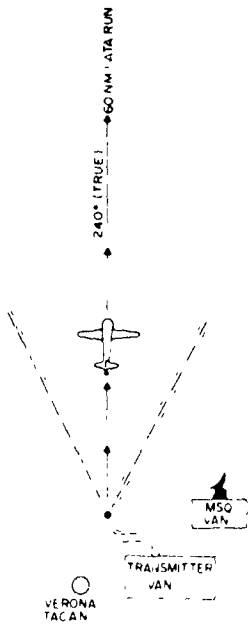

Figure 30
Flight Plan, KC-135 #125 Radials

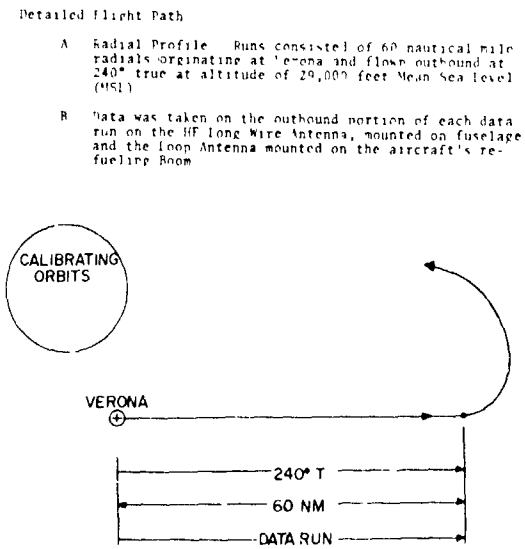

Figure 31
Flight Plan, KC-135 #125

SECTION V

DATA ANALYSIS AND EVALUATION

Measured flight test data is shown in Figures 32 through 45. The data is shown as a plot of relative signal level as a function of elevation angle for the conditions specified in the legends.

To more clearly evaluate the computed data of Figures 1 through 14 and the measured data of Figures 32 through 45, the composite plots shown in Figures 46 through 59 were prepared. Before discussing these composite patterns, the rationale used for plotting them as shown will be discussed. For the case of horizontal polarization, if the pattern of the airborne probe were cosine in distribution, as shown in Figure 60-A, then the comparative pattern data should differ as a function of the cosine. This factor was taken into account when preparing the composites by vertically displacing the measured data to provide a "best fit" between the measured and computed data which most closely followed the cosine variation.

Correspondingly for the case of vertical polarization, as shown in Figure 60-B, the airborne probe has an isotropic distribution over the 0 to 90° sector shown. If this isotropic distribution truly existed, then the measured and computed pattern data should be precisely coincident. Therefore, for the case of vertical polarization, the measured pattern was vertically displaced to provide composite patterns which were most coincident over those elevation angles for which measured data was taken.

PRECEDING PAGE BLANK

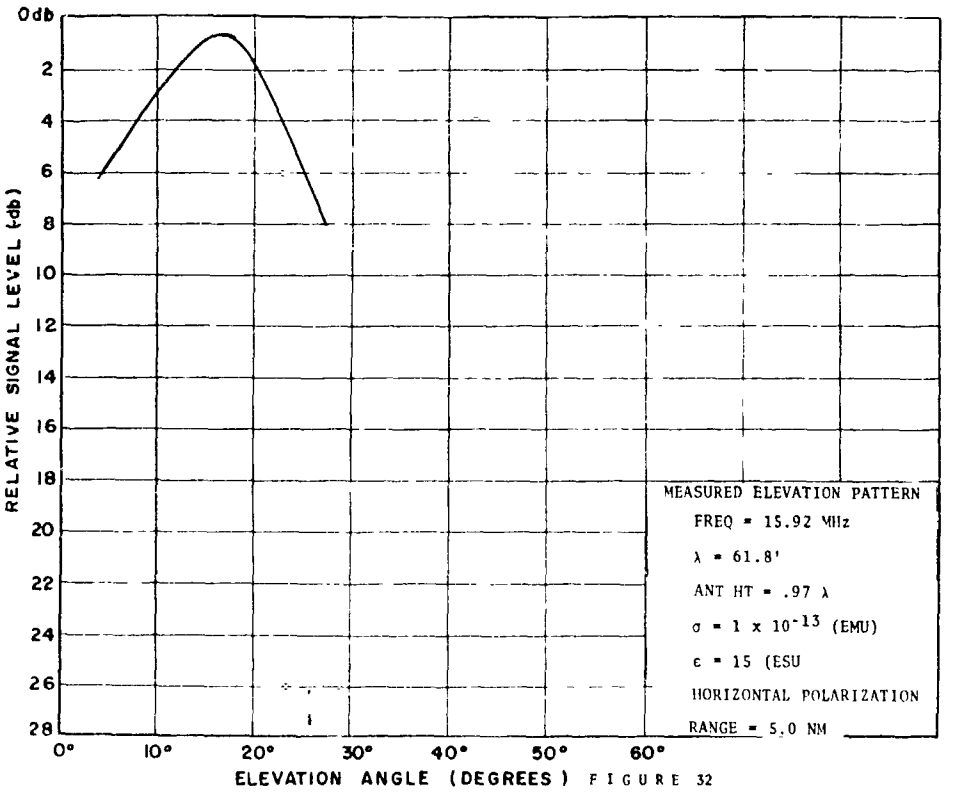

FIGURE 32

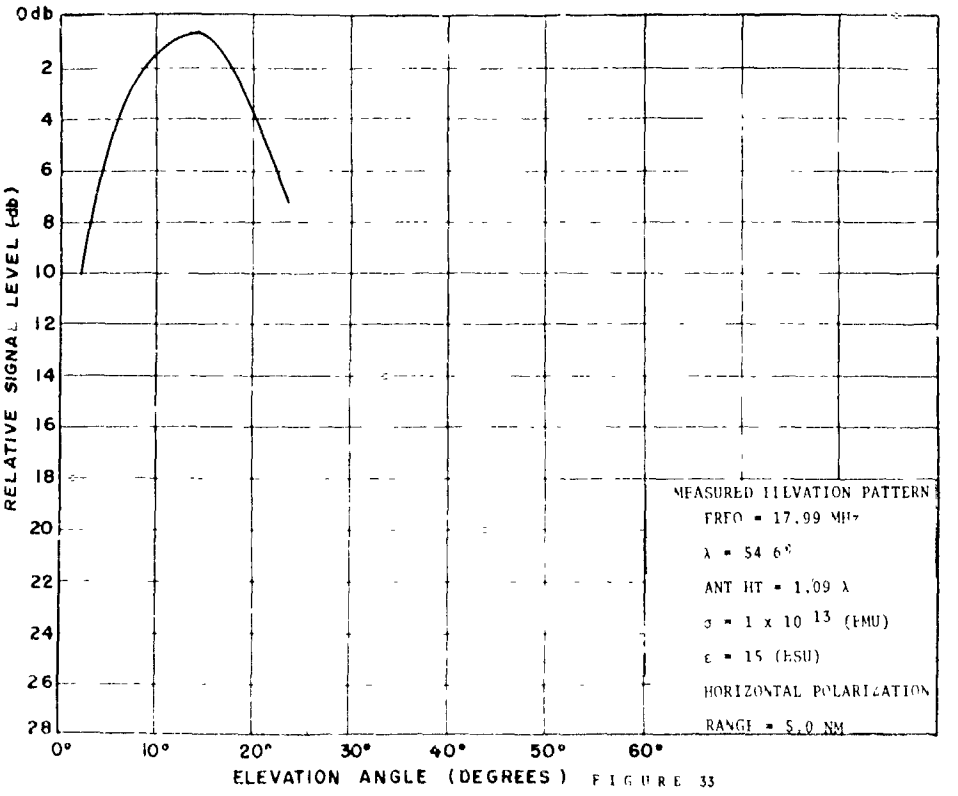

FIGURE 33

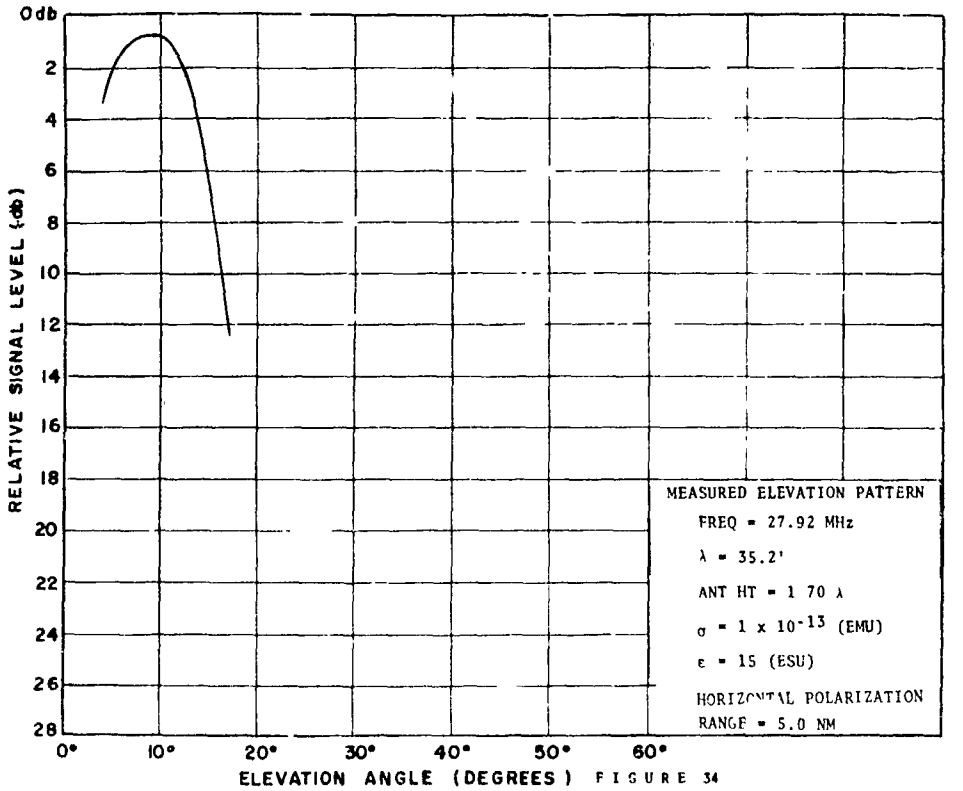

FIGURE 34

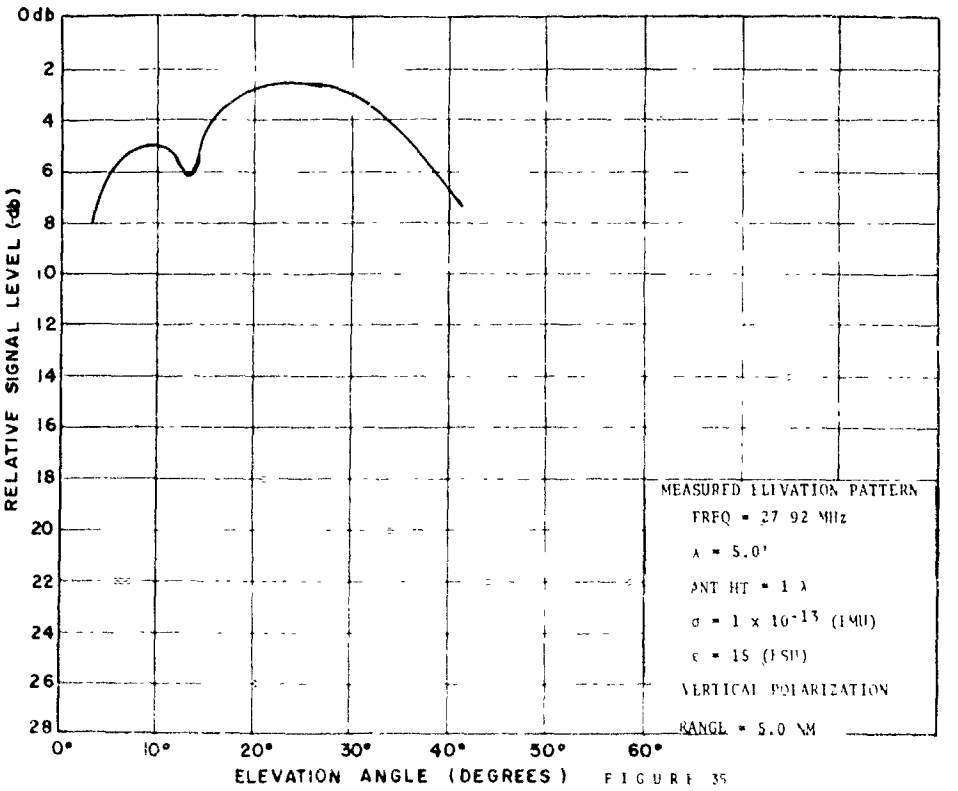

FIGURE 35

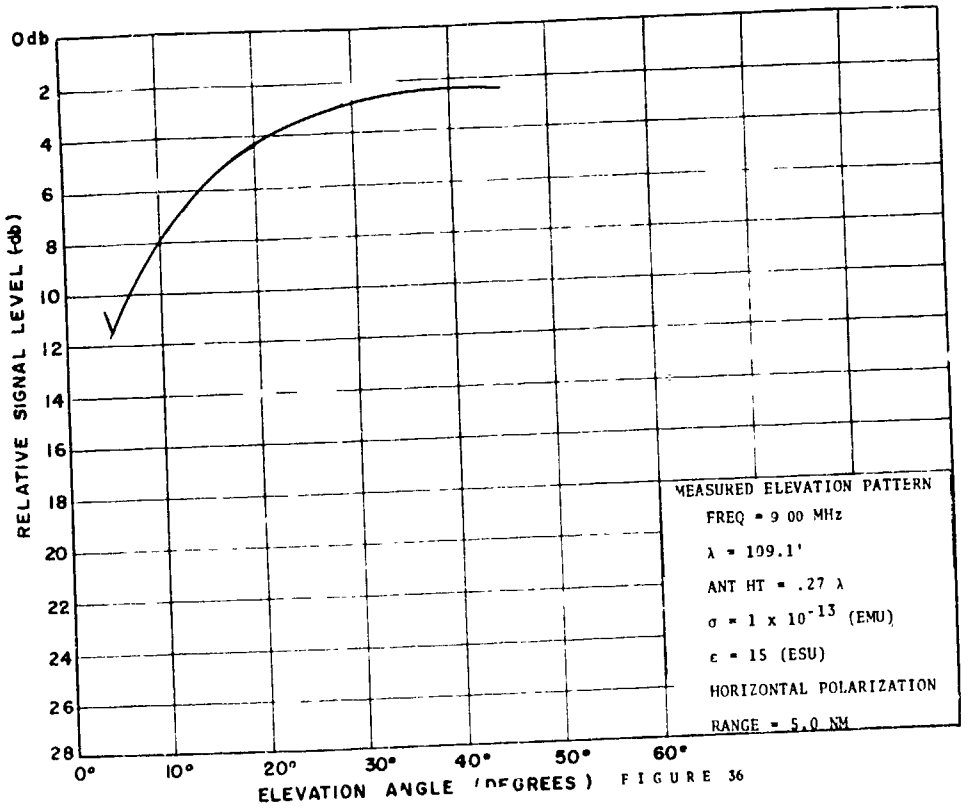

FIGURE 36

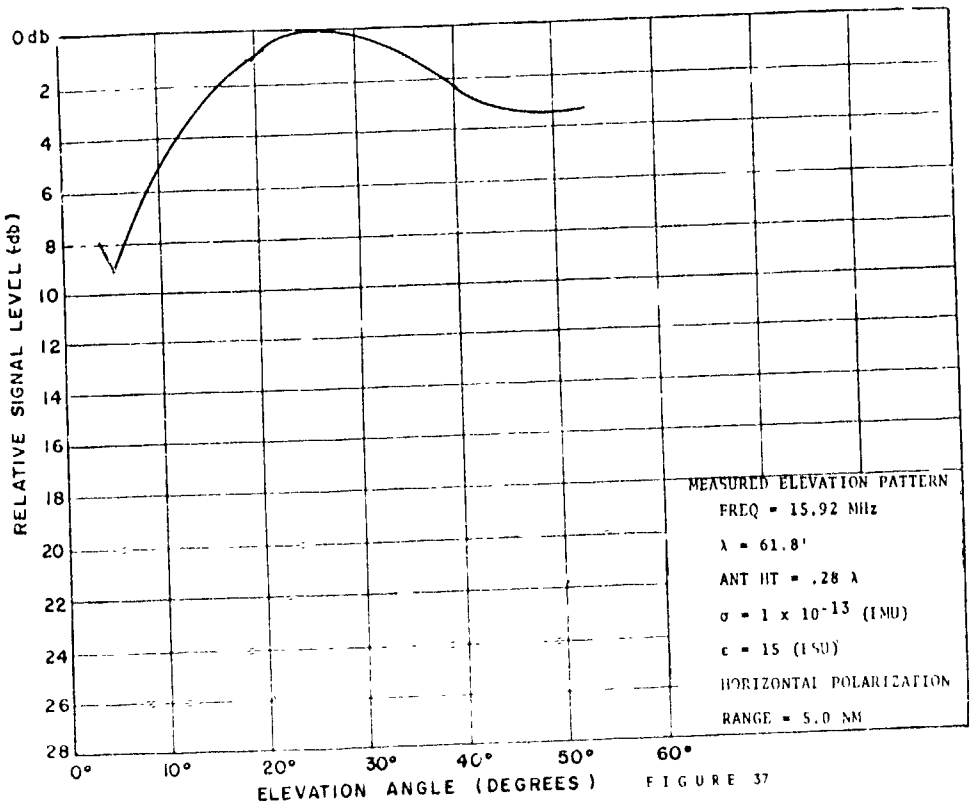

FIGURE 37

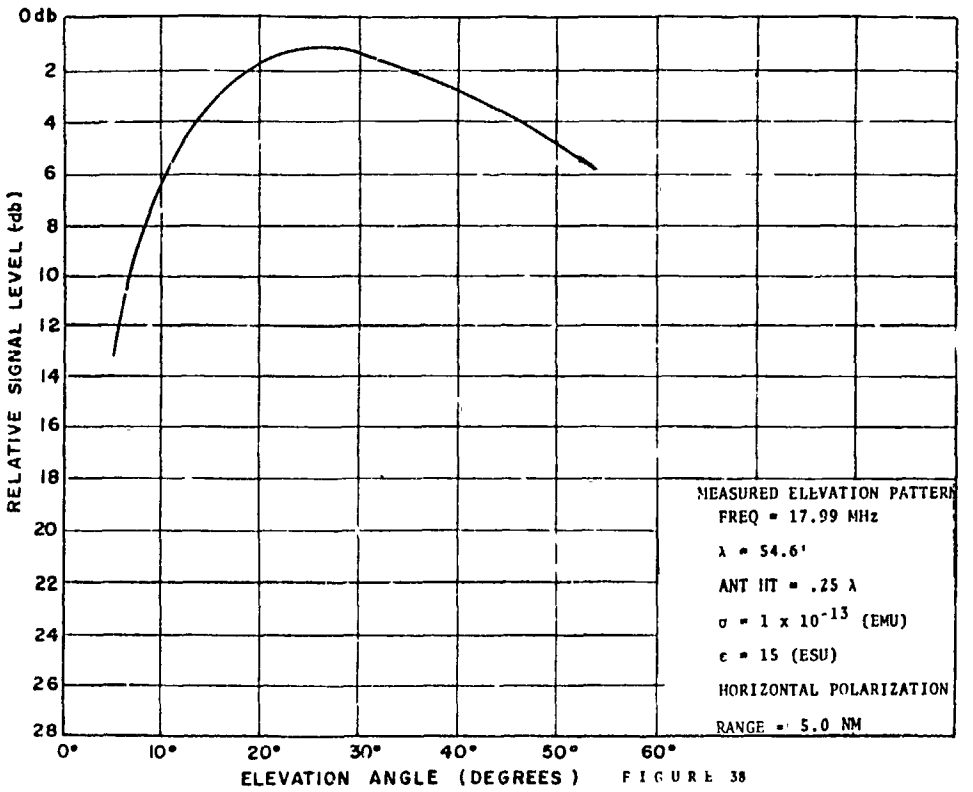

FIGURE 38

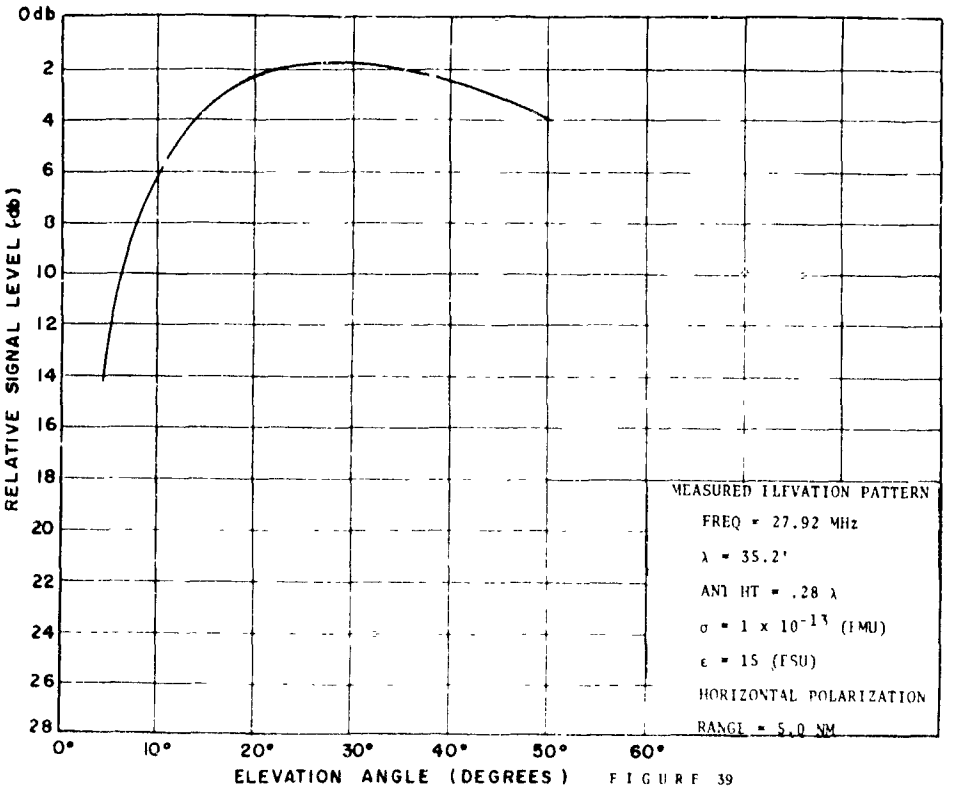

FIGURE 39

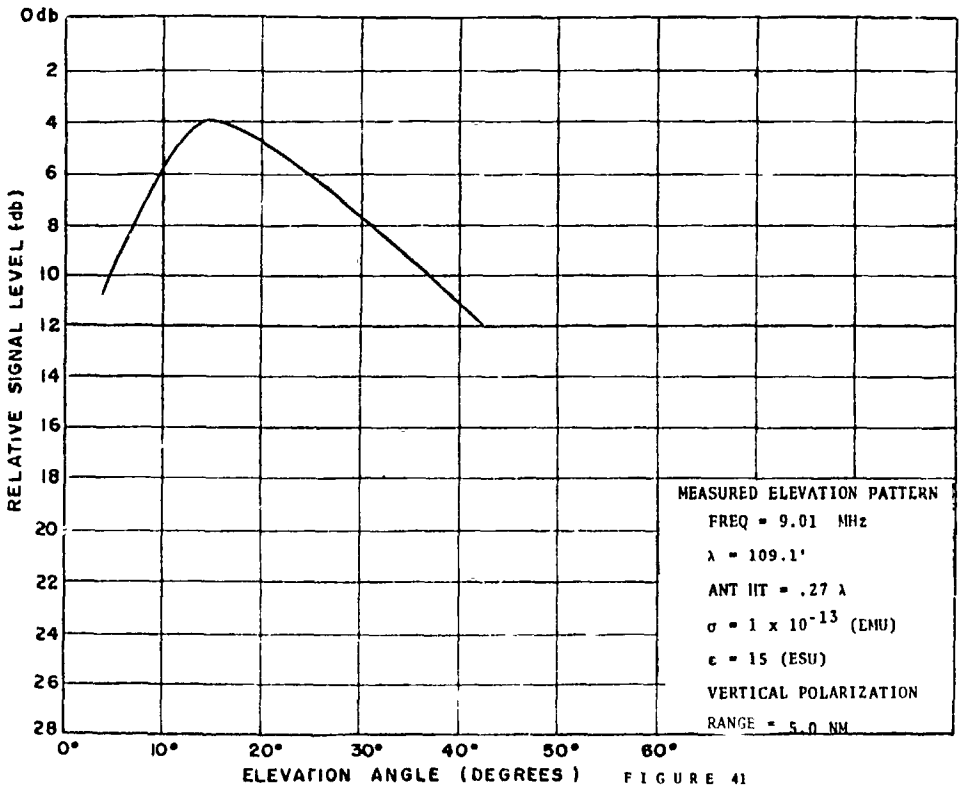

FIGURE 41

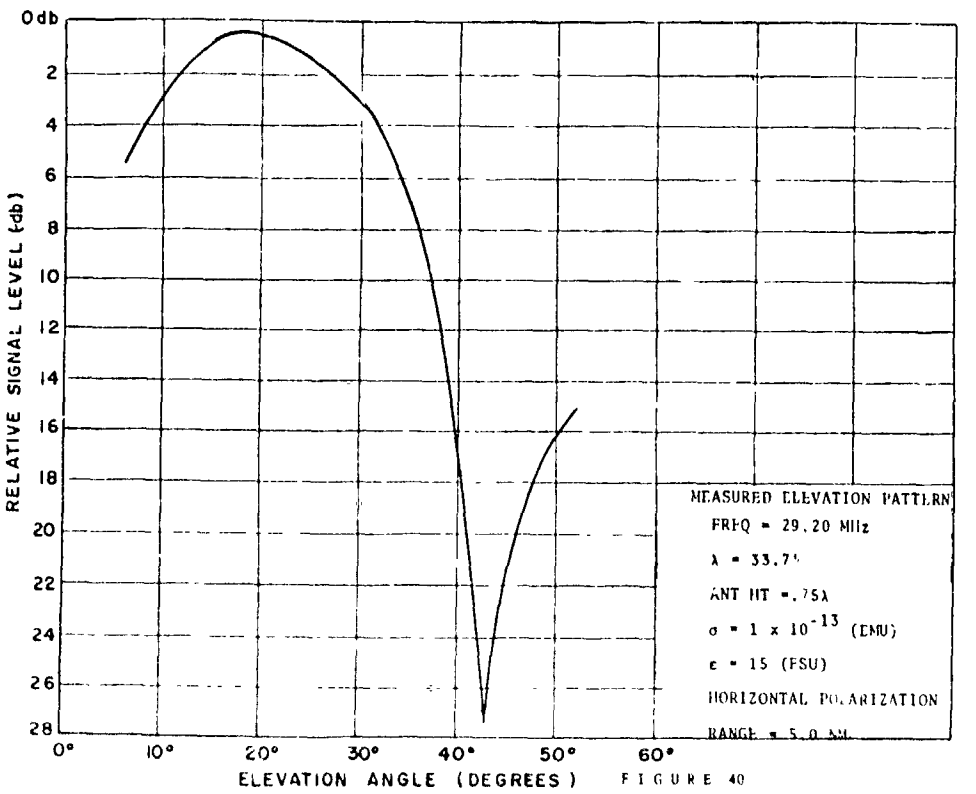

FIGURE 40

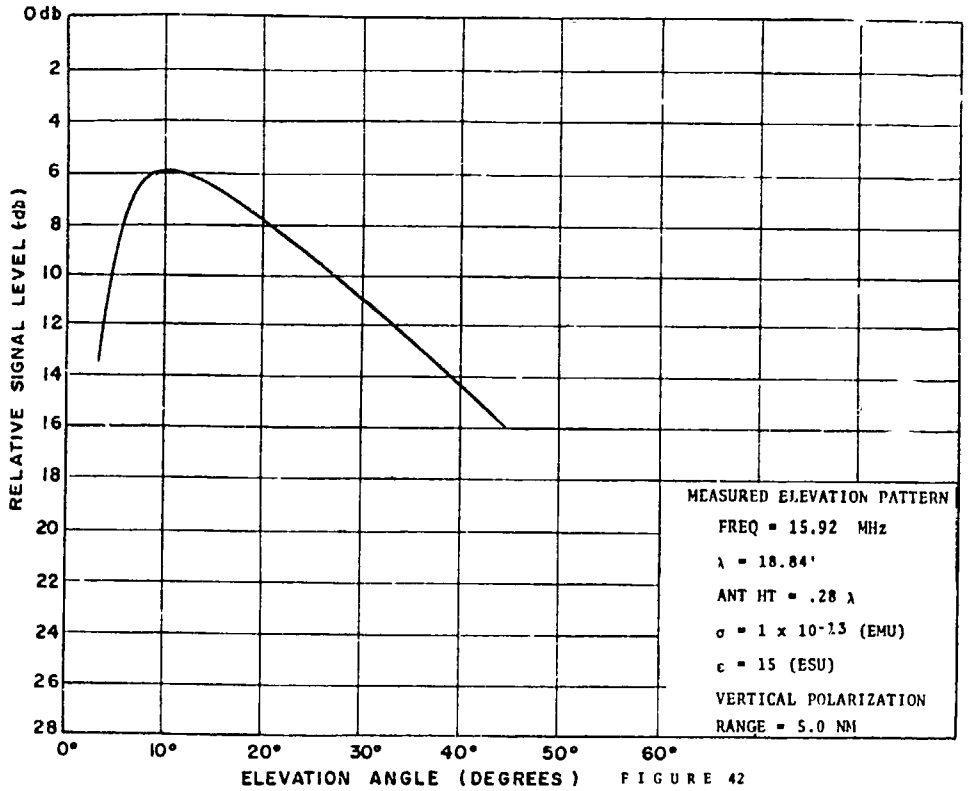

FIGURE 42

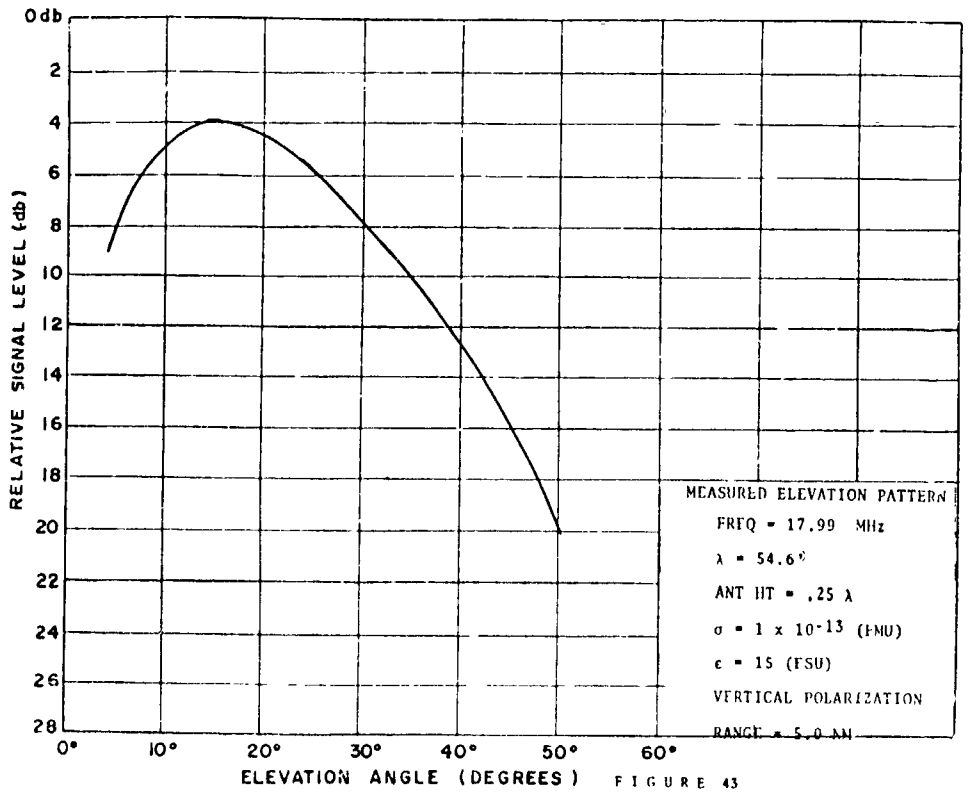

FIGURE 43

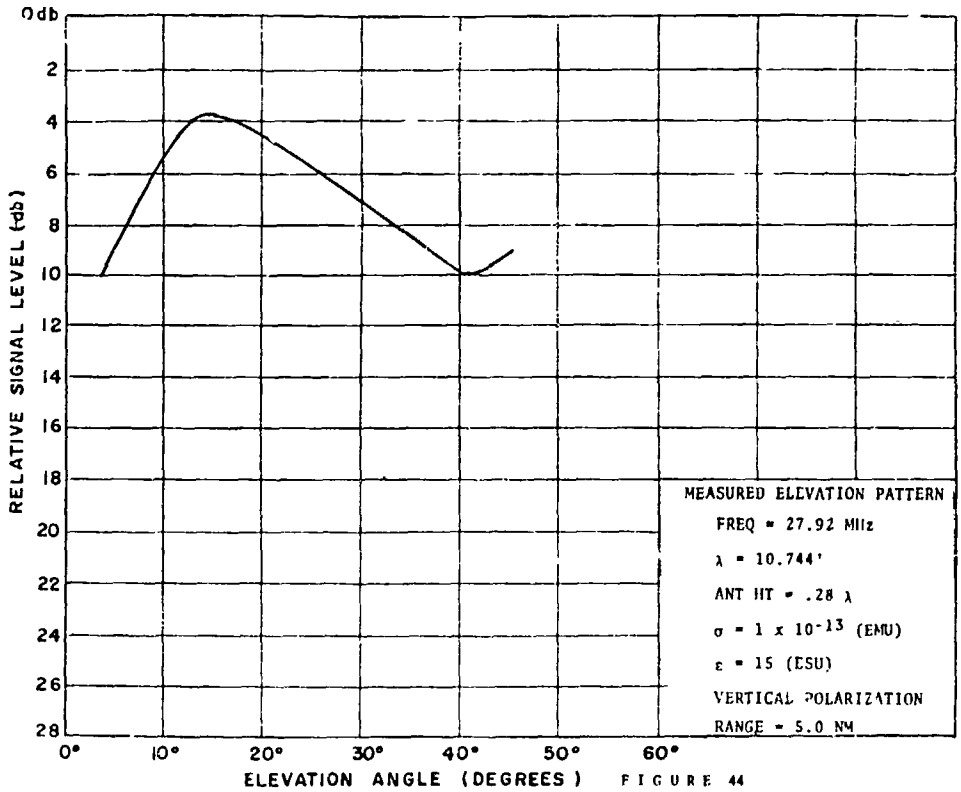

FIGURE 44

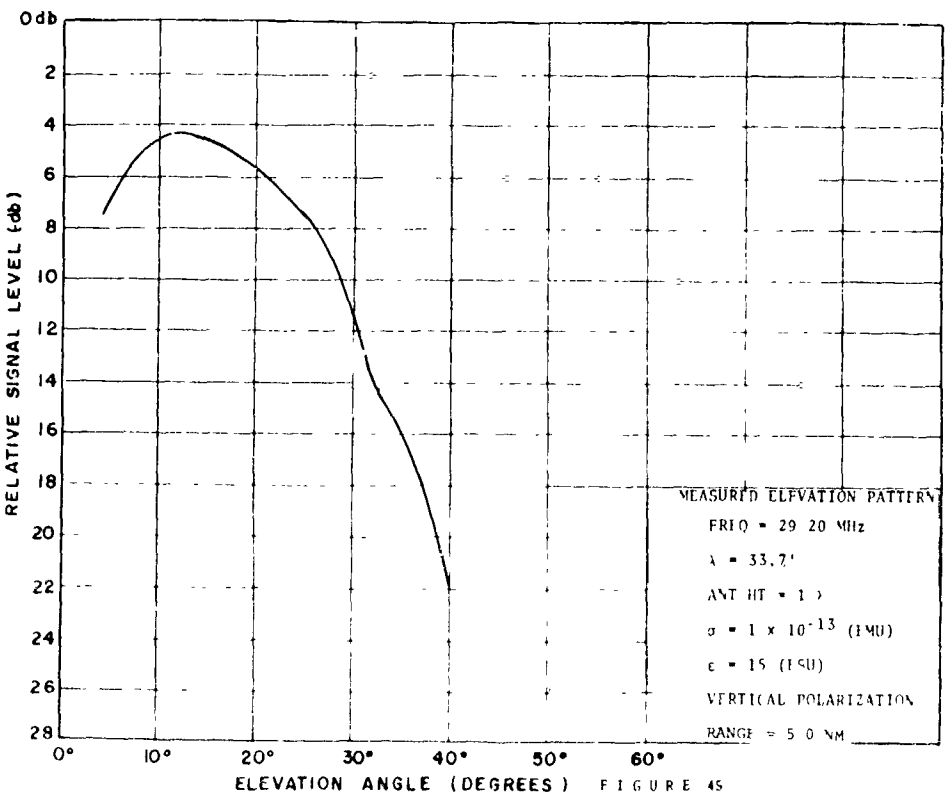

FIGURE 45

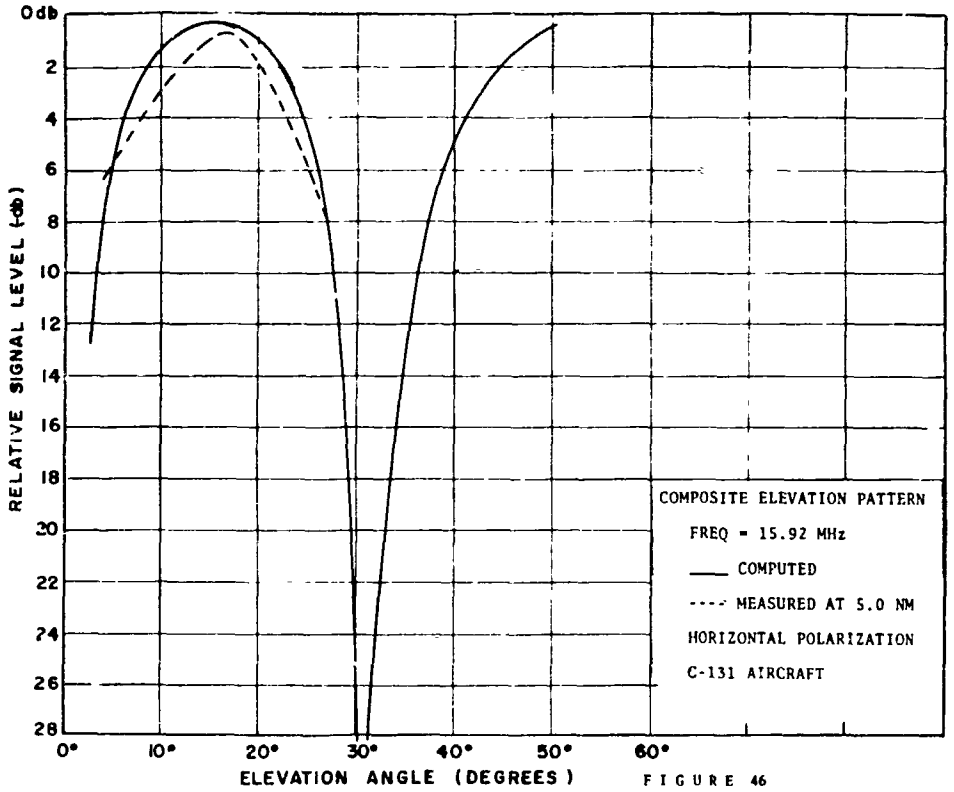

FIGURE 46

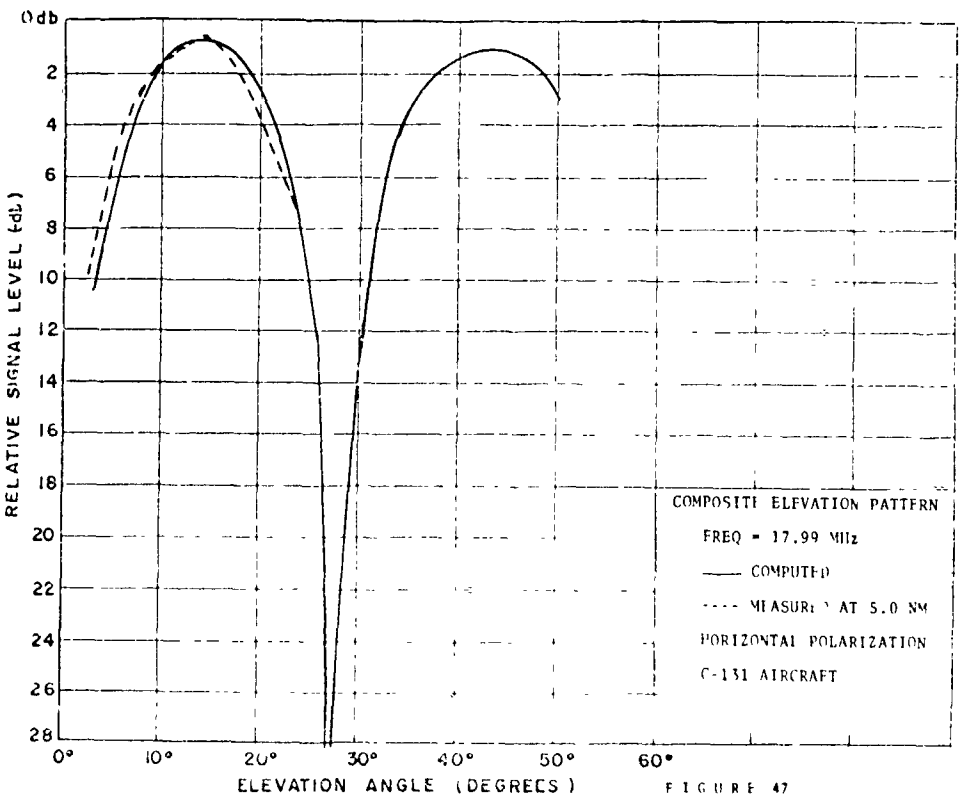

FIGURE 47

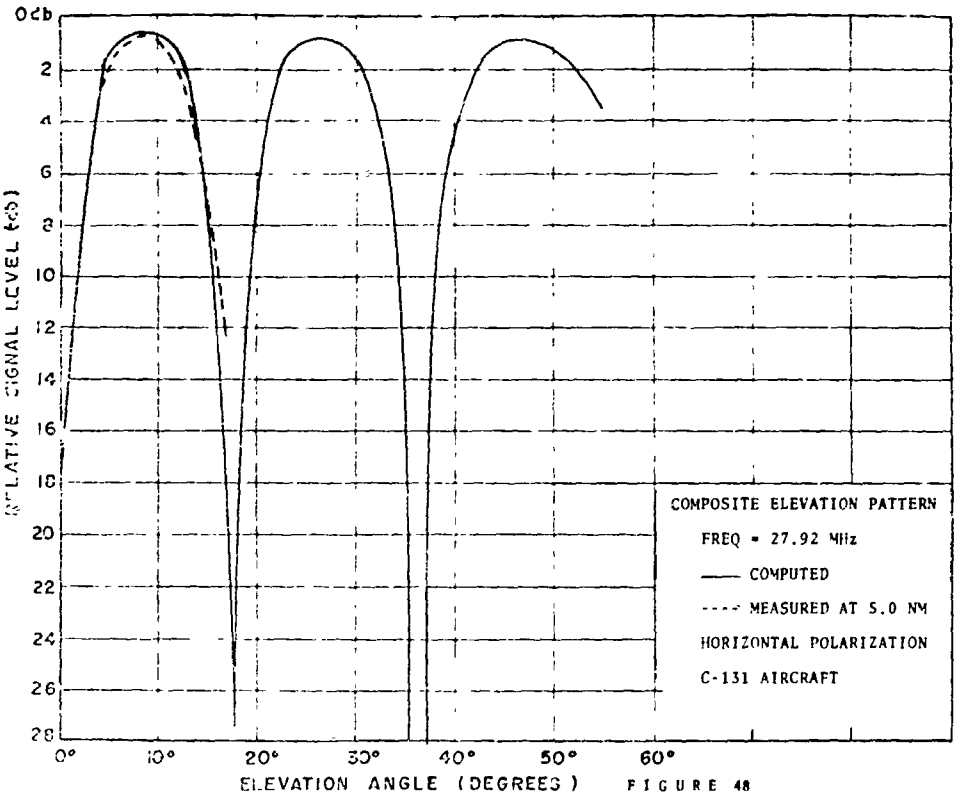

FIGURE 48

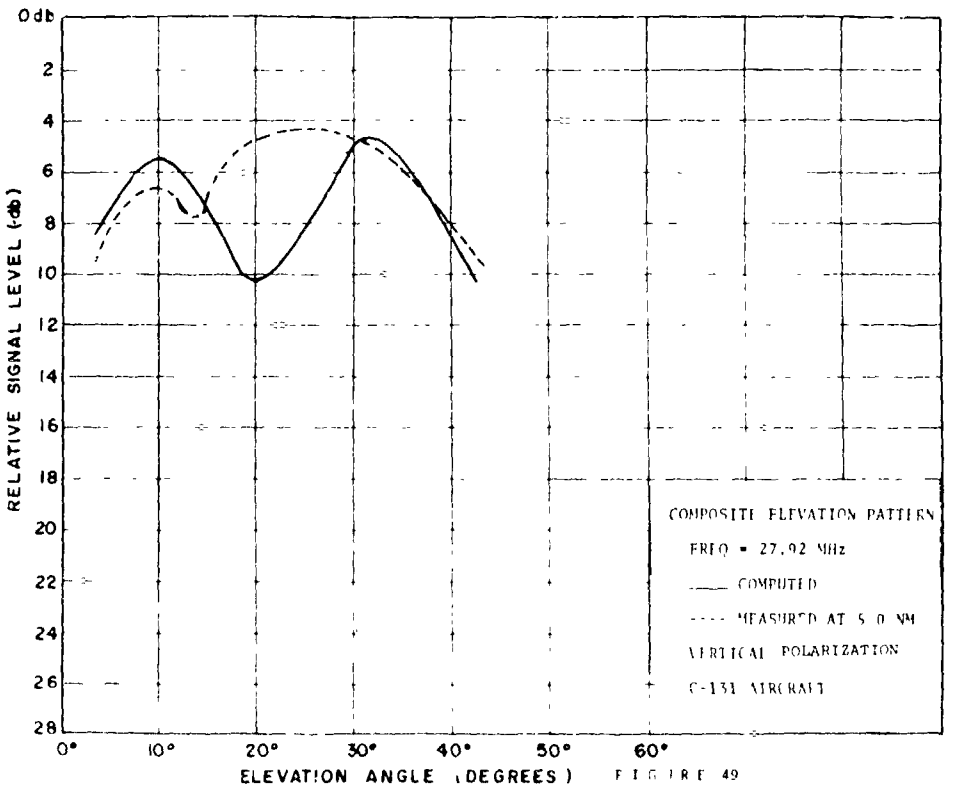

FIGURE 49

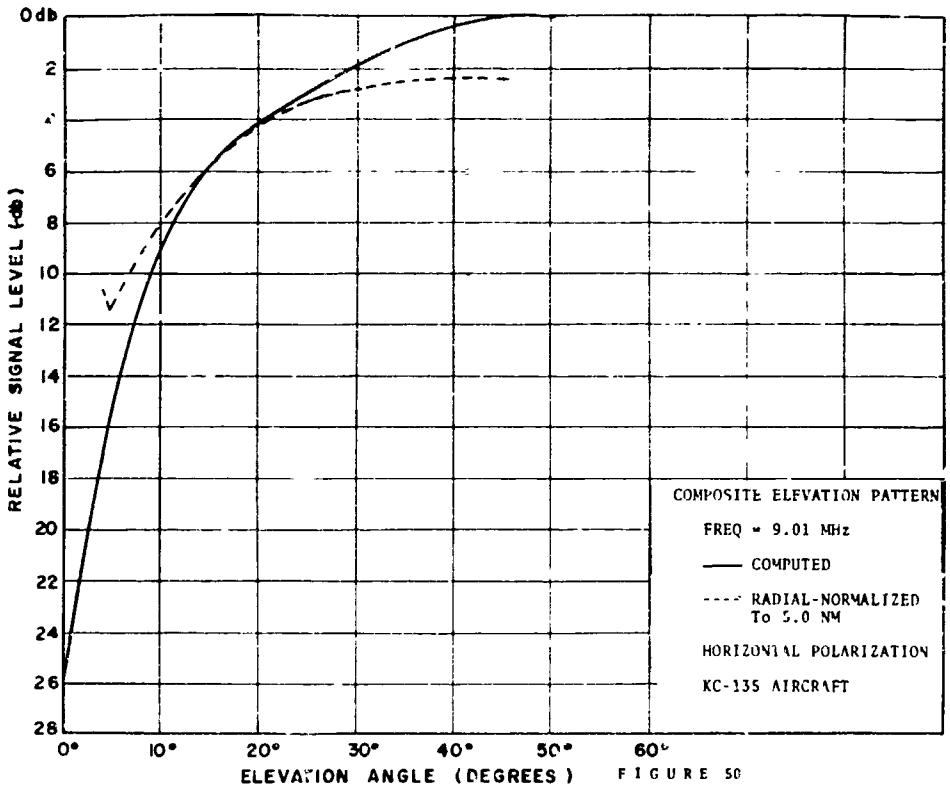

FIGURE 50

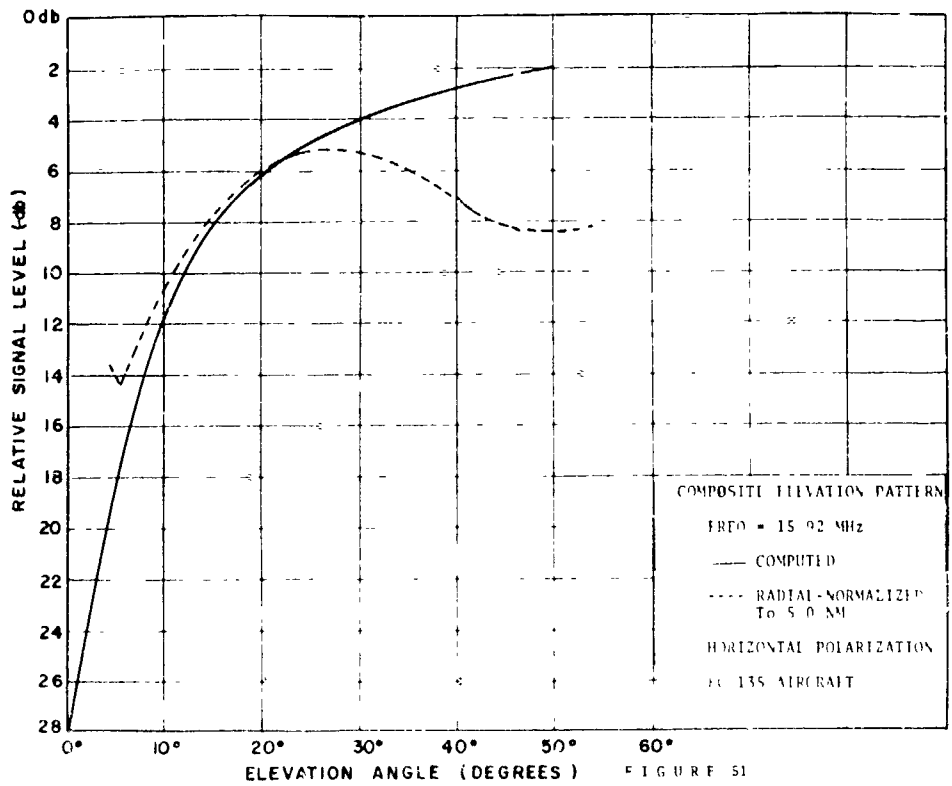

FIGURE 51

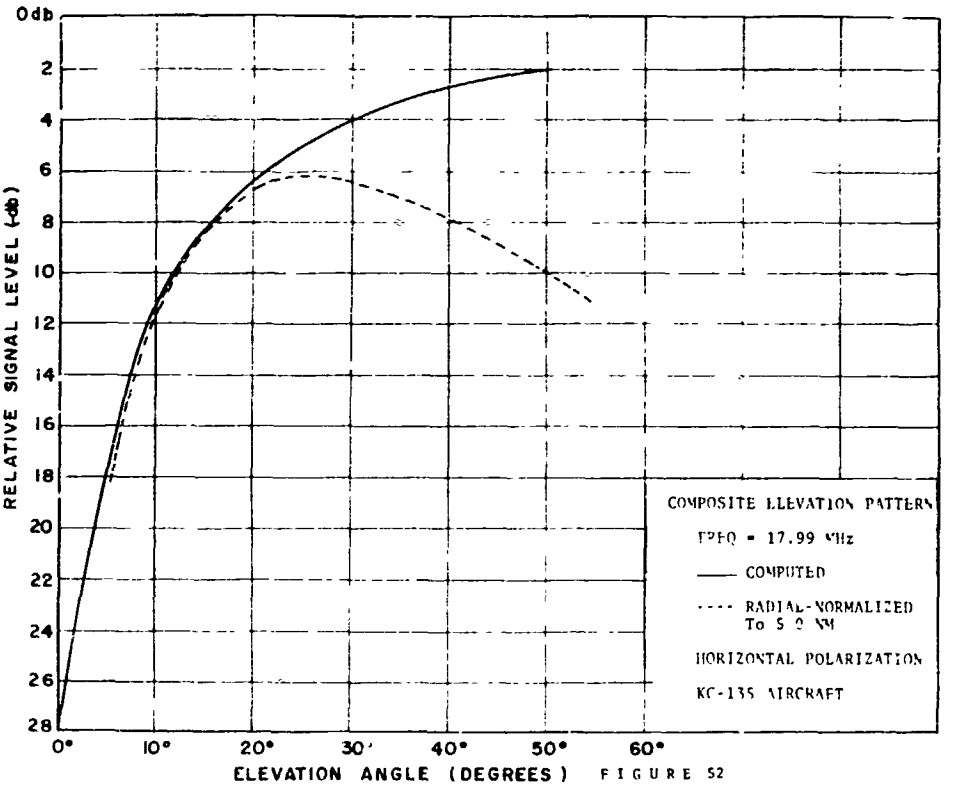

FIGURE 52

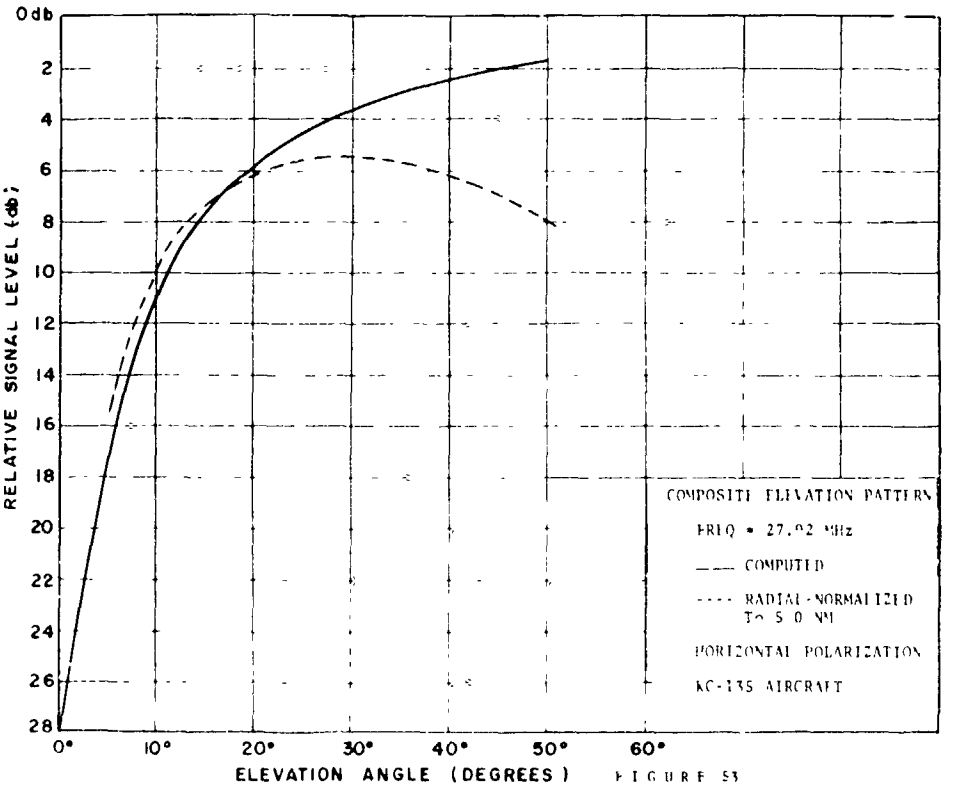

FIGURE 53

Examination of Figures 46 through 48 and 50 through 53, all of which are for horizontal polarization, reveal variations between the measured and computed data which do not differ at all angles by the cosine of the angle PSI (ψ), Figure 60-A. Correspondingly, the data of Figures 49 and 55 through 58, all of which are for vertically polarized loop antennas, reveal variations between the measured and computed patterns which should not exist if the loop truly radiated isotropically as shown in Figure 60-B. This departure from the cosine and isotropic free space distributions, for horizontal and vertical polarization, respectively, was attributed to the proximity of the receiving loop to the aircraft upon which it was mounted. This conclusion was based on consideration of the following factors:

Horizontal Polarization:

- A stable transmitting source
- Repeatable pre-post calibration curves
- Use of horizontally polarized dipole over extremely flat ground

Vertical Polarization:

- A stable transmitting source
- Repeatable pre-post calibration curves
- Excellent agreement of the analytical results with that of the other authors[1,2,6] provided a high degree of confidence in the predicted antenna pattern profiles

Examination of the composite data of Figure 49 reveals poor correlation between measured and computed data for angles between 15° and 30°. There may be many factors responsible for this behavior. However, it is felt that the Brewster Angle effects, particular to operation in the vertical mode, is of prime consideration. This effect can be accounted for in the following way. For the case of vertical polarization, the phase of the reflection coefficient varies most rapidly near those elevation angles at which the magnitude of the reflection coefficient is at a minimum. These combined effects result in an erratic variation in signal level at these angles, when the composite far field pattern, obtained from the interaction of the direct and reflected waves is plotted. For the appropriate frequency and ground conditions represented in Figure 49, the Brewster Angle exists between 15° and 20°. It is in this region that the discrepancy exists between the measured and computed data of Figure 49.

The data of Figures 54 and 59 also requires separate consideration since the airborne antenna used was not a loop, but a fuselage mounted long wire. Figure 54, a composite for the horizontal mode, indicates very good agreement between the measured and computed data.

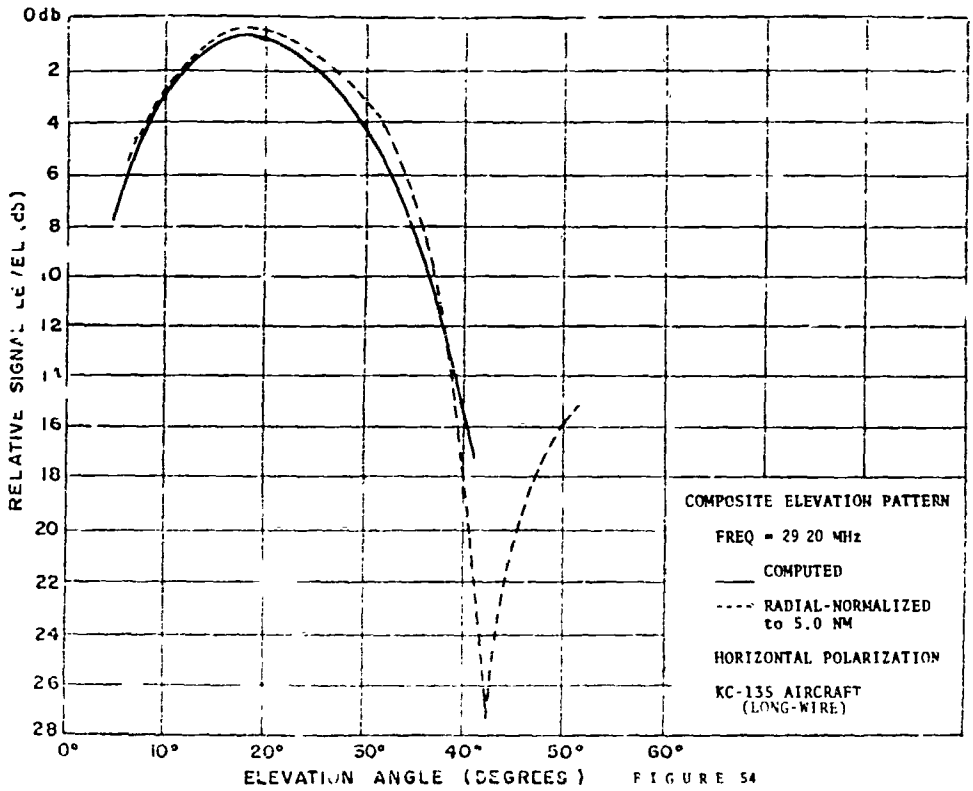

FIGURE 54

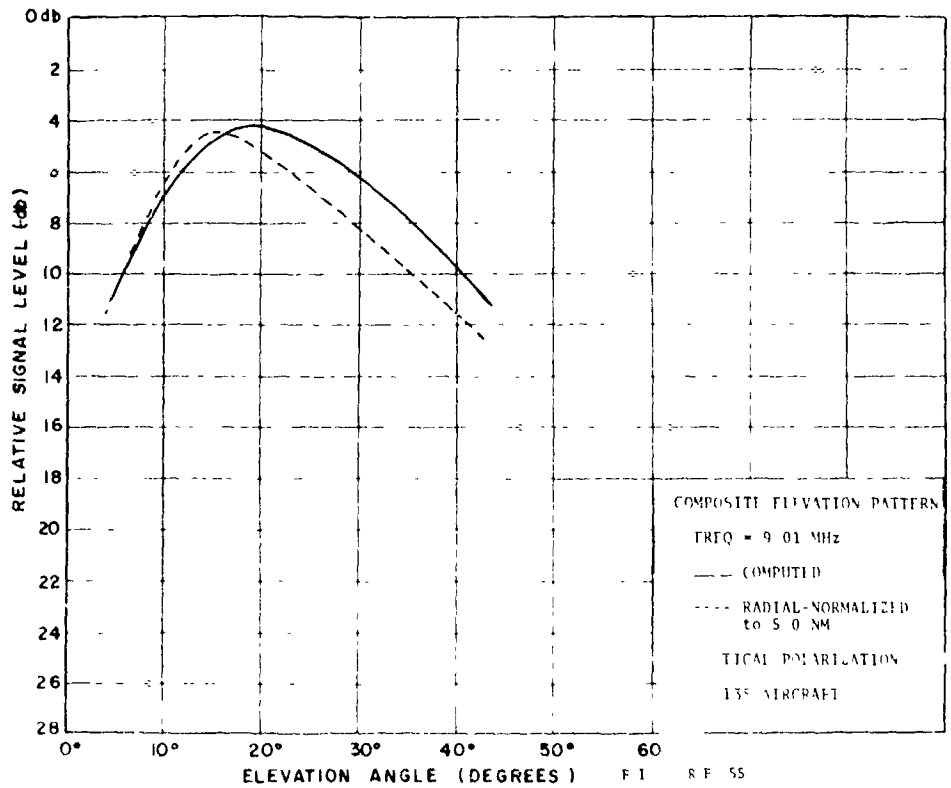

FIGURE 55

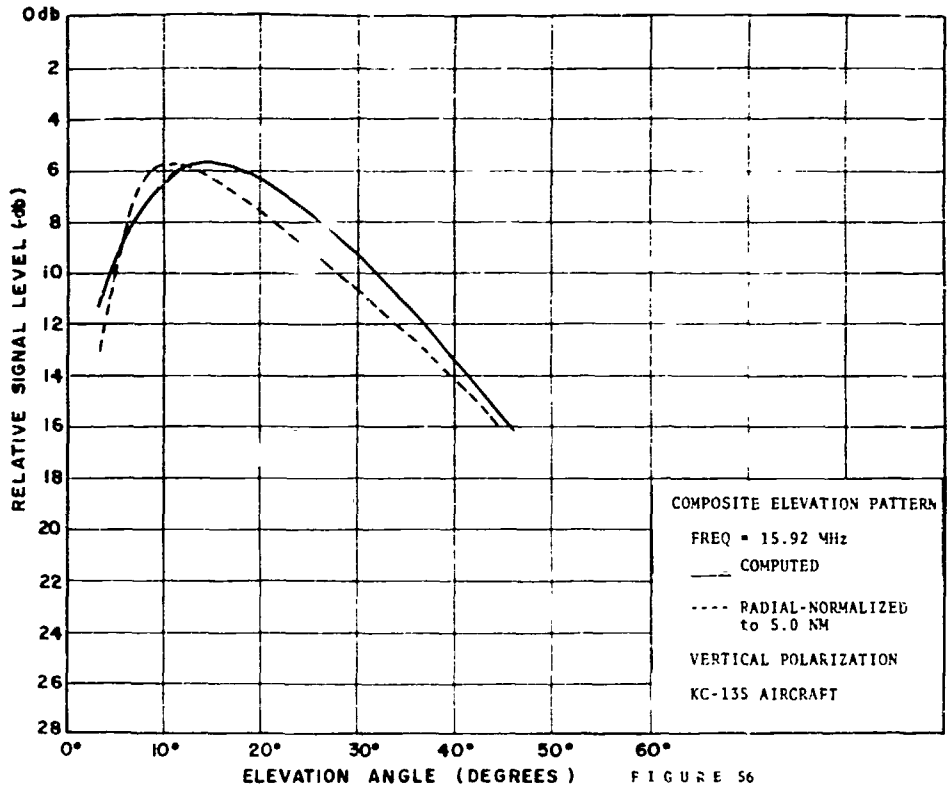

FIGURE 56

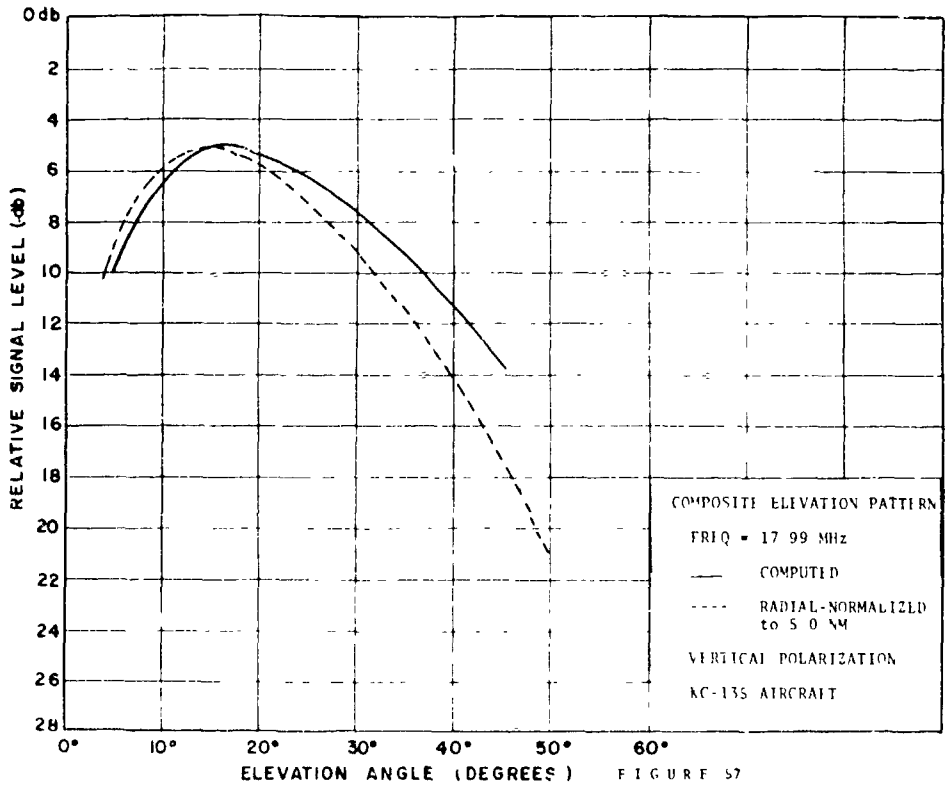

FIGURE 57

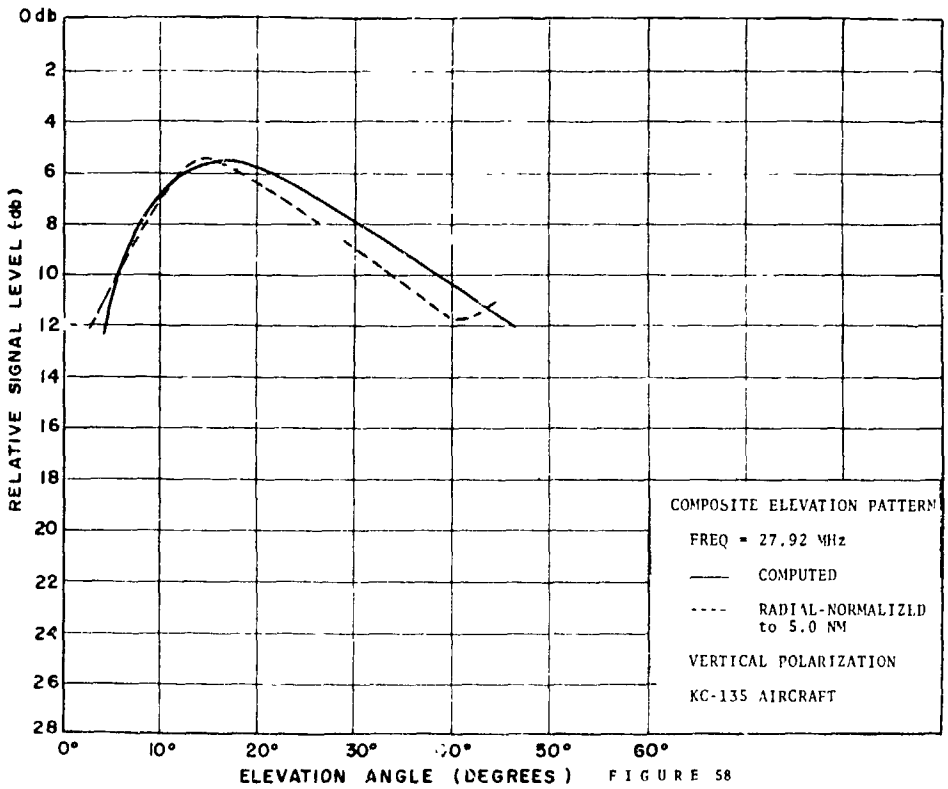

FIGURE 58

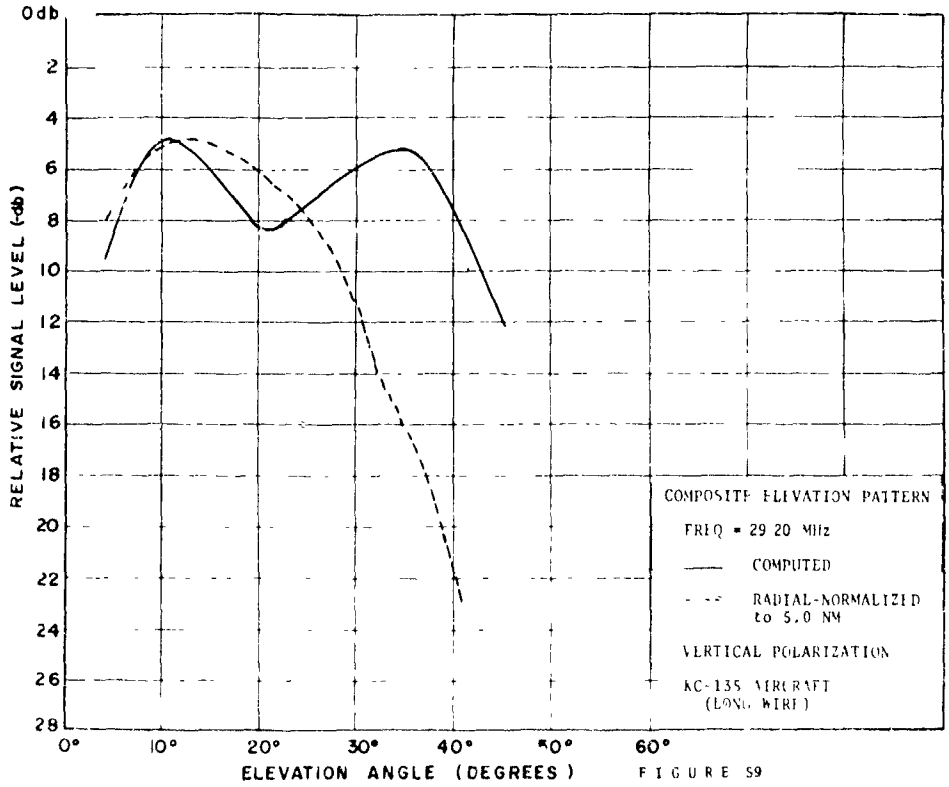

FIGURE 59

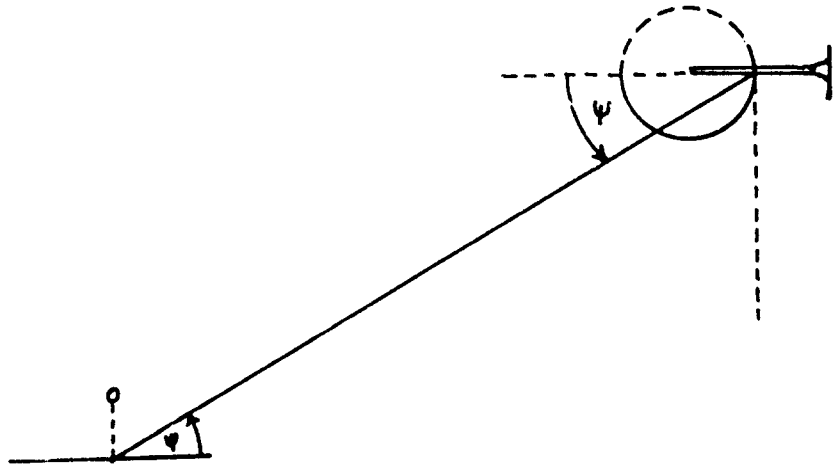

(A) Horizontal Polarization

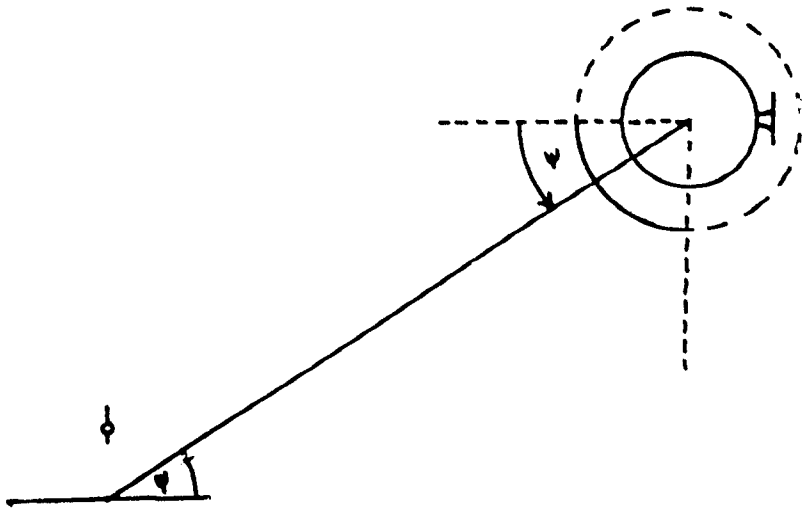

(B) Vertical Polarization

Figure 60. Free Space Pattern of Loop Antenna

However, this is not the case for vertical polarization, as seen in Figure 59. The patterns closely track one another up to about 25°, but beyond that point they diverge. This behavior beyond 25° may be accounted for in Figure 61 which is a plot taken from Reference (8), of the elevation pattern of a vertically polarized long wire antenna mounted on a 1/25 scale model of a KC-135 aircraft. The data shown covers an angular sector of 90°, i.e., from the axis of the aircraft to a point immediately below it. The response of the long wire from 5° to 25° is seen to closely follow that of the computed portion of Figure 59, however, from 25° to 40° the response drops off by approximately 7 dB. It is within this 25° to 40° sector that the greatest discrepancy exists between the measured and computed data of Figure 59. Therefore, the most reliable portion of the data of Figure 59 is contained within the 5° to 25° sector.

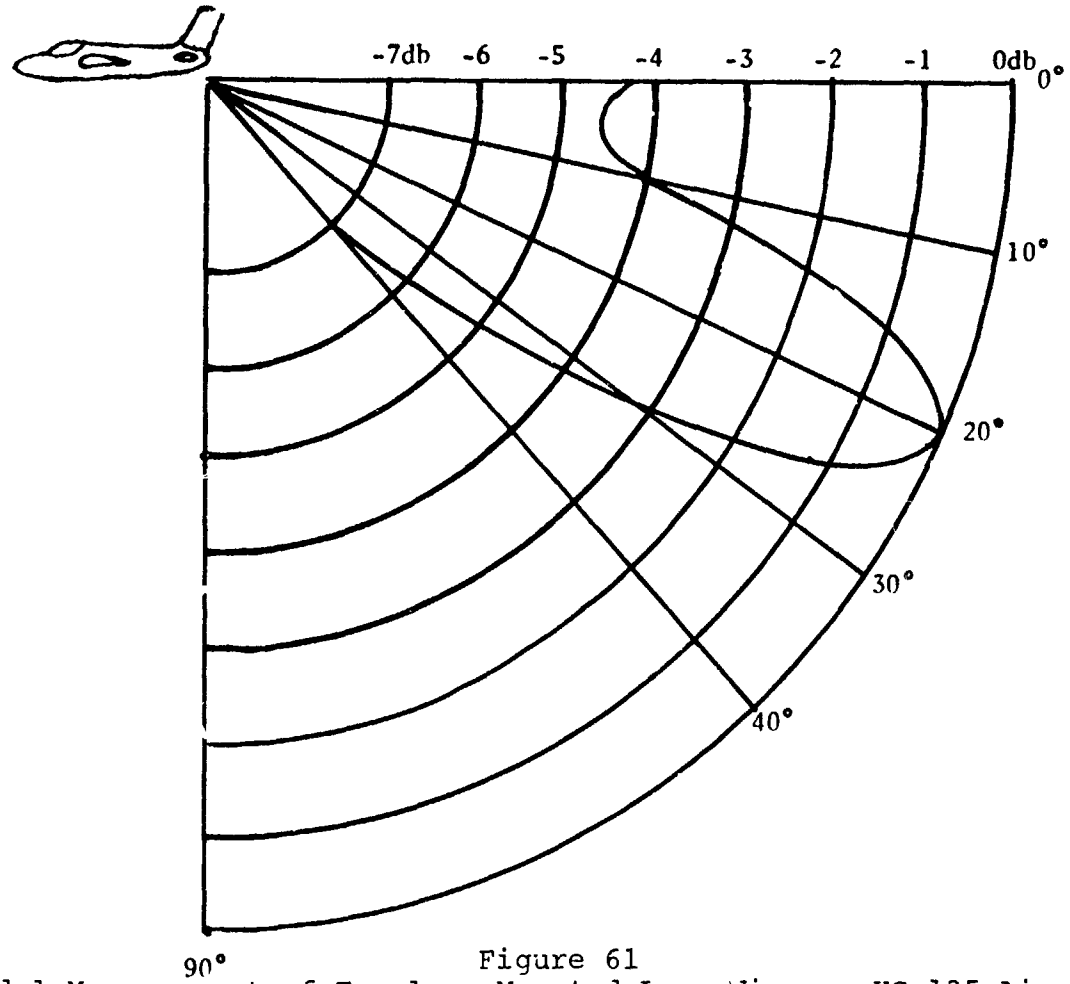

Figure 61
Model Measurement of Fuselage Mounted Long Wire on KC-135 Aircraft

Based on the foregoing considerations, direct use was made of the stepped calibration curves, obtained before and after each of the profile measurements, in calculating the absolute gain of the "unit", i.e., the aircraft and its associated antenna as a single unit. In determining the dipole's gain at each of the operating frequencies, the signal attenuation due to operation over an imperfectly conducting ground was deducted directly from the theoretical gain that would be obtained over a perfectly conducting ground. The signal attenuation at each of the operating frequencies was extrapolated directly from the computed data of Figures 1 through 14. Tables IV-A and IV-B list the absolute power gain of the dipole at the various elevation angles indicated.

In addition to ground losses, various other loss factors must be considered. These have been divided into two groups: those related to the airborne receiving system, shown in Table V, and those related to the ground transmitting system. (Shown in Table VI).

TABLE IV a

Aircraft	Polarization	Frequency	Dipole Free Space (db/iso)	Gain Over Ground (db)	Maximum Combined Gain (db)	Ground Attenuation (db)	Absolute Dipole Gain G_2
C-131#799	Horizontal	15.92	2.15	6.0	8.15	-.5 @ 15°	7.6 dbi
C-131#799	Horizontal	17.99	2.15	6.0	8.15	-.5 @ 14°	7.6 dbi
C-131#799	Horizontal	27.92	2.15	6.0	8.15	-.5 @ 9°	7.6 dbi
C-131#799	Vertical	27.92	2.15	6.0	8.15	-4.4 @ 32°	3.8 dbi

TABLE IV b

Aircraft	Polarization	Frequency	Dipole Free Space (db/iso)	Gain Over Ground (db)	Maximum Combined Gain (db)	Ground Attenuation (db)	Absolute Dipole Gain G_2
KC135#125	Horizontal	9.01	2.15	6.0	8.15	-2.2 @ 40°	6.0 dbi
KC135#125	Horizontal	15.92	2.15	6.0	8.15	-2.2 @ 40°	6.0 dbi
KC135#125	Horizontal	17.99	2.15	6.0	8.15	-2.85 @ 40°	5.3 dbi
KC135#125	Horizontal	27.92	2.15	6.0	8.15	-2.26 @ 40°	5.9 dbi
KC135#125	Horizontal	29.2	2.15	6.0	8.15	-.5 @ 15°	7.6 dbi
KC135#125	Vertical	9.01	2.15	6.0	8.15	4.1 @ 21°	4.0 dbi
KC135#125	Vertical	15.92	2.15	6.0	8.15	-5.8 @ 15°	2.4 dbi
KC135#125	Vertical	17.99	2.15	6.0	8.15	-4.8 @ 16°	3.4 dbi
KC135#125	Vertical	27.92	2.15	6.0	8.15	-5.7 @ 18°	2.5 dbi
KC135#125	Vertical	29.2	2.15	6.0	8.15	-4.8 @ 10°	3.4 dbi

It is not to be inferred that the loss date of Tables V and VI includes all possible loss sources involved in flight measurements of this type. However, those factors which were expected to most significantly alter the accuracy of the gain data of the receiving unit are listed.

TABLE V

C-131 #799 INSERTION LOSS BETWEEN RCVR & WING TIP LOOP (100 Feet RF Cable RG-117 A/U)	
FREQUENCY (MHz)	LOSS (db)
9.018	.26
15.922	.31
17.993	.32
27.920	.48
29.200	.49

KC-135 #125 INSERTION LOSS BETWEEN RCVR & BOOM MOUNTED LOOP (130 Feet RF Cable RG-9A/U)	
FREQUENCY (MHz)	LOSS (db)
9.018	.67
15.922	.70
17.993	.78
27.920	1.28
29.200	1.30

INSERTION LOSS (db) TX LINE LONG WIRE KC-135 #125 (5 Ft RF Cable RG-115/U)	
FREQUENCY (MHz)	LOSS (db)
29.20	0

AIRBORNE RECEIVING SYSTEM LOSSES (db)

TABLE VI

INSERTION LOSS (db) FOR DIPOLE TX LINE 150 Foot (Belden 8210)	
FREQUENCY (MHz)	LOSS (db)
9.018	3.0
15.922	3.1
17.993	3.15
27.920	3.28
29.200	3.30

GROUND TRANSMITTING SYSTEM LOSS Due to Mismatch	
FREQUENCY (MHz)	LOSS (db)
9.018	0
15.922	0
17.993	0
27.920	0
29.200	0

MEASURED GROUND TRANSMITTER SYSTEM LOSSES

SECTION VI

GAIN CALCULATIONS

The following discussion outlines the procedure for determining the absolute gain of the receiving unit as a function of its aspect angle relative to the ground-based transmitting dipole.

Figure 62 is a diagram of the field setup.

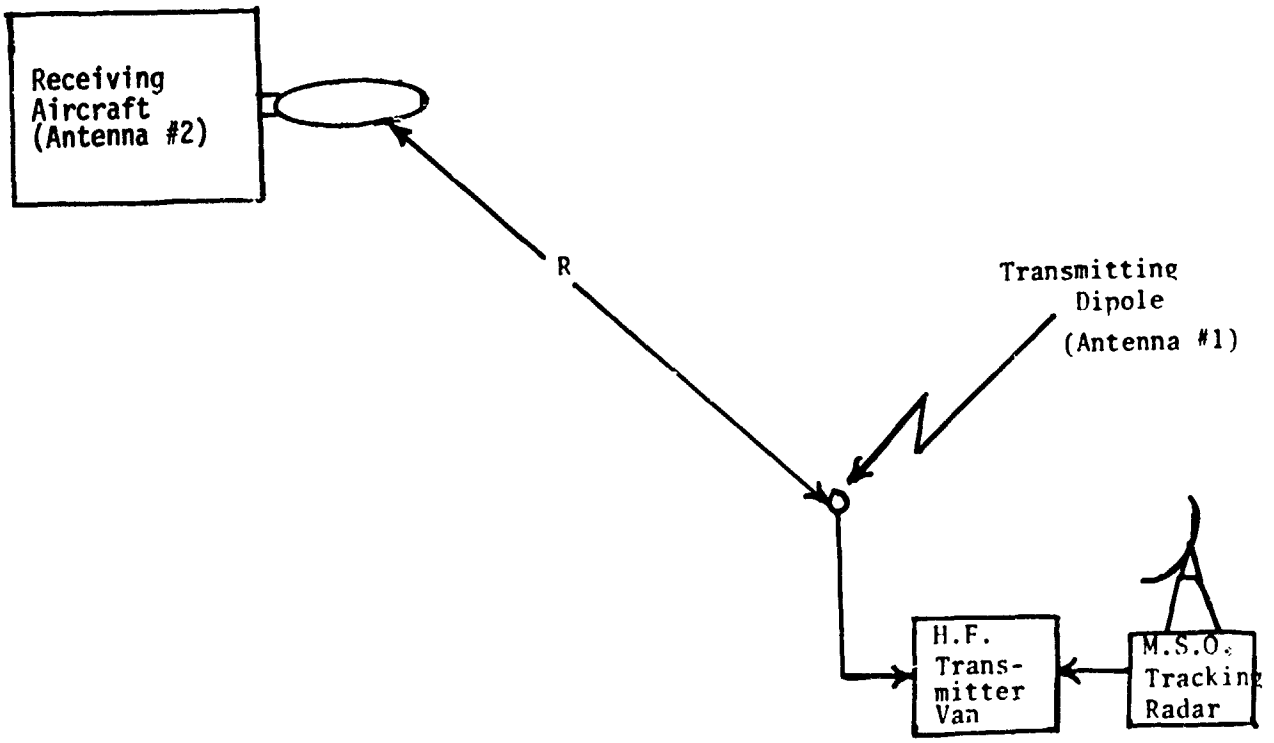

Figure 62. Field Setup

$$PD_2 = \frac{PR_2 + PL_2}{Ae_2} \qquad \text{(Equation 1)}$$

where

PD_2 = Power density impinging on the Receive Antenna

PR_2 = Power measured at the receiver input (extrapolated directly from the recorded patterns in a plane perpendicular to the dipole axis

PL_2 = Power loss due to cable attenuation, impedance mismatch etc. as listed in Table V

Ae_2 = Effective aperture of Antenna #2

where $Ae_2 = \frac{G_u \lambda^2}{4\pi}$

G_u = Gain of the unit (i.e. aircraft and its associated antenna)

λ = Wavelength of operating frequency

PD_2 can also be expressed as follows:

$$PD_2 = \frac{PRAD_1}{4\pi R^2} \qquad \text{(Equation 2)}$$

where:

PD_2 = Power density impinging on the Receive Antenna, 2.

$PRAD_1$ = Power radiated by the Transmit Antenna, 1.

R = Slant Range between Antennas 1 and 2.

Equating Equations 1 and 2

$$\frac{PR_2 + PL_2}{Ae_2} = \frac{PRAD_1}{4\pi R^2} \therefore$$

$$PRAD_1 = \frac{(PR_2 + PL_2)(4\pi R^2)}{Ae_2} \qquad \text{(Equation 3)}$$

Recalling

$$Ae_2 = \frac{G_u \lambda^2}{4\pi} \qquad \text{(Equation 4)}$$

and substituting Equation 4 into Equation 3

$$PRAD_1 = \frac{(PR_2 + PL_2)(4\pi R^2)}{\frac{G_u \lambda^2}{4\pi}}$$

$$PRAD_1 = \frac{(PR_2 + PL_2)(4\pi R)^2}{G_u \lambda^2} \qquad \text{(Equation 5)}$$

where

$$\lambda = \frac{c}{f}$$

where c = Speed of light in meters per second

f = Frequency in MHz

$$\lambda^2 = \left(\frac{c}{f}\right)^2 = \left(\frac{300}{\text{Freq/MHz}}\right)^2 \qquad \text{(Equation 6)}$$

Substituting Equation 6 into 5:

$$PRAD_1 = \frac{(PR_2 + PL_2)(4\pi R)^2}{(G_u)\left(\frac{300^2}{f^2}\right)} \qquad \text{(Equation 7)}$$

$$PRAD_1 = \frac{(PR_2 + PL_2)(4\pi R)^2(f^2)}{(G_u)(300)^2}$$

Letting $K = \frac{(4\pi R)^2}{(300)^2}$ where

R = Range in meters $K = 1.5 \times 10^5$ for R = 5 N.M.

$$PRAD_1 = \frac{(PR_2 + PL_2)(K)(f^2)}{G_u} \quad \therefore$$

$$G_u = \left[\frac{(PR_2 + PL_2)(K)(f^2)}{P_{IN}(G_1)}\right] \qquad \text{(Equation 8)}$$

where $PRAD_1 = (P_{IN})(G_1)$

P_{IN} = $P_{incident} - P_{reflected} - P_{loss}$ from Table VI)

G_1 = Gain of Antenna 1, obtained from Tables IV-A and IV-B.

Table VII-A

AIRCRAFT	ANTENNA	POLAR-IZATION	FREQ (MHz)	PROBE ELEV ANGLE	POWER RECEIVED DBM	PG_1 DIPOLE ABSOLUTE POWER GAIN	POWER RAD WATTS	G_u = UNITS GAIN
C-131	Wing Tip Loop	HOR	15.9	15°	-58.2	7.69 dbi	129.36	-33.2 dbi
C-131	Wing Tip Loop	HOR	17.9	13°	-53.2	7.68 dbi	128.92	-27.22 dbi
C-131	Wing Tip Loop	HOR	27.9	9°	-56.0	7.64 dbi	127.77	-26.4 dbi
C-131	Wing Tip Loop	VERT	27.9	14°	-68.0	1.4 dbi	26.5	-27.0 dbi

Table VII-B

AIRCRAFT	ANTENNA	POLAR-IZATION	FREQ (MHz)	PROBE ELEV ANGLE	POWER RECEIVED DBM	PG_1 DIPOLE ABSOLUTE POWER GAIN	POWER RAD WATTS	G_u = UNITS GAIN
KC-135	Boom Mtd Loop	HOR	9.0	15°	-79.0	2.15 dbi	32.80	-53.3 dbi
KC-135	Boom Mtd Loop	HOR	15.9	15°	-83.0	0 dbi	20.0	-50.1 dbi
KC-135	Boom Mtd Loop	HOR	17.9	15°	-83.0	0 dbi	20.0	-49.2 dbi
KC-135	Boom Mtd Loop	HOR	27.9	15°	-75.0	1.2 dbi	25.0	-37.2 dbi
KC-135	Boom Mtd Loop	VERT	9.0	15°	-84.0	4 dbi	50.0	-60.0 dbi
KC-135	Boom Mtd Loop	VERT	15.9	15°	-78.0	2.4 dbi	34.76	-47.6 dbi
KC-135	Boom Mtd Loop	VERT	17.9	15°	-82.0	2.2 dbi	32.64	-50.3 dbi
KC-135	Boom Mtd Loop	VERT	27.9	15°	-80.0	2.8 dbi	36.48	-45.0 dbi
KC-135	Long Wire	HOR	29.2	20°	-55.0	7.2 dbi	141.8	-25.0 dbi
KC-135	Long Wire	VERT	29.2	11°	-45.0	3.4 dbi	40.0	-10.0 dbi

Using this approach, Tables VII-A and VII-B were prepared. They are consolidations of all pertinent data required to obtain the "Units" gain as a function of operating frequency. The data was determined at those "Probe Elevation Angles" specified in the tables. Using the "Units" gain obtained at each of these particular angles, the absolute gain at all other angles was then determined by taking the relative difference in signal level with respect to that point.

Based on the earlier assumptions in the Data Analysis Section, that variations between the measured and computed data were due to the proximity of the airborne antenna to the aircraft, gain contours have been plotted as shown in Figures 63 through 76. The contours are plots of these variations, in decibels (dB), as a function of the elevation angle PSI (ψ). The gain data is shown relative to the energy distribution from an isotropic source.

The power gain data shown in Figures 63 through 76 may be used in the following manner to determine the absolute power of a typical high frequency antenna installation as shown in Figure 77.

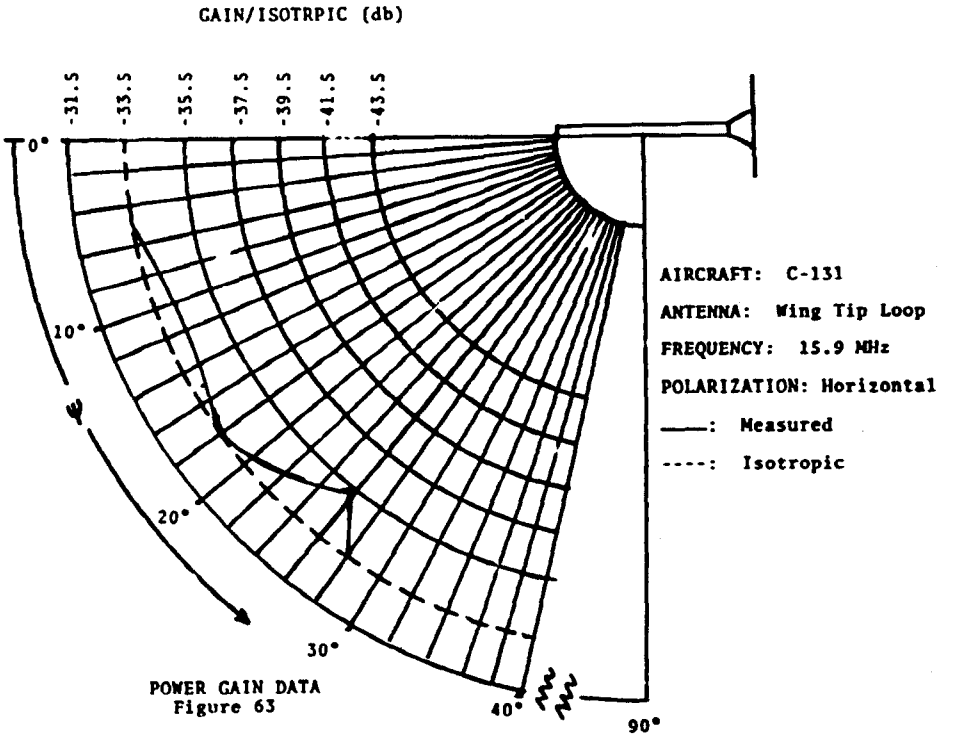

Figure 63. Power Gain Data

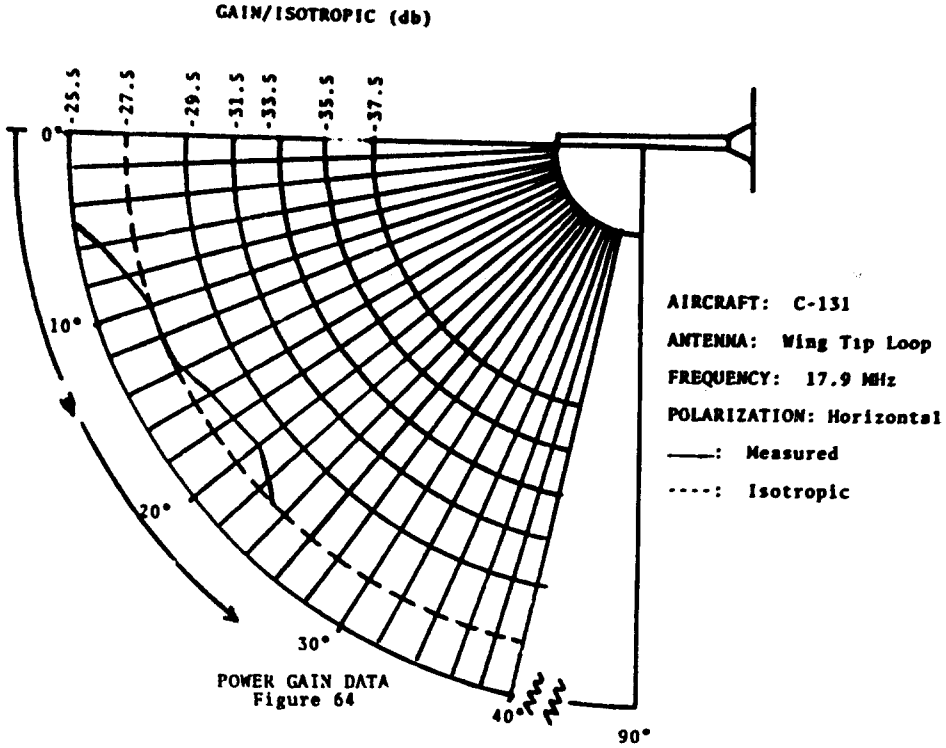

POWER GAIN DATA
Figure 64

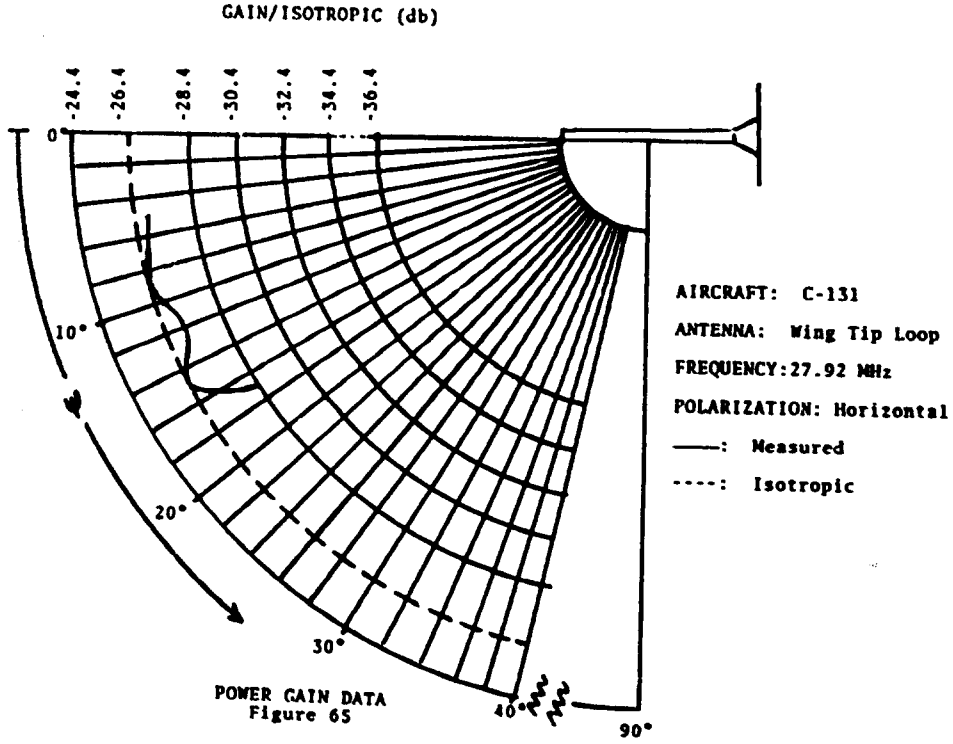

POWER GAIN DATA
Figure 65

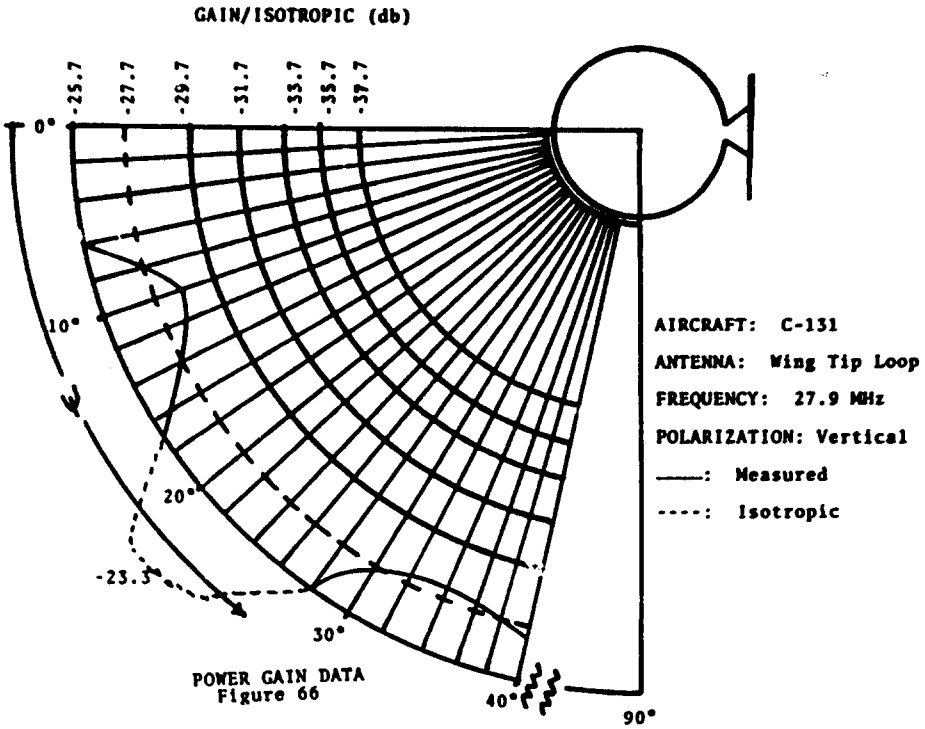

POWER GAIN DATA
Figure 66

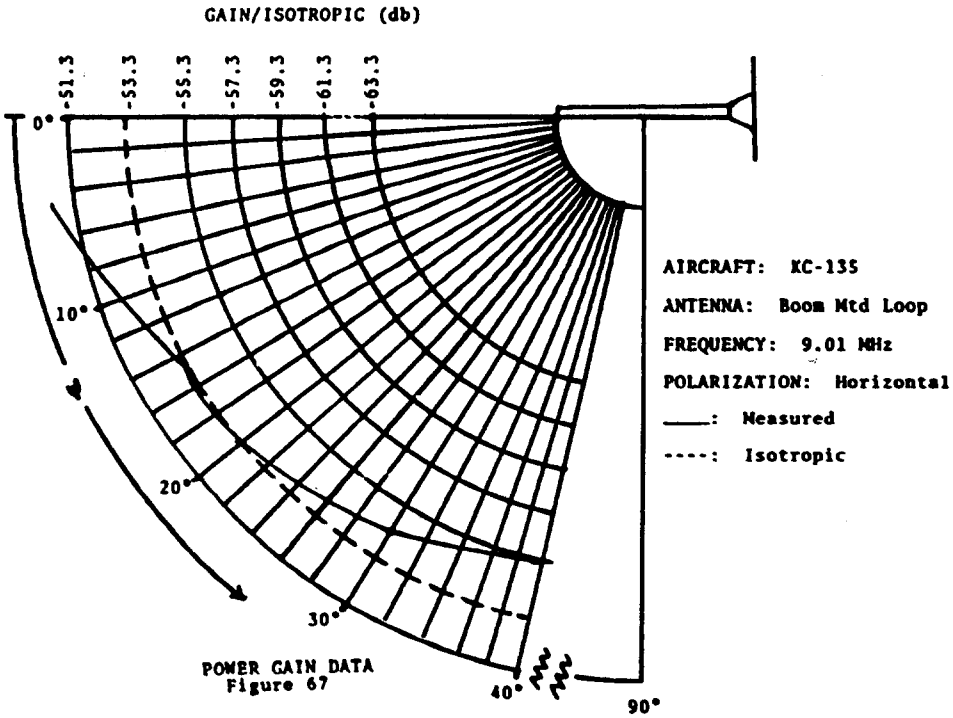

POWER GAIN DATA
Figure 67

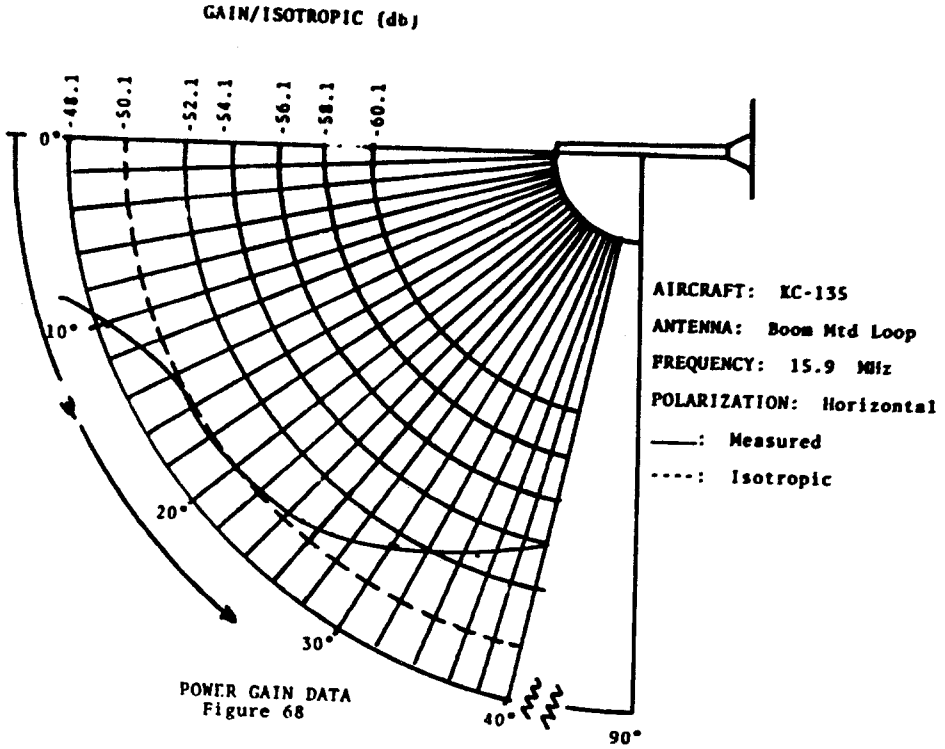

POWER GAIN DATA
Figure 68

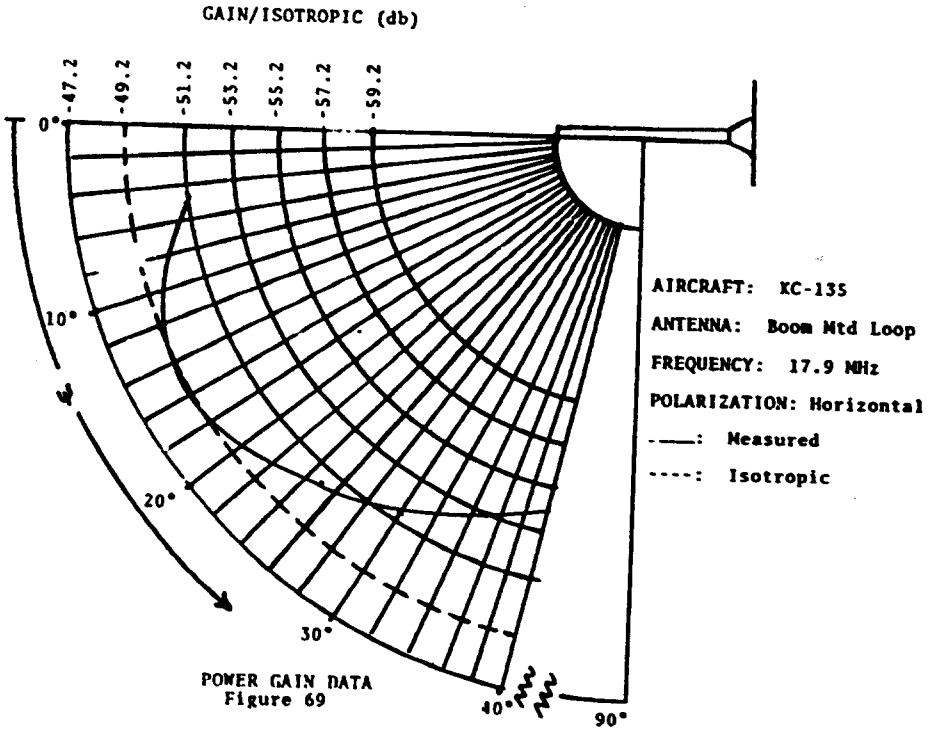

POWER GAIN DATA
Figure 69

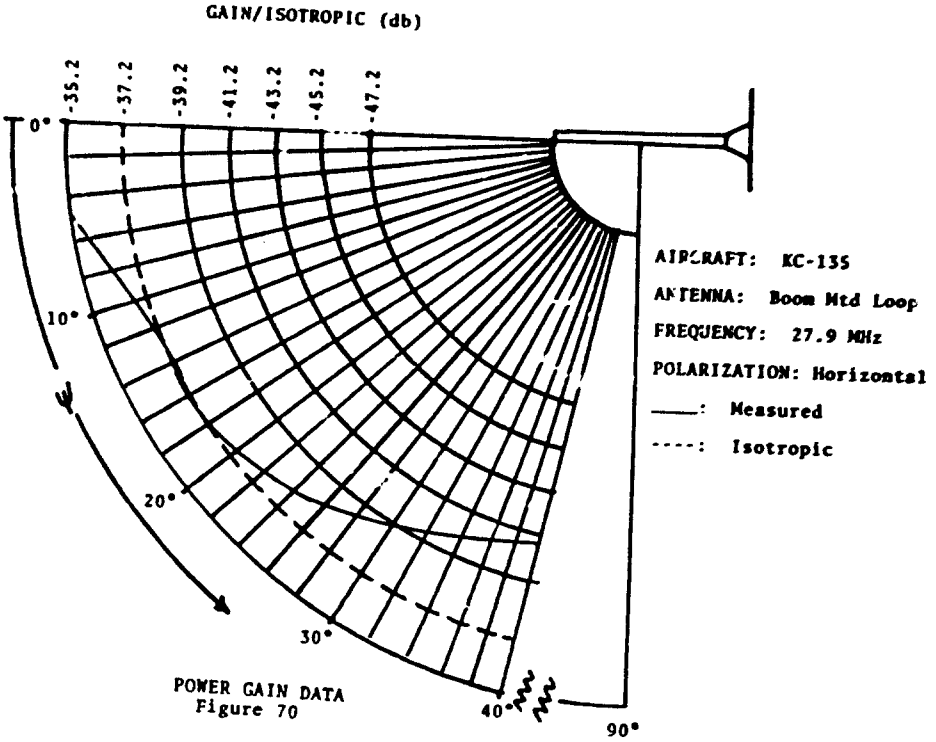

POWER GAIN DATA
Figure 70

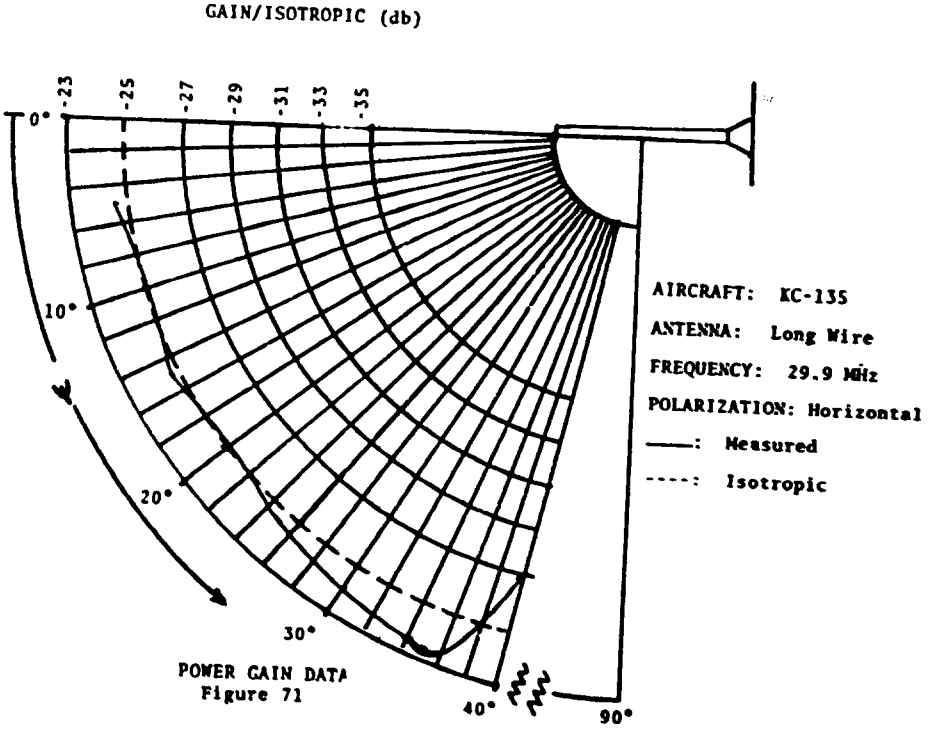

POWER GAIN DATA
Figure 71

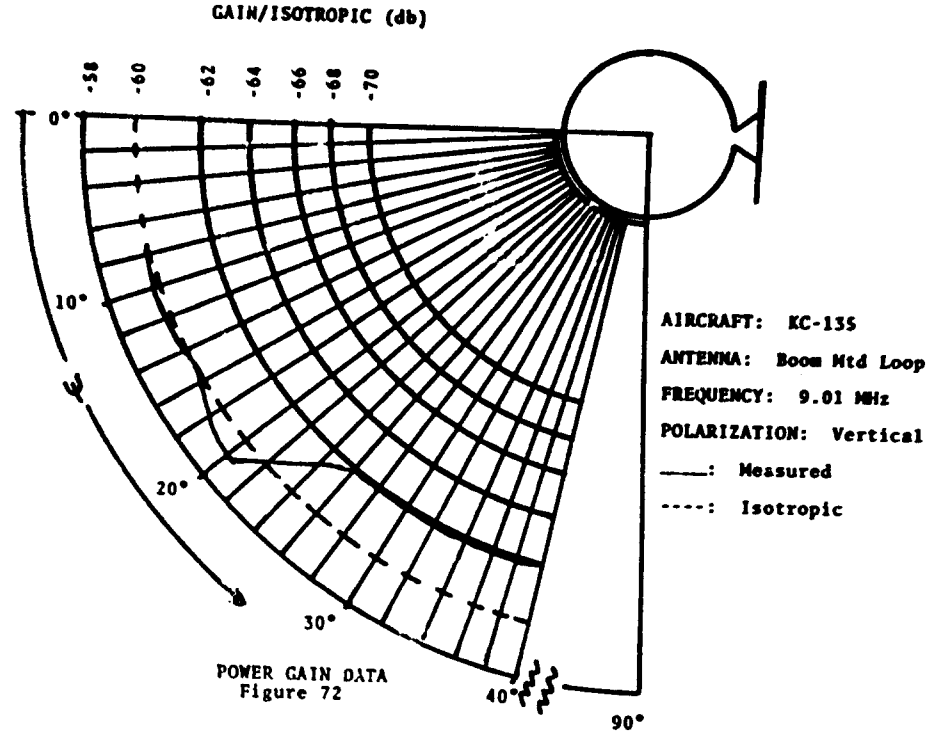

POWER GAIN DATA
Figure 72

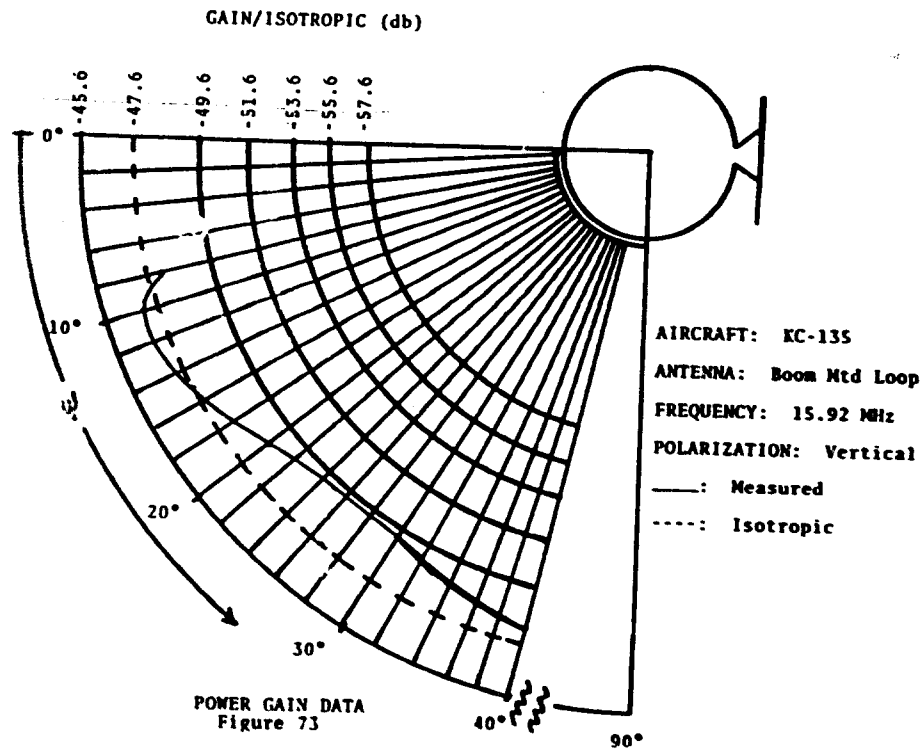

POWER GAIN DATA
Figure 73

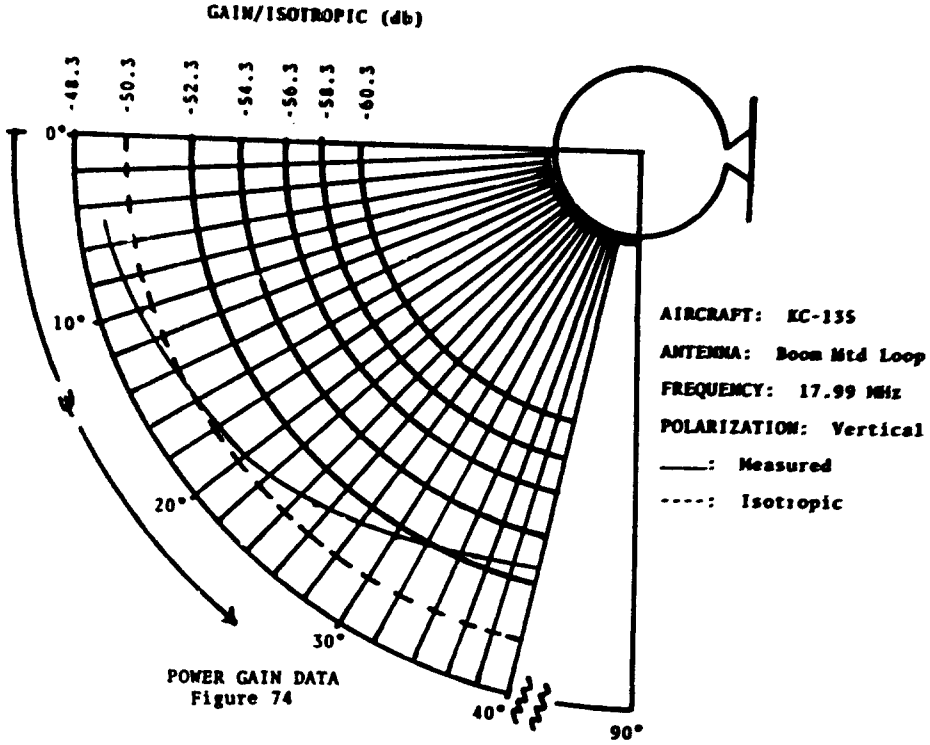

POWER GAIN DATA
Figure 74

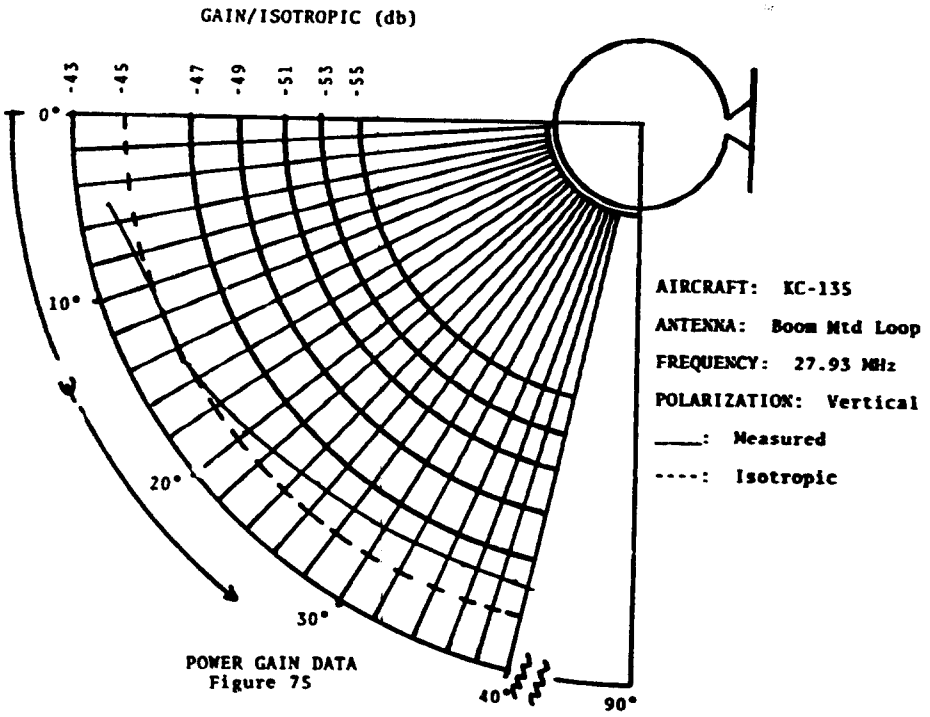

POWER GAIN DATA
Figure 75

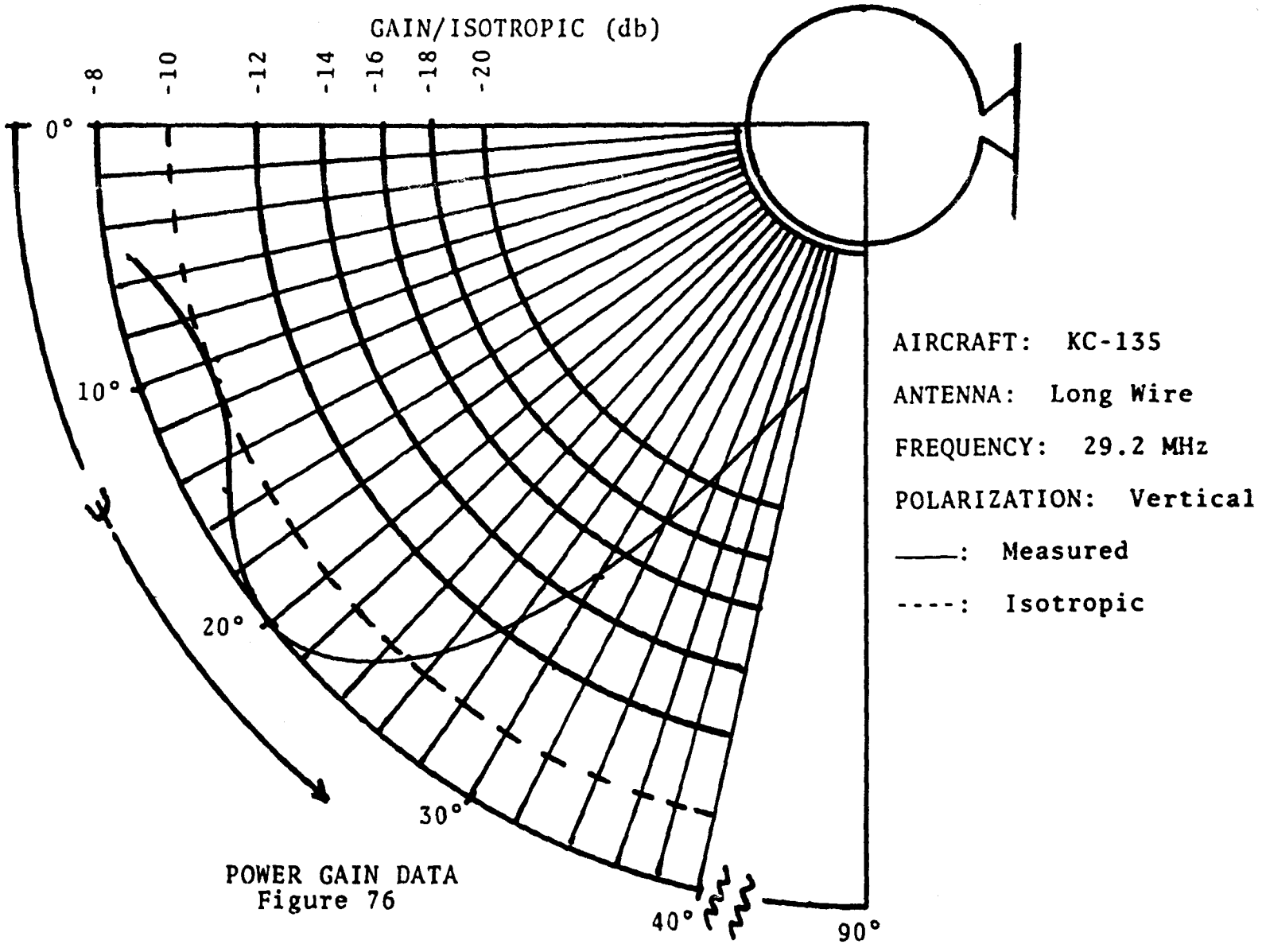

POWER GAIN DATA
Figure 76

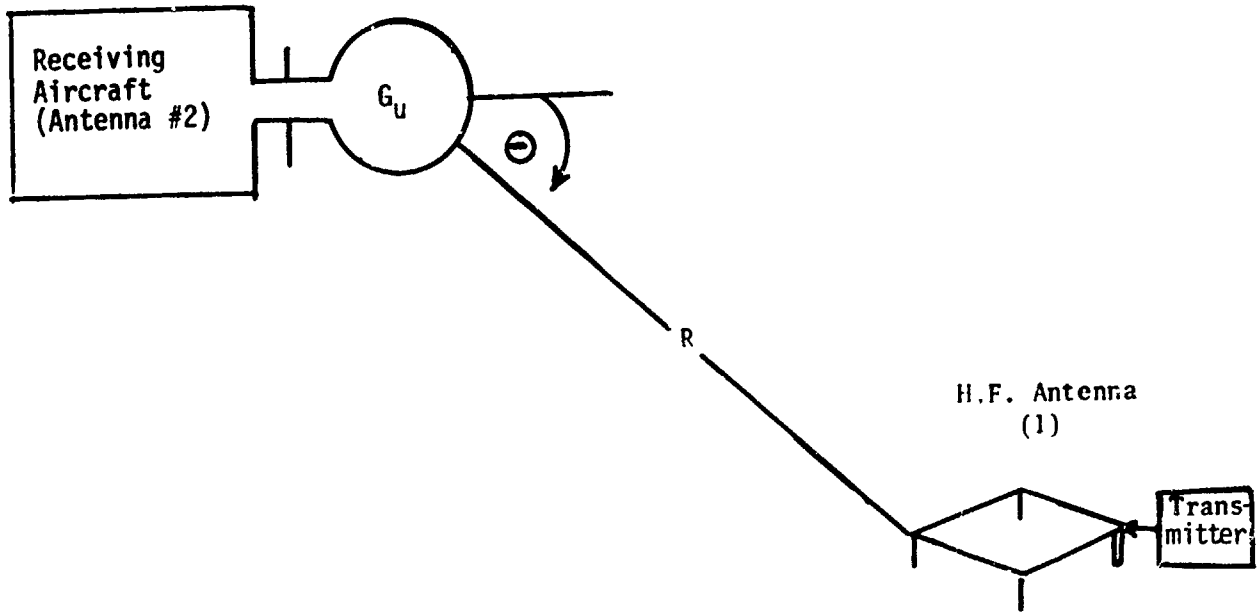

Figure 77. HF Antenna Installation

$$G_u = \frac{(PR_2 + PL_2)(K)(f^2)}{PRAD_1}$$

where: G_u at the appropriate frequency and Theta (Θ)Angle is obtained from Figures 63 through 76

$K = \frac{(4\pi R^2)}{(300)^2 \text{meters}}$ for the appropriate Slant Range (meters)

f = Frequency (MHz)

$PRAD_1$ = Power radiated by antenna under test (#1)

Solving for "$PRAD_1$"

$$PRAD_1 = \frac{(PR_2 + PL_2)(K)(f^2)}{G_u}$$

Substitute "$PRAD_1$" into the following:

$$PRAD_1 = (G_1)\ (PIN_1)$$

where:

G_1 = Gain of unknown antenna.

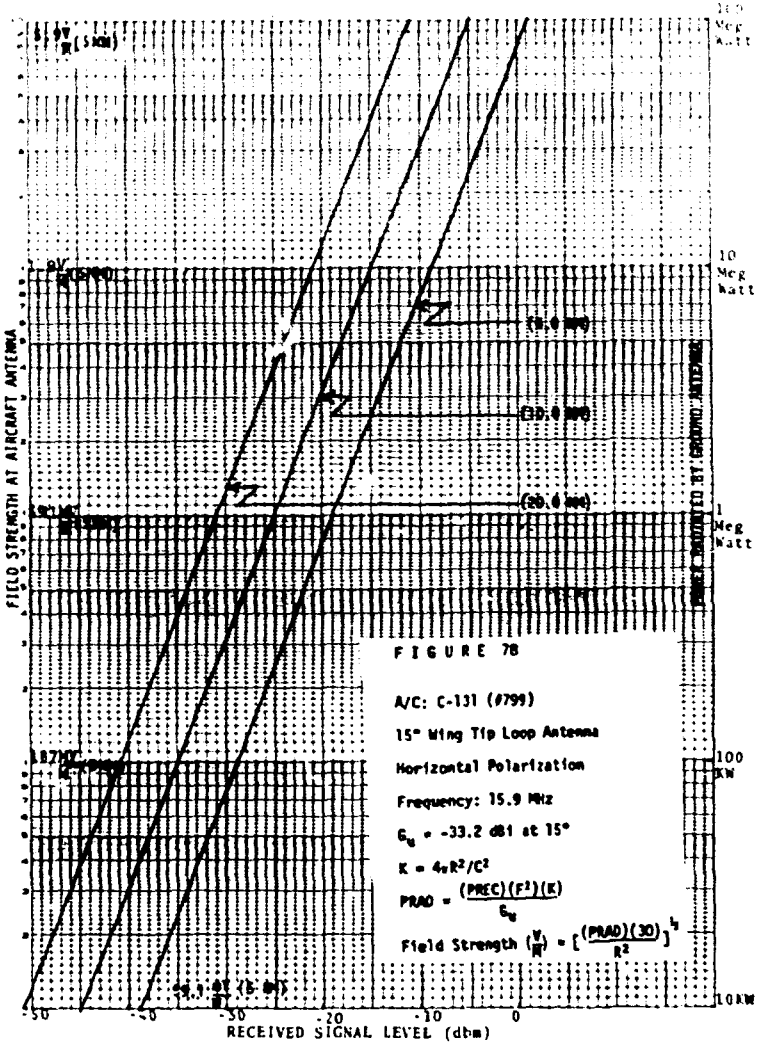

FIGURE 78

A/C: C-131 (#799)

15° Wing Tip Loop Antenna

Horizontal Polarization

Frequency: 15.9 MHz

G_u = -33.2 dBi at 15°

$K = 4\pi R^2/C^2$

$PRAD = \frac{(PREC)(F^2)(K)}{G_u}$

Field Strength $(\frac{V}{M}) = [\frac{(PRAD)(30)}{R^2}]^{\frac{1}{2}}$

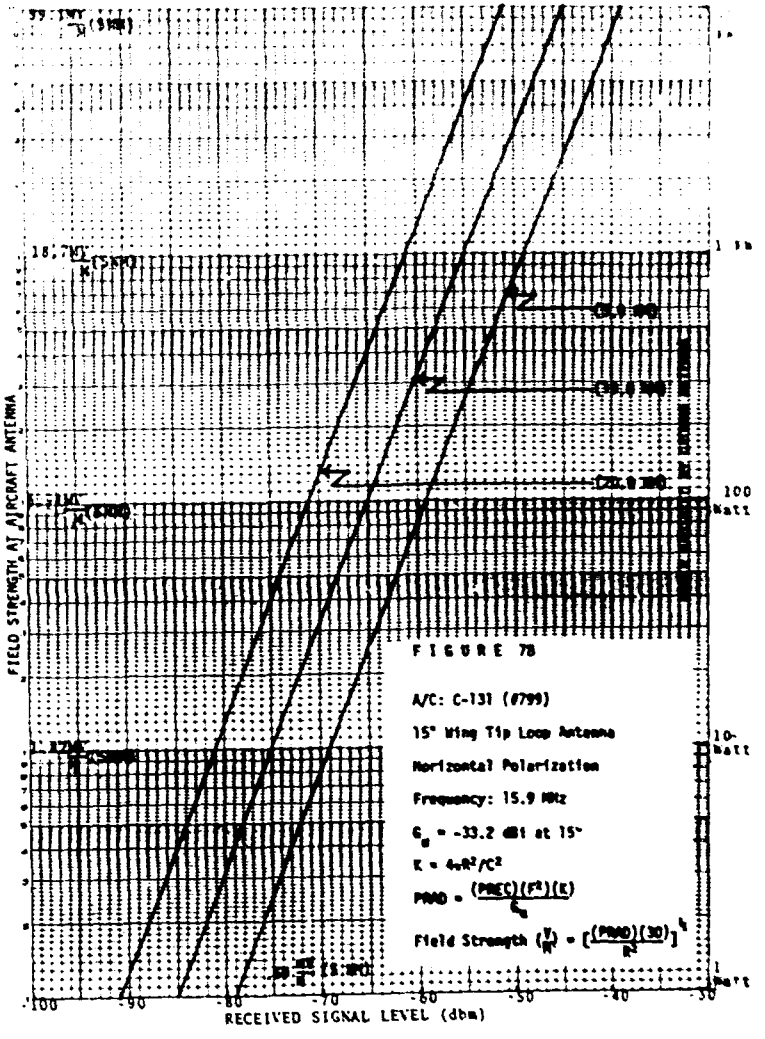

FIGURE 78

A/C: C-131 (#799)

15° Wing Tip Loop Antenna

Horizontal Polarization

Frequency: 15.9 MHz

G_u = -33.2 dBi at 15°

$K = 4\pi R^2/C^2$

$PRAD = \frac{(PREC)(F^2)(K)}{G_u}$

Field Strength $(\frac{V}{M}) = [\frac{(PRAD)(30)}{R^2}]^{\frac{1}{2}}$

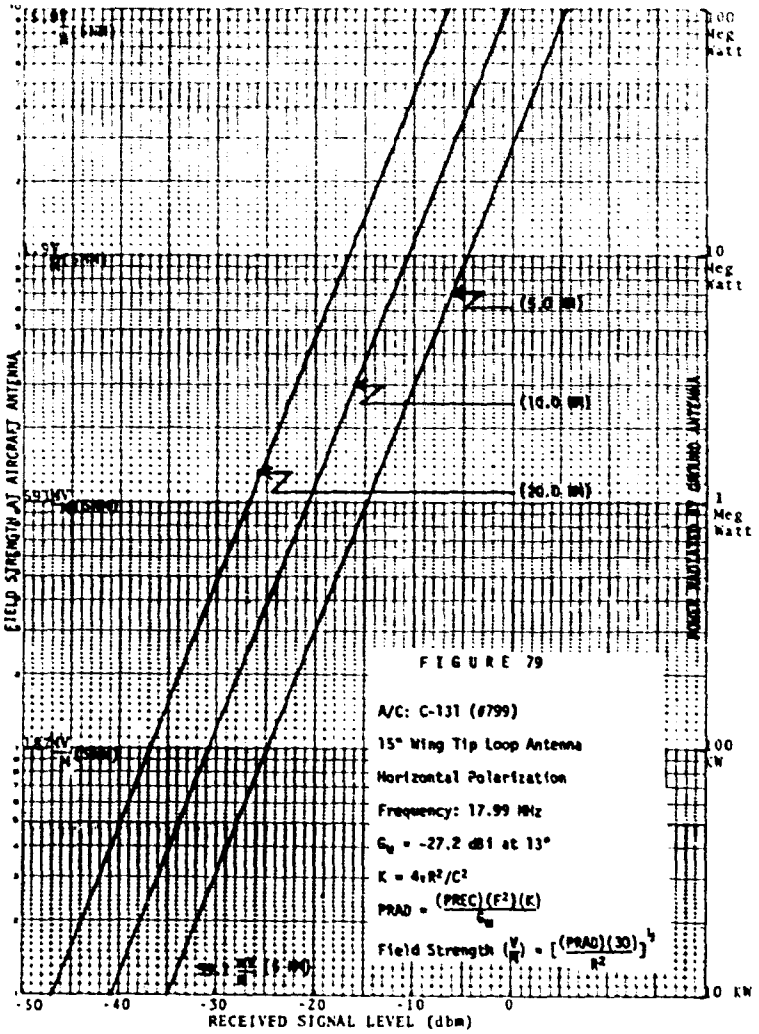
FIELD STRENGTH AT AIRCRAFT ANTENNA
RECEIVED SIGNAL LEVEL (dbm)
-50
-40
-30
-20
-10
0
100 Meg Watt
10 Meg Watt
1 Meg Watt
100 KW
0 KW
(5.0 MW)
(10.0 MW)
(20.0 MW)
FIGURE 79
A/C: C-131 (#799)
15° Wing Tip Loop Antenna
Horizontal Polarization
Frequency: 17.99 MHz
G_{eq} = -27.2 dBi at 13°
$K = 4\pi R^2/C^2$
$PRAD = \frac{(PREC)(F^2)(K)}{G_{eq}}$
Field Strength $(\frac{V}{M}) = [\frac{(PRAD)(30)}{R^2}]^{\frac{1}{2}}$

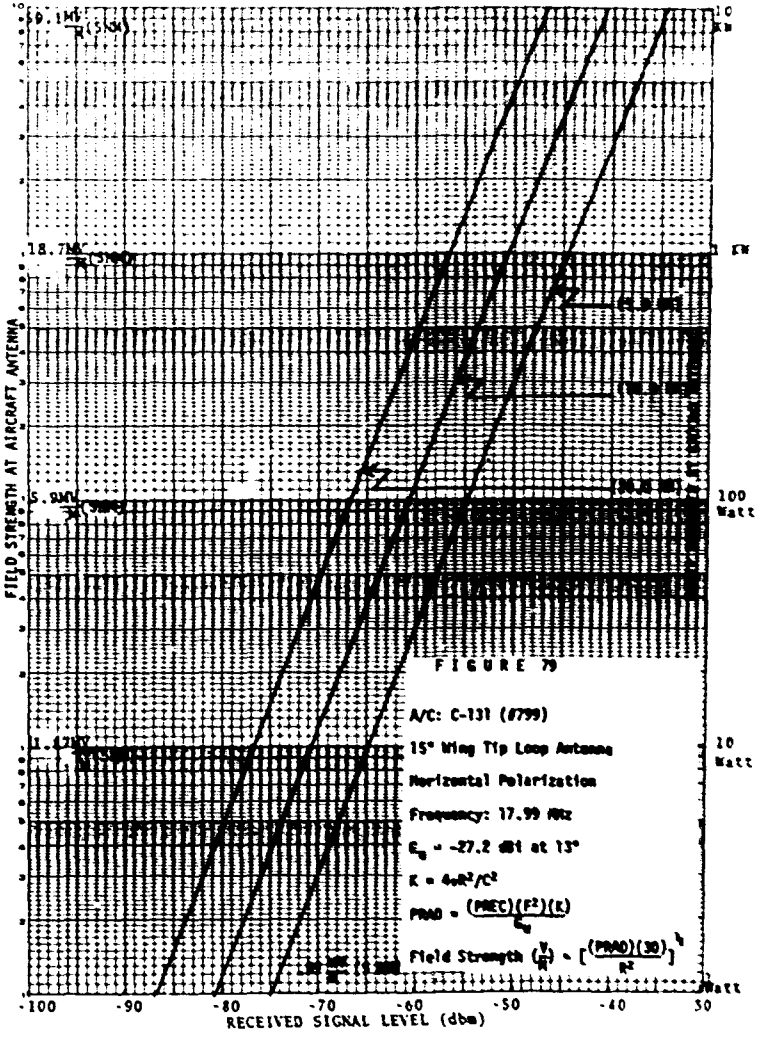
FIELD STRENGTH AT AIRCRAFT ANTENNA
RECEIVED SIGNAL LEVEL (dbm)
-100
-90
-80
-70
-60
-50
-40
30
10 KW
1 KW
100 Watt
10 Watt
FIGURE 79
A/C: C-131 (#799)
15° Wing Tip Loop Antenna
Horizontal Polarization
Frequency: 17.99 MHz
G_{eq} = -27.2 dBi at 13°
$K = 4\pi R^2/C^2$
$PRAD = \frac{(PREC)(F^2)(K)}{G_{eq}}$
Field Strength $(\frac{V}{M}) = [\frac{(PRAD)(30)}{R^2}]^{\frac{1}{2}}$

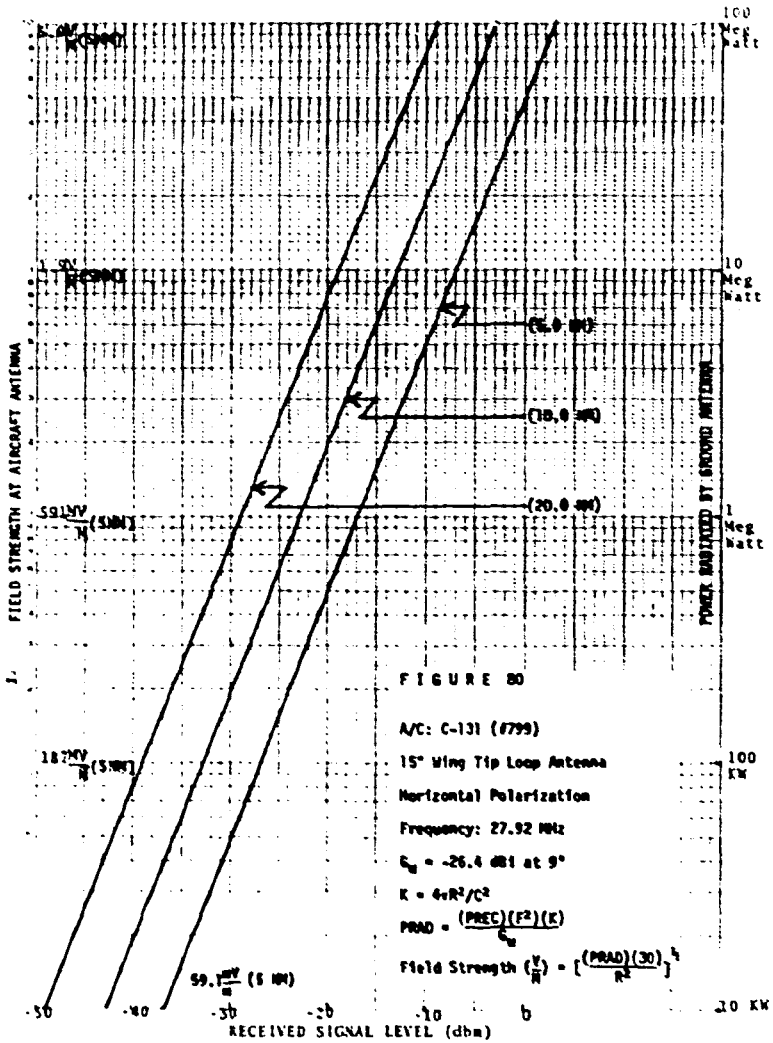

FIGURE 80

A/C: C-131 (#799)

15° Wing Tip Loop Antenna

Horizontal Polarization

Frequency: 27.92 MHz

G_w = -26.4 dBi at 9°

$K = 4\pi R^2/C^2$

$PRAD = \frac{(PREC)(F^2)(K)}{G_w}$

Field Strength $(\frac{V}{M}) = [\frac{(PRAD)(30)}{R^2}]^{\frac{1}{2}}$

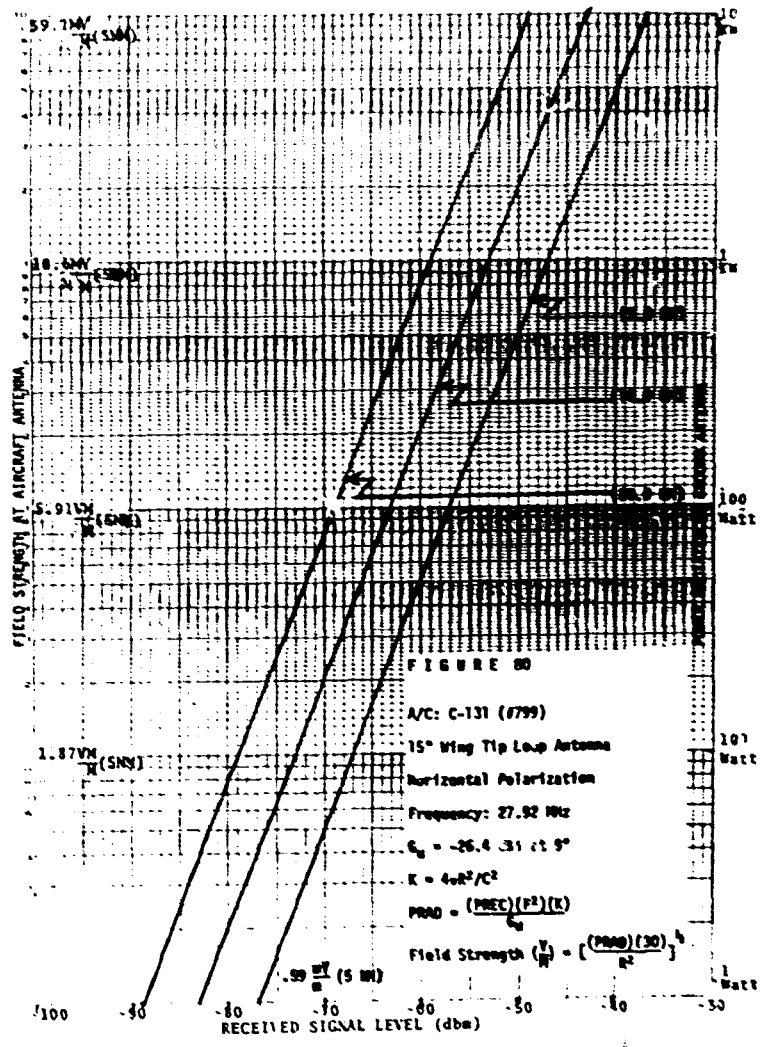

FIGURE 80

A/C: C-131 (#799)

15° Wing Tip Loop Antenna

Horizontal Polarization

Frequency: 27.92 MHz

G_w = -26.4 dBi at 9°

$K = 4\pi R^2/C^2$

$PRAD = \frac{(PREC)(F^2)(K)}{G_w}$

Field Strength $(\frac{V}{M}) = [\frac{(PRAD)(30)}{R^2}]^{\frac{1}{2}}$

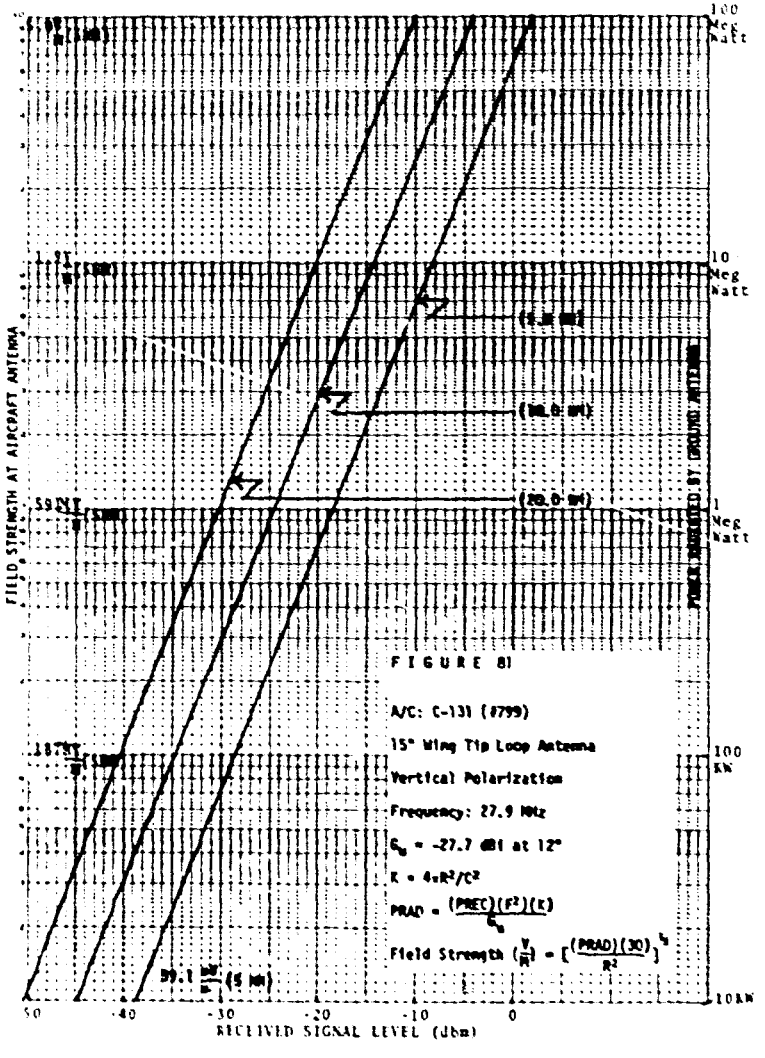
FIELD STRENGTH AT AIRCRAFT ANTENNA
RECEIVED SIGNAL LEVEL (dbm)
POWER RADIATED BY GROUND ANTENNA
100 Meg Watt
10 Meg Watt
1 Meg Watt
100 KW
10KW
(20.0 NM)
(10.0 NM)
(5.0 NM)
59.1 mV/m (5 NM)
FIGURE 81
A/C: C-131 (#799)
15" Wing Tip Loop Antenna
Vertical Polarization
Frequency: 27.9 MHz
G_w = -27.7 dBi at 12°
$K = 4\pi R^2/C^2$
$PRAD = \frac{(PREC)(F^2)(K)}{G_w}$
Field Strength $(\frac{V}{M}) = [\frac{(PRAD)(30)}{R^2}]^{1/2}$

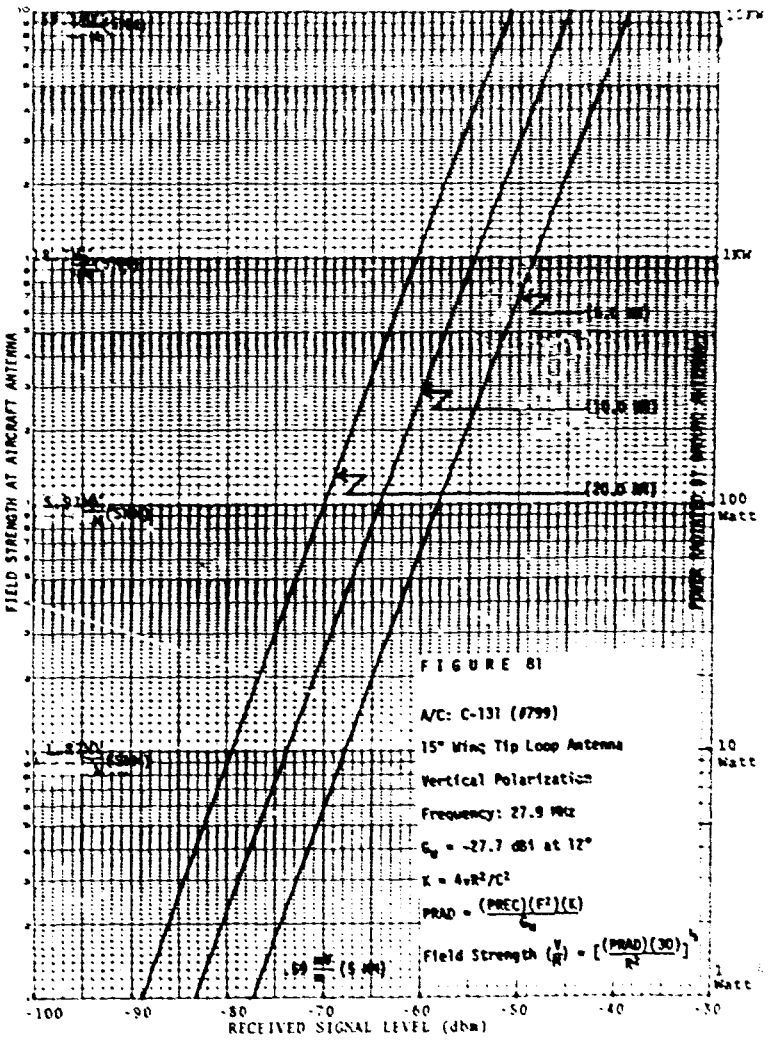
FIELD STRENGTH AT AIRCRAFT ANTENNA
RECEIVED SIGNAL LEVEL (dbm)
POWER RADIATED BY GROUND ANTENNA
1KW
100 Watt
10 Watt
1 Watt
(20.0 NM)
(10.0 NM)
(5.0 NM)
59 mV/m (5 NM)
FIGURE 81
A/C: C-131 (#799)
15" Wing Tip Loop Antenna
Vertical Polarization
Frequency: 27.9 MHz
G_w = -27.7 dBi at 12°
$K = 4\pi R^2/C^2$
$PRAD = \frac{(PREC)(F^2)(K)}{G_w}$
Field Strength $(\frac{V}{M}) = [\frac{(PRAD)(30)}{R^2}]^{1/2}$

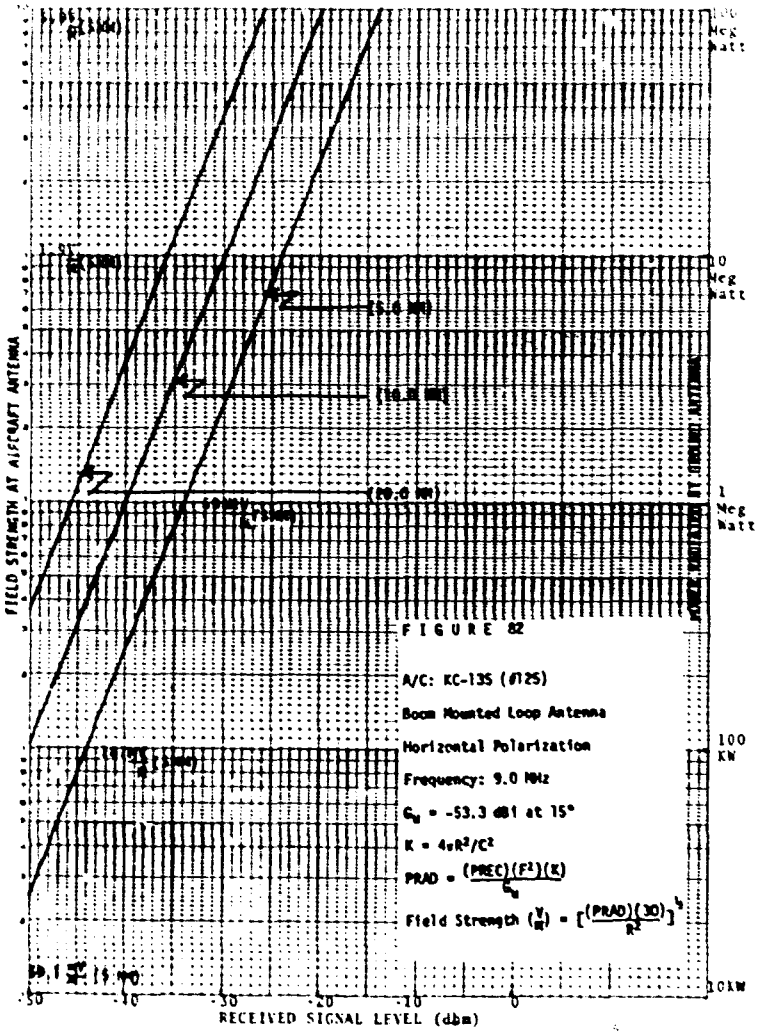
FIELD STRENGTH AT AIRCRAFT ANTENNA
RECEIVED SIGNAL LEVEL (dbm)
POWER RADIATED BY GROUND ANTENNA
100 Meg Watt
10 Meg Watt
1 Meg Watt
100 KW
10KW
(5.0 MM)
(10.0 MM)
(20.0 MM)
FIGURE 82
A/C: KC-135 (#125)
Boom Mounted Loop Antenna
Horizontal Polarization
Frequency: 9.0 MHz
G_u = -53.3 dBi at 15°
$K = 4\pi R^2/C^2$
$PRAD = \frac{(PREC)(F^2)(K)}{G_u}$
Field Strength $(\frac{V}{M}) = [\frac{(PRAD)(30)}{R^2}]^{1/2}$

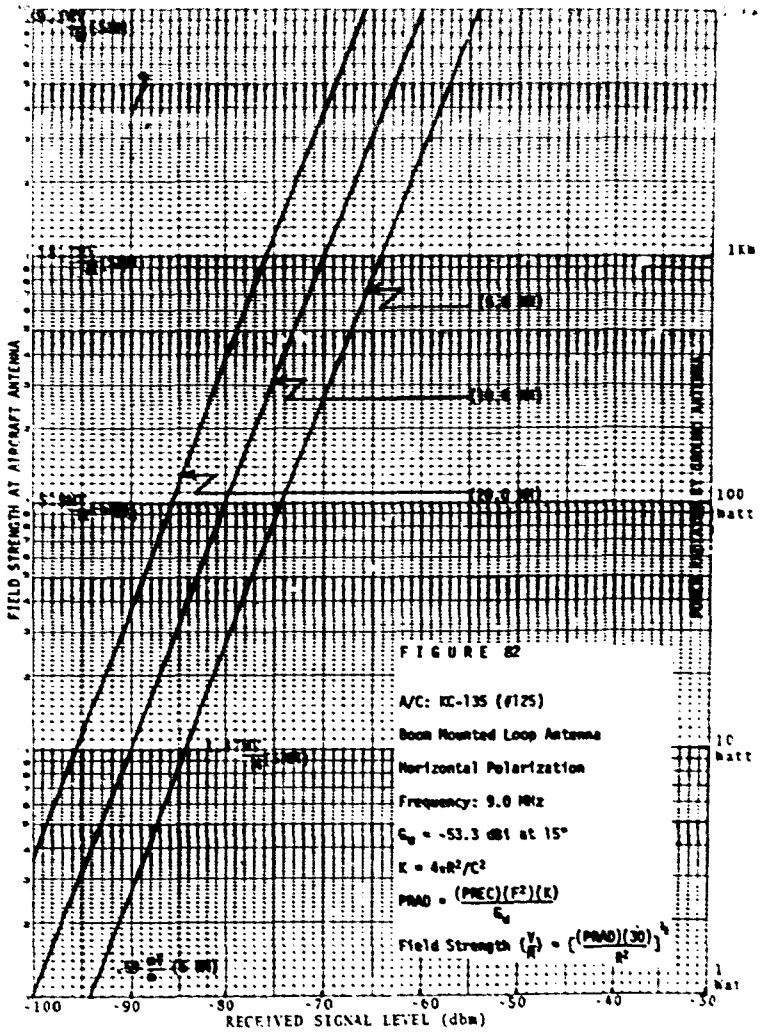
FIELD STRENGTH AT AIRCRAFT ANTENNA
RECEIVED SIGNAL LEVEL (dbm)
POWER RADIATED BY GROUND ANTENNA
1Kw
100 Watt
10 Watt
1 Wat
(5.0 MM)
(10.0 MM)
(20.0 MM)
FIGURE 82
A/C: KC-135 (#125)
Boom Mounted Loop Antenna
Horizontal Polarization
Frequency: 9.0 MHz
G_u = -53.3 dBi at 15°
$K = 4\pi R^2/C^2$
$PRAD = \frac{(PREC)(F^2)(K)}{G_u}$
Field Strength $(\frac{V}{M}) = [\frac{(PRAD)(30)}{R^2}]^{1/2}$

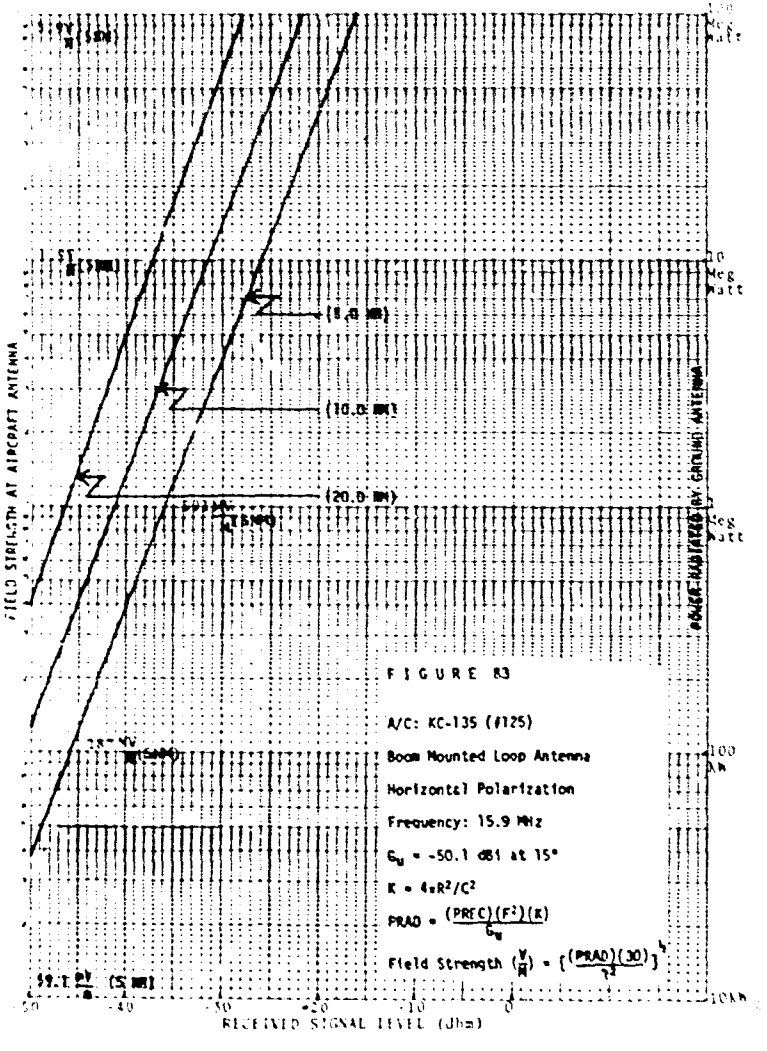

FIGURE 83

A/C: KC-135 (#125)

Boom Mounted Loop Antenna

Horizontal Polarization

Frequency: 15.9 MHz

G_u = -50.1 dBi at 15°

$K = 4\pi R^2/C^2$

$PRAD = \frac{(PREC)(F^2)(K)}{G_u}$

Field Strength $(\frac{V}{M}) = [\frac{(PRAD)(30)}{r^2}]^{\frac{1}{2}}$

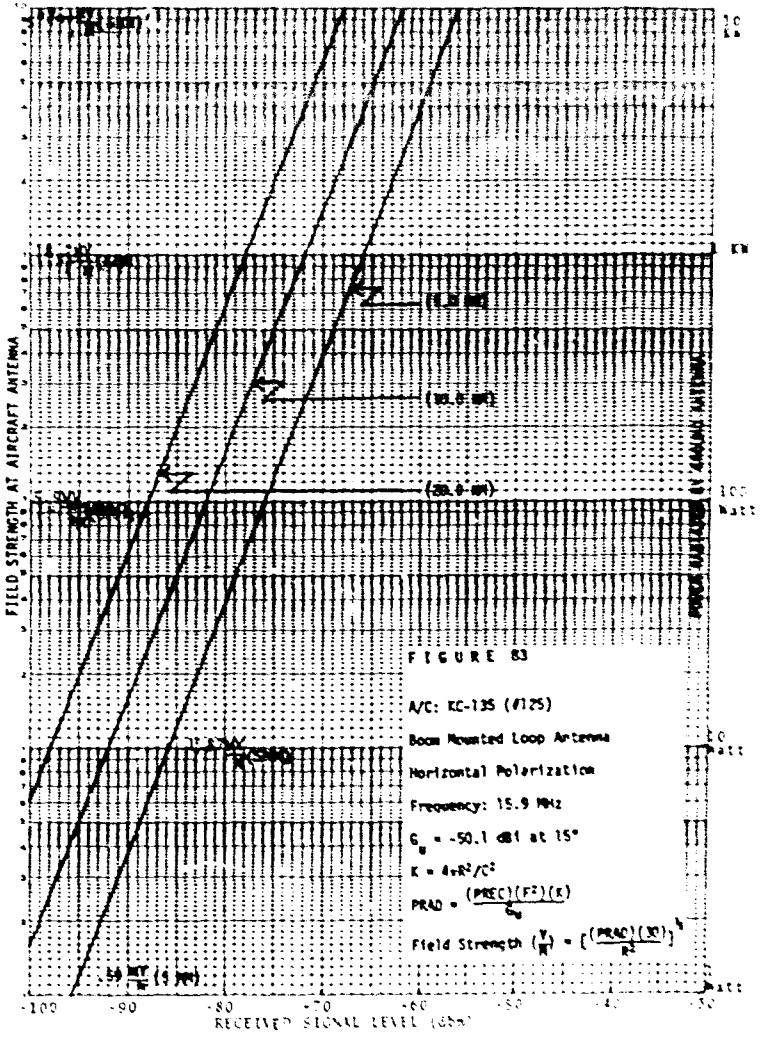

FIGURE 83

A/C: KC-135 (#125)

Boom Mounted Loop Antenna

Horizontal Polarization

Frequency: 15.9 MHz

G_u = -50.1 dBi at 15°

$K = 4\pi R^2/C^2$

$PRAD = \frac{(PREC)(F^2)(K)}{G_u}$

Field Strength $(\frac{V}{M}) = [\frac{(PRAD)(30)}{R^2}]^{\frac{1}{2}}$

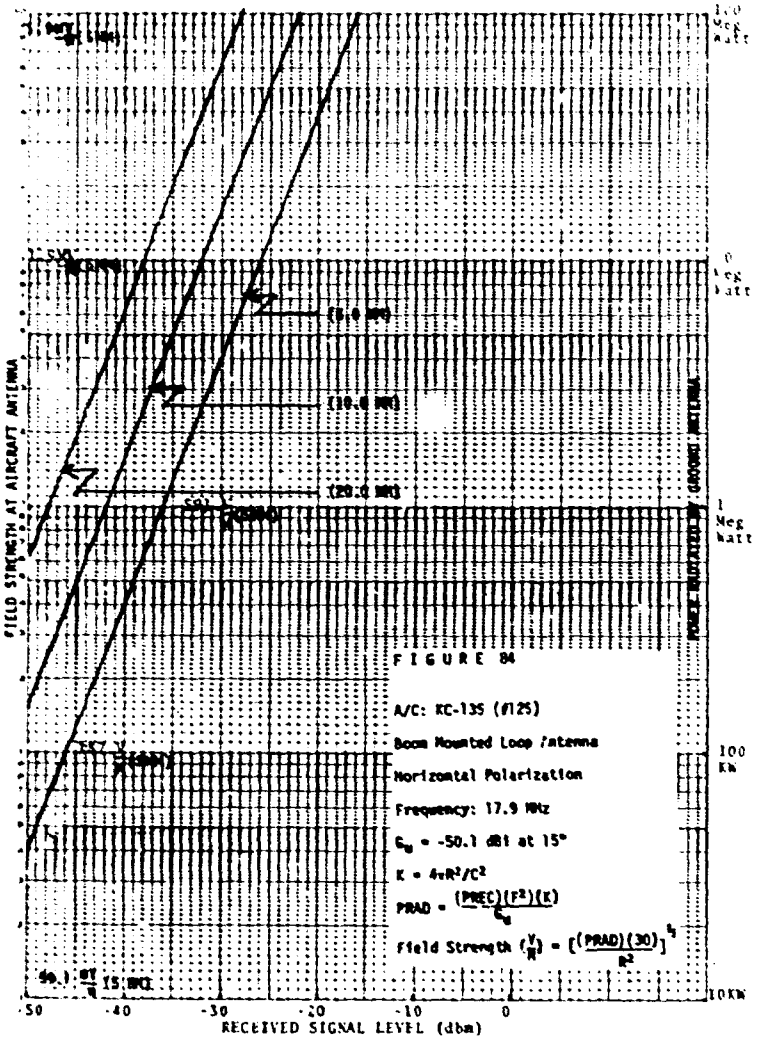
FIELD STRENGTH AT AIRCRAFT ANTENNA
RECEIVED SIGNAL LEVEL (dbm)
-50
-40
-30
-20
-10
0
100 Meg Watt
0 Meg Watt
1 Meg Watt
100 Kw
10Kw
(10.0 NM)
(20.0 NM)
FIGURE 84
A/C: KC-135 (#125)
Boom Mounted Loop Antenna
Horizontal Polarization
Frequency: 17.9 MHz
G_u = -50.1 dBi at 15°
$K = 4\pi R^2/C^2$
$PRAD = \frac{(PREC)(F^2)(K)}{G_u}$
Field Strength $(\frac{V}{M}) = [\frac{(PRAD)(30)}{R^2}]^{\frac{1}{2}}$

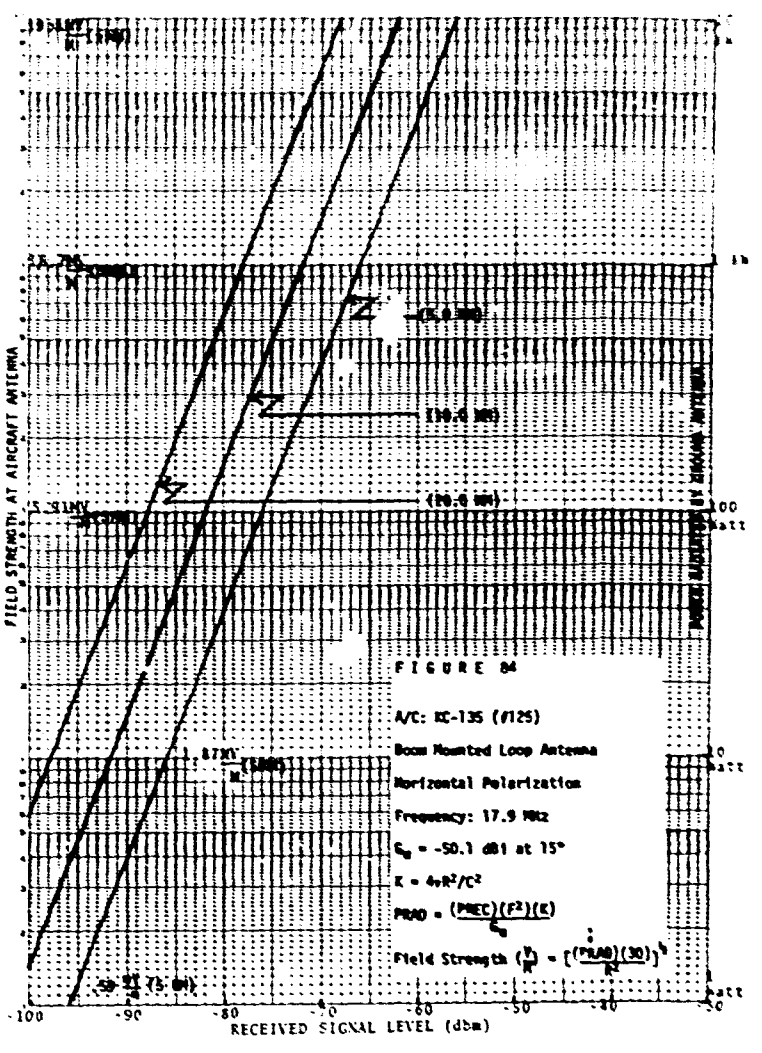
FIELD STRENGTH AT AIRCRAFT ANTENNA
RECEIVED SIGNAL LEVEL (dbm)
-100
-90
-80
-70
-60
-50
-40
-30
100 Watt
10 Watt
1 Watt
(10.0 NM)
FIGURE 84
A/C: KC-135 (#125)
Boom Mounted Loop Antenna
Horizontal Polarization
Frequency: 17.9 MHz
G_u = -50.1 dBi at 15°
$K = 4\pi R^2/C^2$
$PRAD = \frac{(PREC)(F^2)(K)}{G_u}$
Field Strength $(\frac{V}{M}) = [\frac{(PRAD)(30)}{R^2}]^{\frac{1}{2}}$

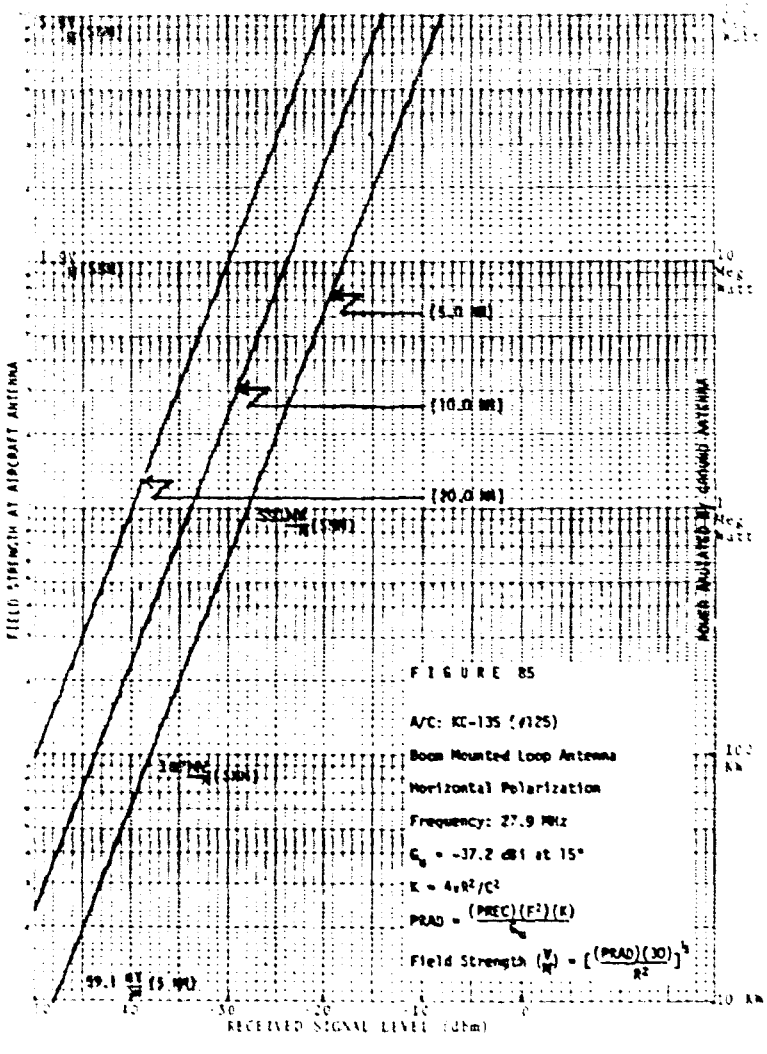

FIGURE 85

A/C: KC-135 (#125)

Boom Mounted Loop Antenna

Horizontal Polarization

Frequency: 27.9 MHz

G_a = -37.2 dBi at 15°

$K = 4\pi R^2/C^2$

$PRAD = \frac{(PREC)(E^2)(K)}{G_a}$

Field Strength $(\frac{V}{M}) = [\frac{(PRAD)(30)}{R^2}]^{\frac{1}{2}}$

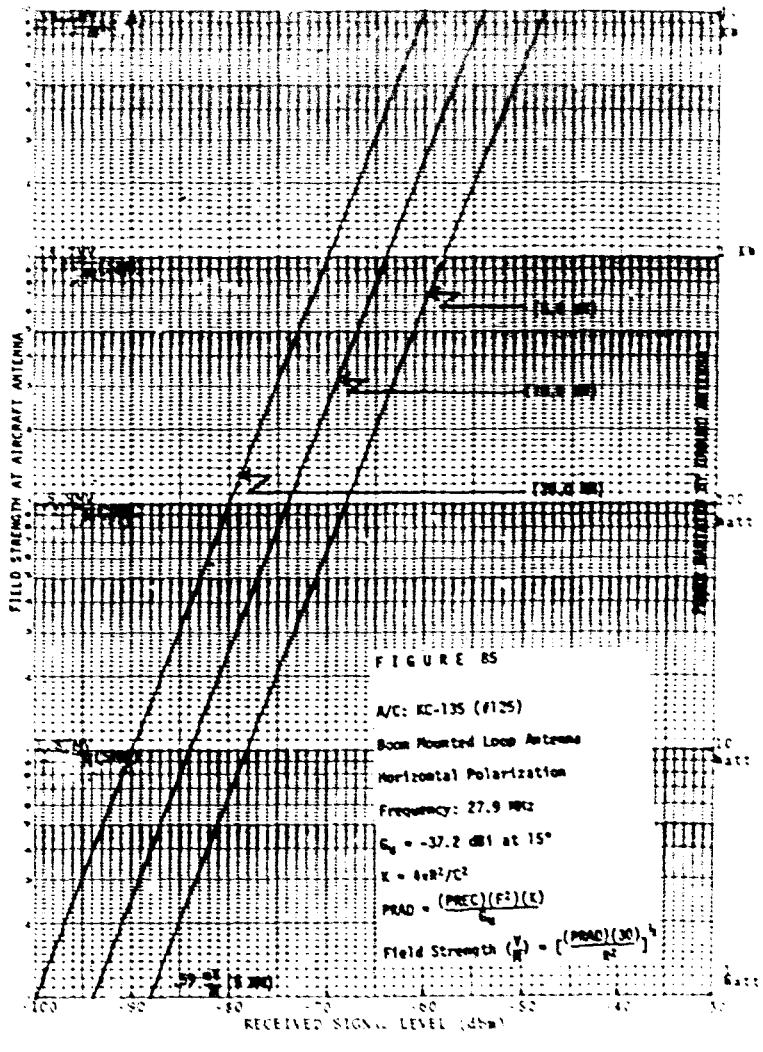

FIGURE 85

A/C: KC-135 (#125)

Boom Mounted Loop Antenna

Horizontal Polarization

Frequency: 27.9 MHz

G_a = -37.2 dBi at 15°

$K = 4\pi R^2/C^2$

$PRAD = \frac{(PREC)(E^2)(K)}{G_a}$

Field Strength $(\frac{V}{M}) = [\frac{(PRAD)(30)}{R^2}]^{\frac{1}{2}}$

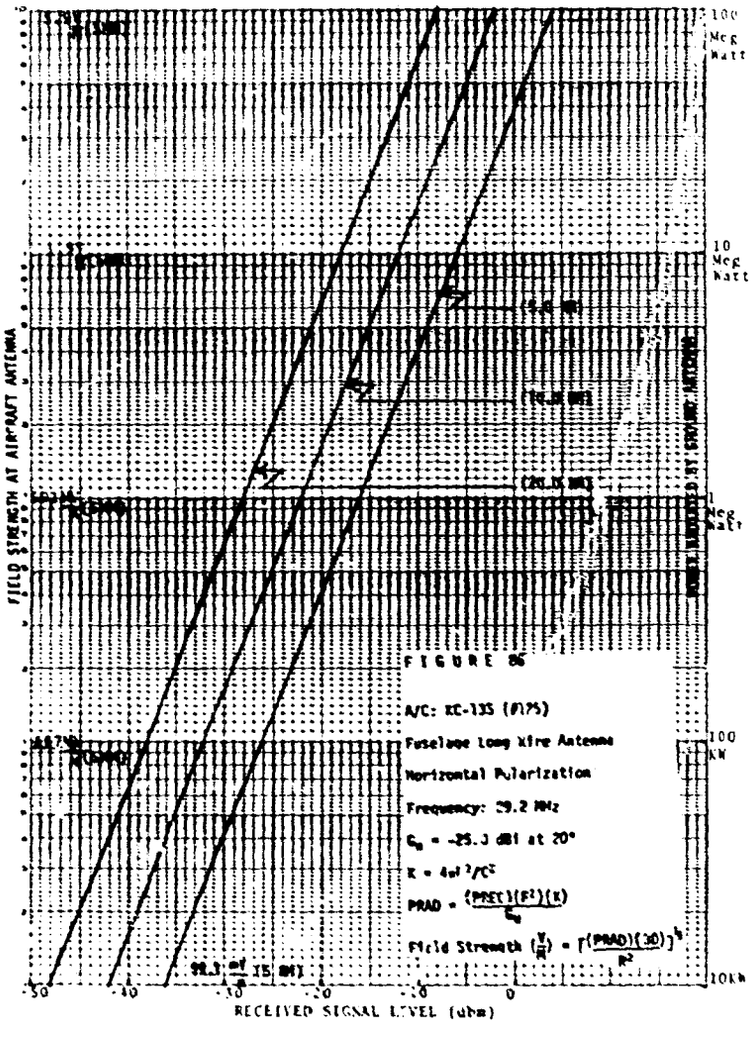
FIELD STRENGTH AT AIRCRAFT ANTENNA
RECEIVED SIGNAL LEVEL (dbm)
-50
-40
-30
-20
-10
0
100 Meg Watt
10 Meg Watt
1 Meg Watt
100 KW
10KW
FIGURE 86
A/C: KC-135 (#175)
Fuselage Long Wire Antenna
Horizontal Polarization
Frequency: 29.2 MHz
G_a = -25.3 dBi at 20°
$K = 4\pi R^2/C^2$
$PRAD = \frac{(PREC)(F^2)(K)}{G_a}$
Field Strength $(\frac{V}{M}) = [\frac{(PRAD)(30)}{R^2}]^{1/2}$

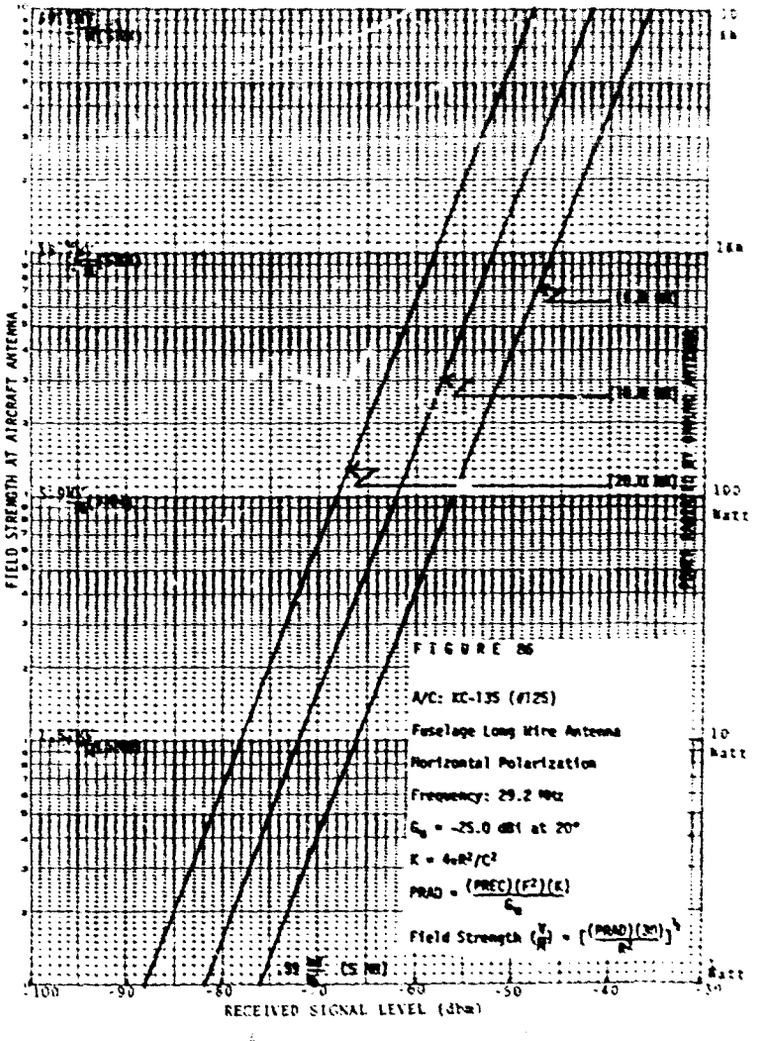
FIELD STRENGTH AT AIRCRAFT ANTENNA
RECEIVED SIGNAL LEVEL (dbm)
-100
-90
-80
-70
-60
-50
-40
-30
100 Watt
10 Watt
FIGURE 86
A/C: KC-135 (#125)
Fuselage Long Wire Antenna
Horizontal Polarization
Frequency: 29.2 MHz
G_a = -25.0 dBi at 20°
$K = 4\pi R^2/C^2$
$PRAD = \frac{(PREC)(F^2)(K)}{G_a}$
Field Strength $(\frac{V}{M}) = [\frac{(PRAD)(30)}{R^2}]^{1/2}$

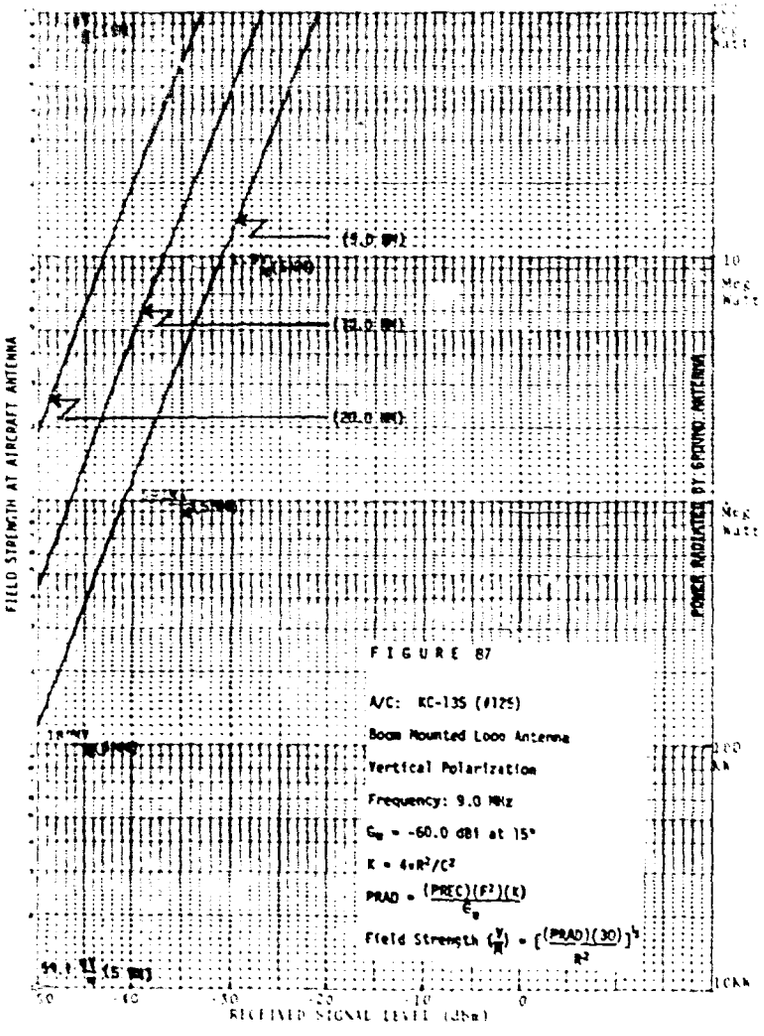

FIGURE 87

A/C: KC-135 (#125)

Boom Mounted Loop Antenna

Vertical Polarization

Frequency: 9.0 MHz

G_a = -60.0 dBi at 15°

$K = 4\pi R^2/C^2$

$PRAD = \frac{(PREC)(F^2)(K)}{G_a}$

Field Strength $(\frac{V}{M}) = [\frac{(PRAD)(30)}{R^2}]^{1/2}$

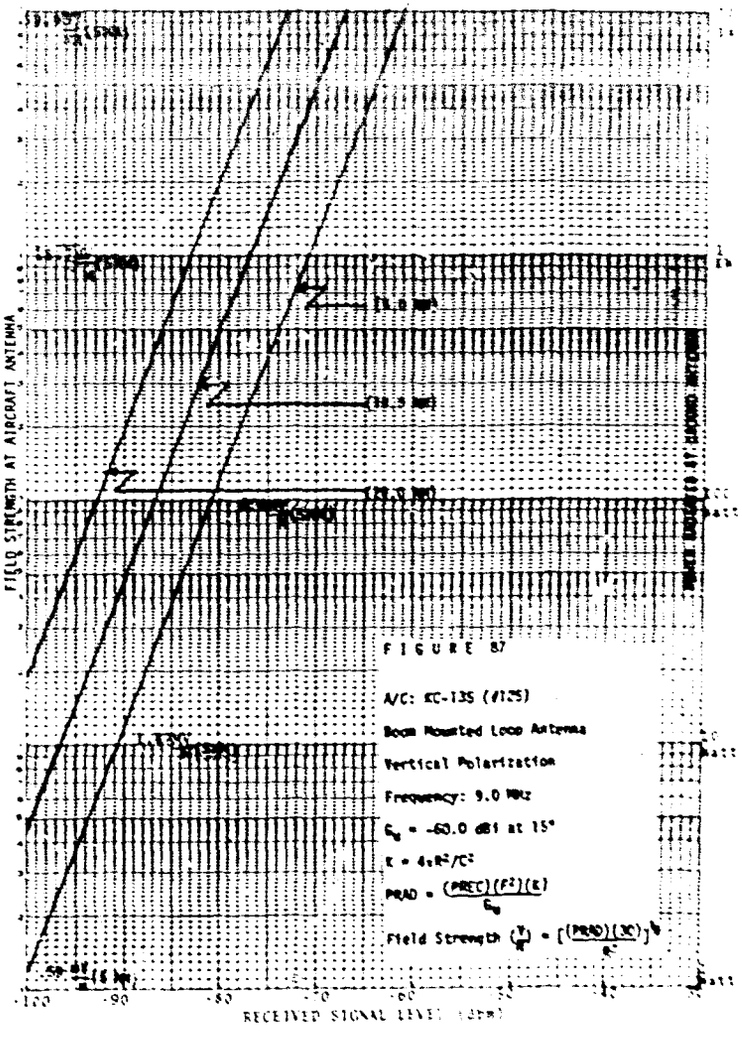

FIGURE 87

A/C: KC-135 (#125)

Boom Mounted Loop Antenna

Vertical Polarization

Frequency: 9.0 MHz

G_a = -60.0 dBi at 15°

$K = 4\pi R^2/C^2$

$PRAD = \frac{(PREC)(F^2)(K)}{G_a}$

Field Strength $(\frac{V}{M}) = [\frac{(PRAD)(30)}{R^2}]^{1/2}$

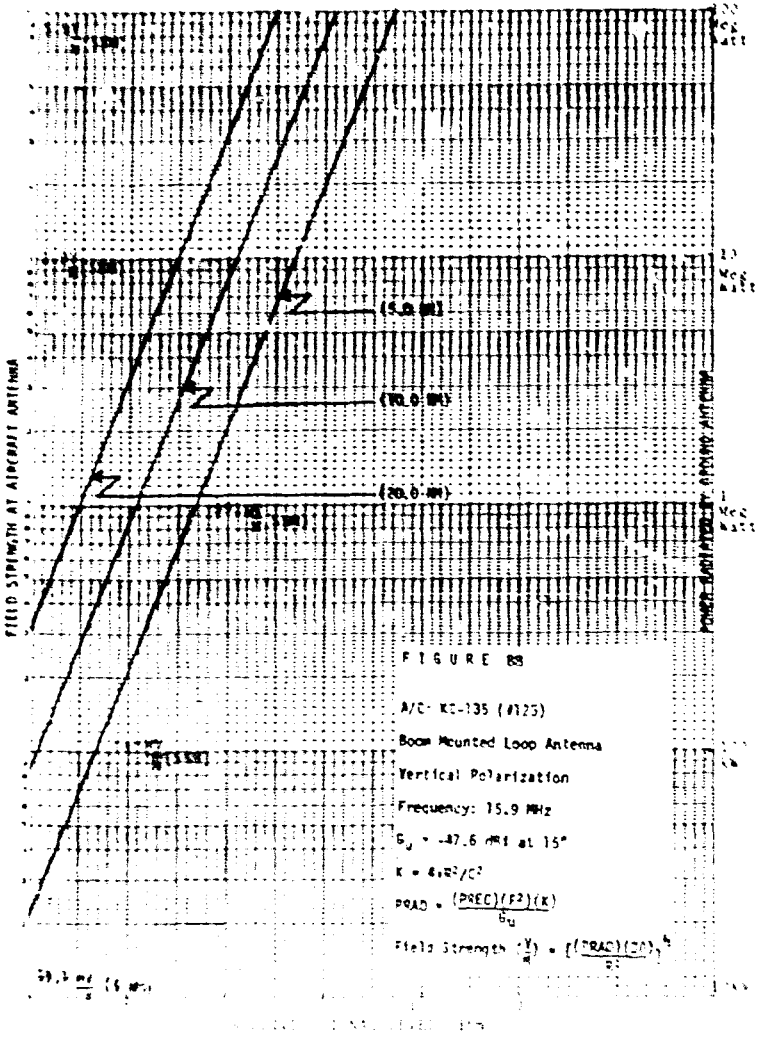

FIGURE 88

A/C: KC-135 (#125)

Boom Mounted Loop Antenna

Vertical Polarization

Frequency: 15.9 MHz

G_u = -47.6 dBi at 15°

$K = 4\pi R^2/C^2$

$PRAD = \frac{(PREC)(F^2)(K)}{G_u}$

Field Strength $(\frac{V}{m}) = \left[\frac{(PRAD)(30)}{R^2}\right]^{1/2}$

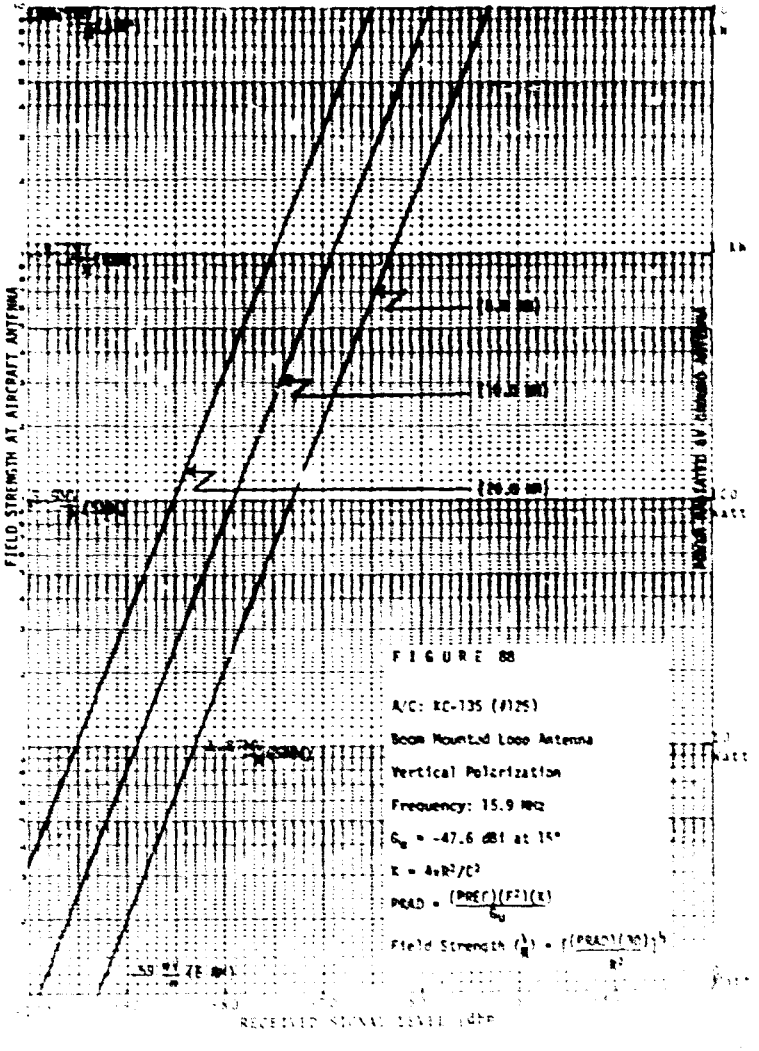

FIGURE 88

A/C: KC-135 (#125)

Boom Mounted Loop Antenna

Vertical Polarization

Frequency: 15.9 MHz

G_u = -47.6 dBi at 15°

$K = 4\pi R^2/C^2$

$PRAD = \frac{(PREC)(F^2)(K)}{G_u}$

Field Strength $(\frac{V}{m}) = \left[\frac{(PRAD)(30)}{R^2}\right]^{1/2}$

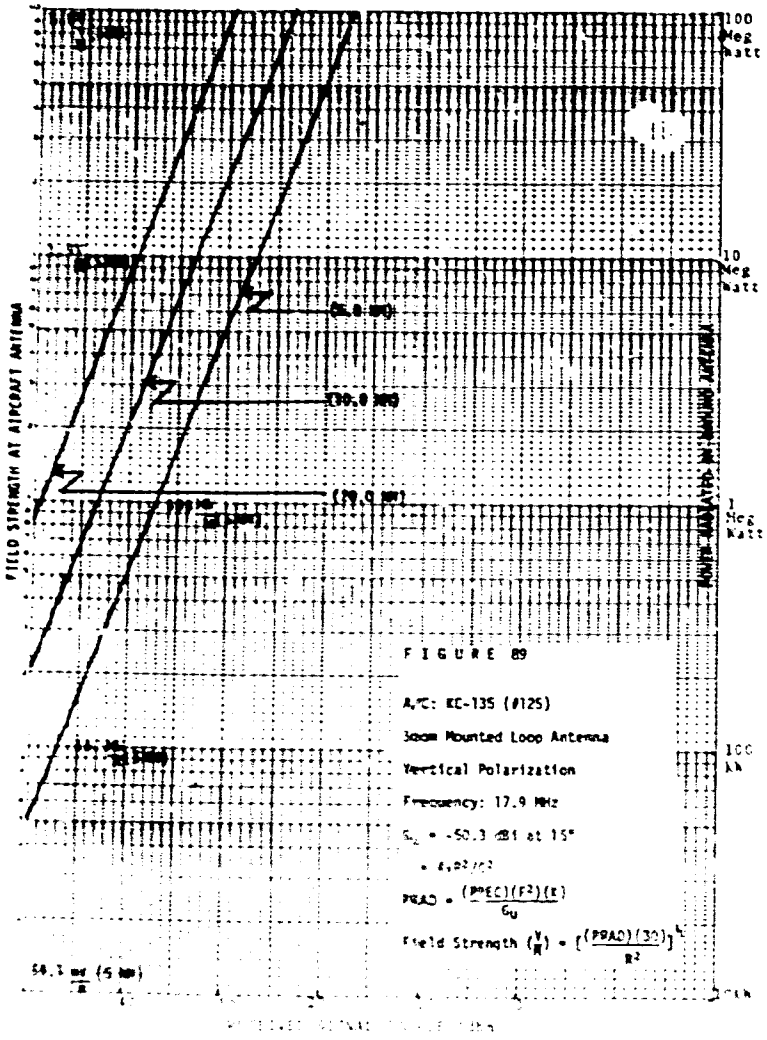
FIELD STRENGTH AT AIRCRAFT ANTENNA
100 Meg Watt
10 Meg Watt
1 Meg Watt
100 kW
(5.0 MM)
(10.0 MM)
(20.0 MM)
FIGURE 89
A/C: KC-135 (#125)
Boom Mounted Loop Antenna
Vertical Polarization
Frequency: 17.9 MHz
G_u = -50.3 dBi at 15°
$K = 4\pi R^2/C^2$
$PRAD = \frac{(PREC)(F^2)(K)}{G_u}$
Field Strength $(\frac{V}{M}) = [\frac{(PRAD)(30)}{R^2}]^{1/2}$

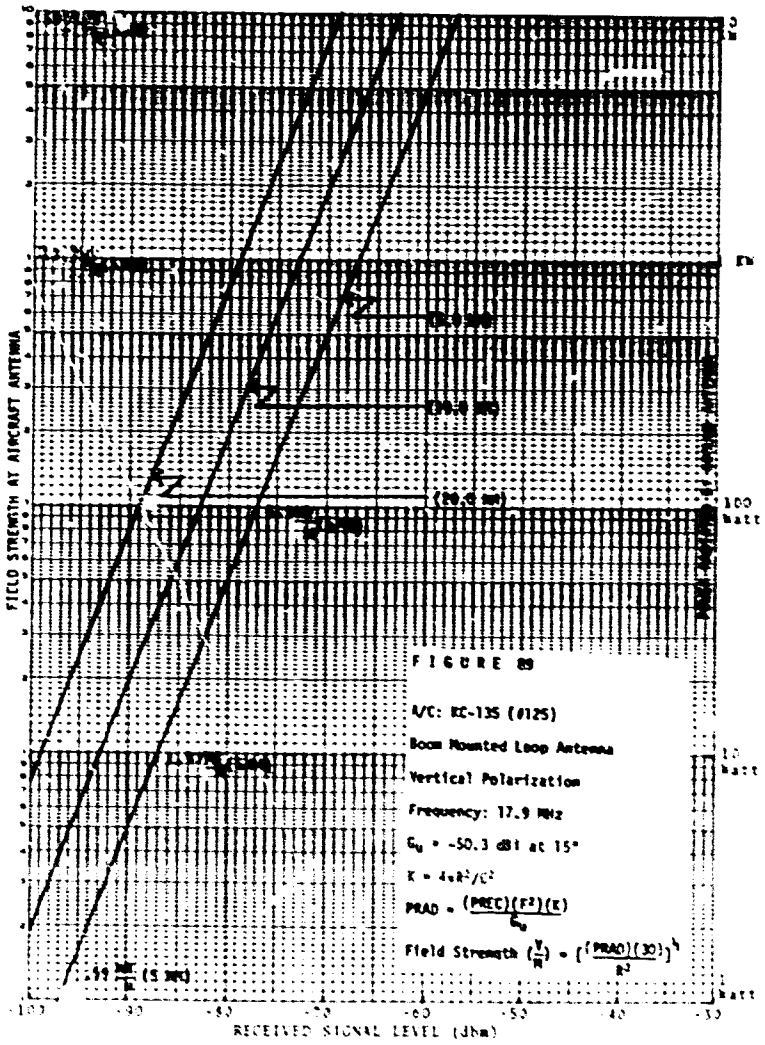
FIELD STRENGTH AT AIRCRAFT ANTENNA
100 Watt
10 Watt
1 Watt
(20.0 MM)
FIGURE 89
A/C: KC-135 (#125)
Boom Mounted Loop Antenna
Vertical Polarization
Frequency: 17.9 MHz
G_u = -50.3 dBi at 15°
$K = 4\pi R^2/C^2$
$PRAD = \frac{(PREC)(F^2)(K)}{G_u}$
Field Strength $(\frac{V}{M}) = [\frac{(PRAD)(30)}{R^2}]^{1/2}$
-100
-90
-80
-70
-60
-50
-40
-30
RECEIVED SIGNAL LEVEL (dbm)

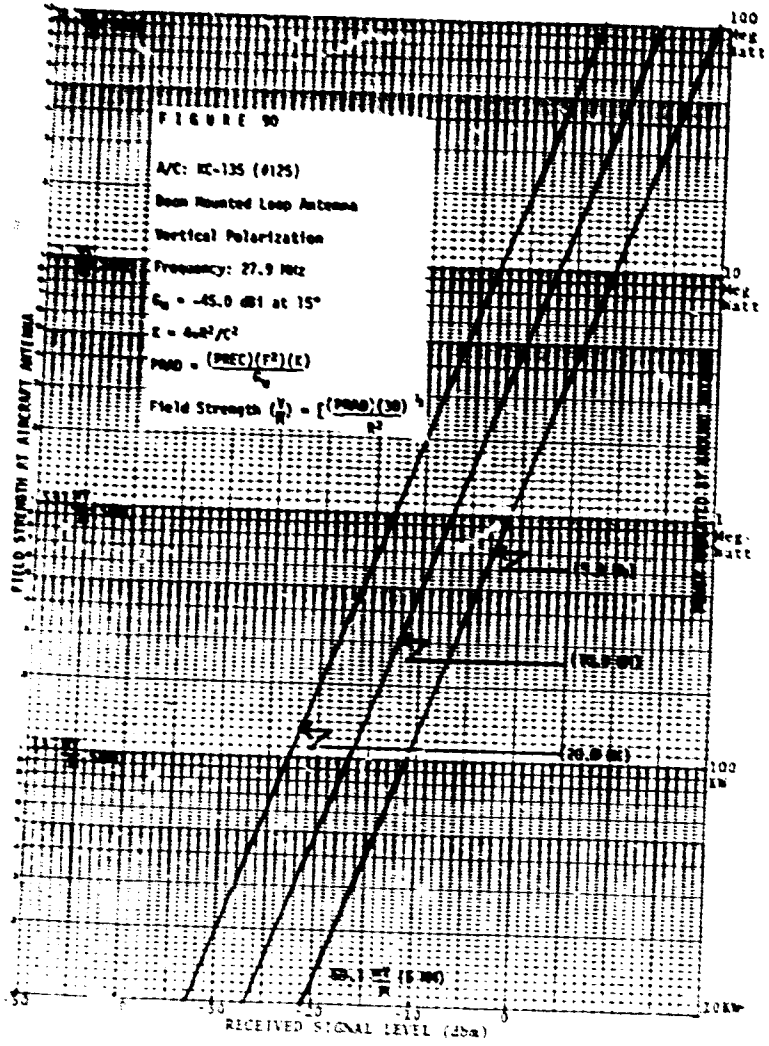
FIGURE 90
A/C: KC-135 (#125)
Boom Mounted Loop Antenna
Vertical Polarization
Frequency: 27.9 MHz
G_u = -45.0 dBi at 15°
K = 4πR²/C²
PRAD = (PREC)(F²)(K) / G_u
Field Strength (V/M) = [(PRAD)(30) / R²]^½
FIELD STRENGTH AT AIRCRAFT ANTENNA
RECEIVED SIGNAL LEVEL (dbm)
100 Meg Watt
10 Meg Watt
1 Meg Watt
100 KW
10 KW

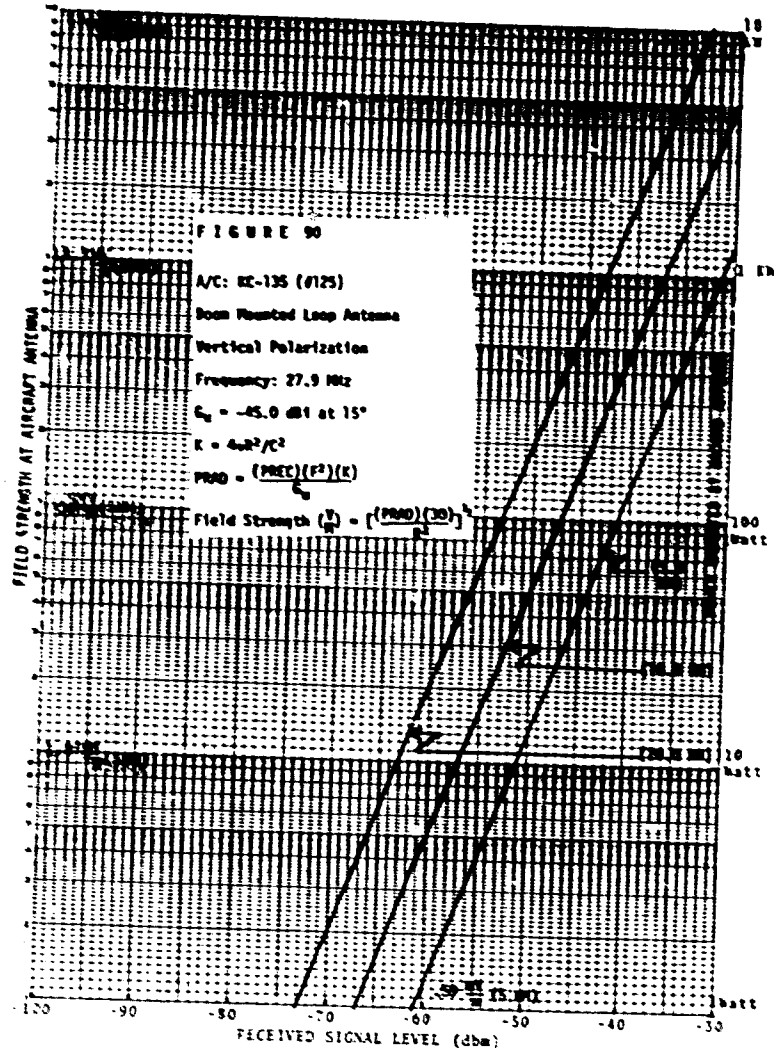
FIGURE 90
A/C: KC-135 (#125)
Boom Mounted Loop Antenna
Vertical Polarization
Frequency: 27.9 MHz
G_u = -45.0 dBi at 15°
K = 4πR²/C²
PRAD = (PREC)(F²)(K) / G_u
Field Strength (V/M) = [(PRAD)(30) / R²]^½
FIELD STRENGTH AT AIRCRAFT ANTENNA
RECEIVED SIGNAL LEVEL (dbm)
100 Watt
10 Watt
1 Watt

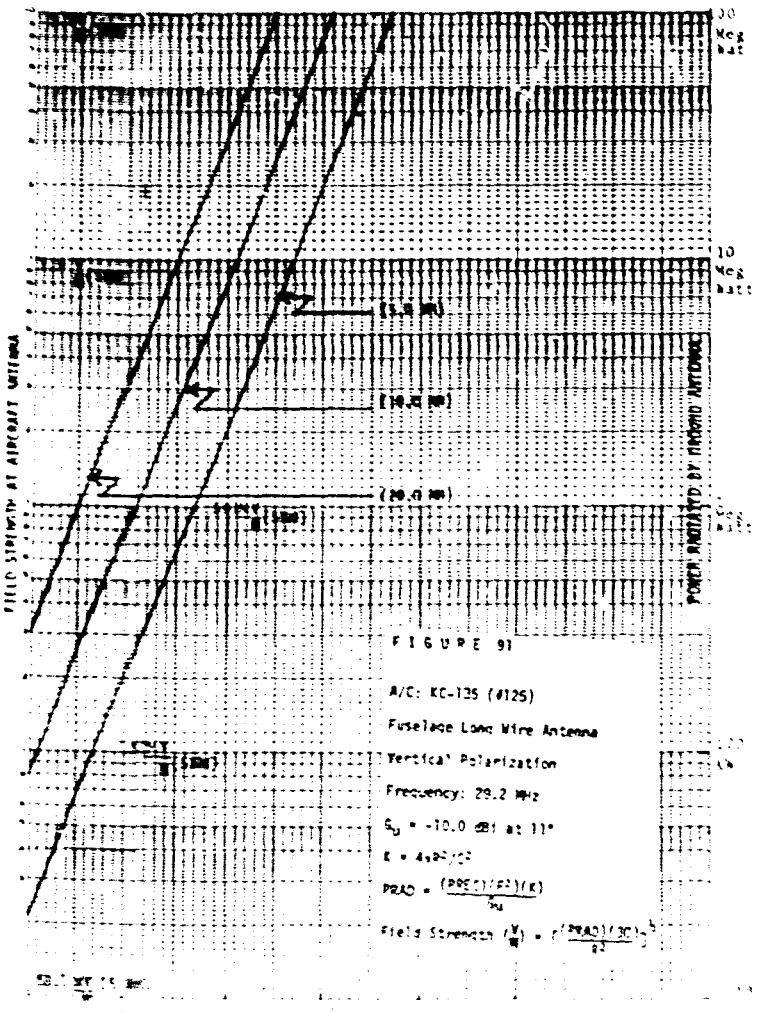

FIGURE 91

A/C: KC-135 (#125)

Fuselage Long Wire Antenna

Vertical Polarization

Frequency: 29.2 MHz

G_u = -10.0 dBi at 11°

$K = 4\pi R^2/C^2$

$PRAD = \frac{(PREC)(F^2)(K)}{G_u}$

Field Strength $(\frac{V}{M}) = [\frac{(PRAD)(30)}{R^2}]^{\frac{1}{2}}$

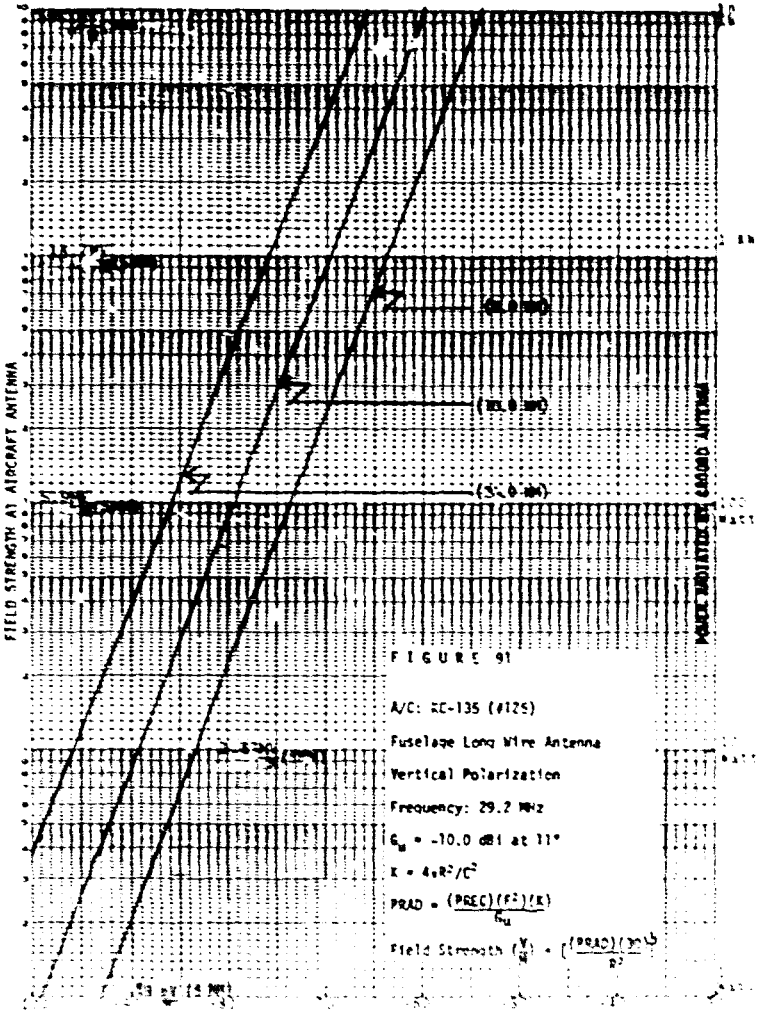

FIGURE 91

A/C: KC-135 (#125)

Fuselage Long Wire Antenna

Vertical Polarization

Frequency: 29.2 MHz

G_u = -10.0 dBi at 11°

$K = 4\pi R^2/C^2$

$PRAD = \frac{(PREC)(F^2)(K)}{G_u}$

Field Strength $(\frac{V}{M}) = [\frac{(PRAD)(30)}{R^2}]^{\frac{1}{2}}$

P_{IN_1} = Power input to Antenna #1

$P_{IN_1} = P_{INC} - P_{REFL} - P_{LOSS}$

$$[G_1 = \frac{(PR_2+PL_2)(K)(f^2)/G_u}{PIN_1}]$$

In order to facilitate use of the gain data of Figures 63 through 76, Figures 78 through 91 were prepared. These figures relate the gain data of Table VII to a variable "PR" Power Received (dBm) at the Airborne Receiver to predict both the power radiated (watts) by the Ground Antenna and Field Strength (volts per meter) impinging on the Airborne Antenna. For example:

> Referring to Figure 80 at a 5.0 nautical mile range and for an assumed receive power of -57 dBm, the power radiated by the Ground Antenna is 100 watts and the Field Strength at the Airborne Antenna is 5.9 $\frac{V}{M}$:

Similar data for ranges of 10 to 20 nautical miles has been included in the graphs of Figures 78 through 91.

The equations used to obtain the data of Figures 78 through 91 are contained in the legends of these figures. The equation for the power radiated by the Ground Antenna was obtained as follows:

$$G_u = (PR_2 + PL_2)(K)(f^2)/PRAD_1 \qquad \text{(Equation 8)}$$

Therefore:

$$PRAD = \frac{(PR_2 + PL_2)(K)(f^2)}{G_u}$$

The Field Strength at the airborne antenna was determined as follows:

$$P_{DEN} = \frac{(\frac{V}{M})^2}{120\pi} \qquad \text{(Equation 1)}$$

$$P_{DEN} = \frac{PRAD}{4\pi R^2} \qquad \text{(Equation 2)}$$

Equating 1 and 2:

$$\frac{(\frac{V}{M})^2}{120\pi} = \frac{PRAD}{4\pi R^2}$$

$$\left(\frac{V}{M}\right)^2 = \frac{PRAD\ (120\pi)}{4\pi R^2}$$

$$\left(\frac{V}{M}\right)^2 = \frac{(PRAD)(30)}{R^2}$$

$$\left(\frac{V}{M}\right) = \left[\frac{(PRAD)(30)}{R^2}\right]^{\frac{1}{2}} \frac{VOLTS}{METER}$$

SECTION VII

CONCLUSIONS

Two aircraft have been calibrated as field probes for making absolute power gain measurements of high frequency, HF, antenna installations, thereby eliminating the need for a reference antenna at each installation. Conventional measurement techniques make use of a reference antenna in close proximity to the test antenna in order to make comparative radiation pattern measurements. The use of a reference is complicated by (a) limited availability of standard HF reference antennas and (b) installation of these physically large structures. The availability of these calibrated test vehicles circumvents the need for a reference antenna at each site; additional cost of the reference antenna installation in remote sites; and additional flight time and data reduction effort required at every test location to check validity of correlation.

The technique used in the calibration consists of establishing a known radiation field by means of a ground based dipole of controlled geometry installed in a site where terrain and ground conductivity are known, thus allowing the field intensity to be accurately calculated. Flight tests were then conducted using precise positioning and attitude control of the aircraft, from which data is obtained to establish the required calibration. The airborne antennas were used in the receive mode, and all flight test measurements were made in the CW mode. Calibration was accomplished for both vertical and horizontal polarization. Substantial correlation was achieved between the theory and experiment to validate the results. The criteria for instrumenting the aircraft and for designing and using the "standard" ground dipole installation have been established.

Based upon the extreme care and control with which flight tests were made, the absolute gain data contained in this report is considered accurate within ± 2.5 dB (Appendix A).

PRECEDING PAGE BLANK

APPENDIX A

In an attempt to realistically estimate the accuracy of the gain data of Tables VII-A and VII-B, the following error budget was prepared. The primary factors involved are:

a. Precise knowledge of ground constants

b. Control of aircraft position and attitude

c. Equipment accuracy

d. Insertion loss

e. Human error, i.e., operator effects

Estimate of Errors:

a. Uncertainty in ground electrical constants about $\pm$ 1.5 dB

b. Throughout the flight tests aircraft attitude instruments were periodically monitored by the pilot to assure that a level attitude was maintained. The stability was maintained within $\pm 2^{\circ}$. It was estimated that a roll of this magnitude would vary the received signal level approximately $\pm$ 0.2 dB.

c. Equipment accuracy: The radiated power, monitored during the tests, was maintained within $\pm$ 0.3 dB across the operating band. Pre- and post-calibration curves were repeatable within $\pm$ 0.2 dB.

d. Cable loss uncertainty was about $\pm$ 0.1 dB.

e. Operator effects probably amounted to $\pm$ 0.2 dB

The total uncertainty is therefore $\pm$ 2.5 dB.

In terms of an RMS error value, consideration of the above variables provides a total RMS of $\pm$ 1.5 dB.

PRECEDING PAGE BLANK